Technical Memorandum NESS 57

DEPARTMENT OF COMMERCE
★ ★
UNITED STATES OF AMERICA

NIMBUS-5 SOUNDER DATA PROCESSING SYSTEM

PART I: Measurement Characteristics and

Data Reduction Procedures

W. L. Smith
H. M. Woolf
P. G. Abel
C. M. Hayden
M. Chalfant
N. Grody

Washington, D.C.
June 1974

noaa NATIONAL OCEANIC AND
ATMOSPHERIC ADMINISTRATION / National Environmental
Satellite Service

ESSA Technical Memoranda

NESCTM 18 On the Statistical Relation Between Geopotential Height and Temperature-Pressure Profiles. W. L. Smith and S. Fritz, November 1969. (PB-189-276)

NESCTM 19 Applications of Environmental Satellite Data to Oceanography and Hydrology. E. Paul McClain, January 1970. (PB-190-652)

NESCTM 20 Mapping of Geostationary Satellite Pictures--An Operational Experiment. R. C. Doolittle, C. L. Bristor, and L. Lauritson, March 1970. (PB-191-189)

NESCTM 22 Publications and Final Reports on Contracts and Grants, 1969--NESC. January 1970. (PB-190-632)

NESCTM 23 Estimating Mean Relative Humidity From the Surface to 500 Millibars by Use of Satellite Pictures. Frank J. Smigielski and Lee M. Mace, March 1970. (PB-191-741)

NESCTM 24 Operational Brightness Normalization of ATS-1 Cloud Pictures. V. R. Taylor, August 1970. (PB-194-638)

NESCTM 25 Aircraft Microwave Measurements of the Arctic Ice Pack. Alan E. Strong and Michael H. Fleming, August 1970. (PB-194-588)

NOAA Technical Memoranda

NESS 21 Geostationary Satellite Position and Attitude Determination Using Picture Landmarks. William J. Dambeck, August 1972. (COM-72-10916)

NESS 26 Potential of Satellite Microwave Sensing for Hydrology and Oceanography Measurements. John C. Alishouse, Donald R. Baker, E. Paul McClain, and Harold W. Yates, March 1971. (COM-71-00544)

NESS 27 A Review of Passive Microwave Remote Sensing. James J. Whalen, March 1971. (COM-72-10546)

NESS 28 Calculation of Clear-Column Radiances Using Airborne Infrared Temperature Profile Radiometer Measurements Over Partly Cloudy Areas. William L. Smith, March 1971. (COM-71-00556)

NESS 29 The Operational Processing of Solar Proton Monitor and Flat Plate Radiometer Data. Henry L. Phillips and Louis Rubin, May 1972. (COM-72-10719)

NESS 30 Limits on the Accuracy of Infrared Radiation Measurements of Sea-Surface Temperature From a Satellite. Charles Braun, December 1971. (COM-72-10898)

NESS 31 Publications and Final Reports on Contracts and Grants, 1970--NESS. December 1971. (COM-72-10303)

NESS 32 On Reference Levels for Determining Height Profiles From Satellite-Measured Temperature Profiles. Christopher M. Hayden, December 1971. (COM-72-50393)

NOAA Technical Memorandum NESS 57

NIMBUS-5 SOUNDER DATA PROCESSING SYSTEM

PART I: Measurement Characteristics and

Data Reduction Procedures

W. L. Smith
H. M. Woolf
P. G. Abel
C. M. Hayden
M. Chalfant
N. Grody

Washington, D.C.
June 1974

UNITED STATES
DEPARTMENT OF COMMERCE
Frederick B. Dent, Secretary

NATIONAL OCEANIC AND
ATMOSPHERIC ADMINISTRATION
Robert M. White, Administrator

National Environmental
Satellite Service
David S. Johnson, Director

NOAA

74   3341

This memorandum was originally prepared
for the GARP Project Office, National Aero-
nautics and Space Administration, Goddard
Space Flight Center, under Contract No.
S-70249-AG.
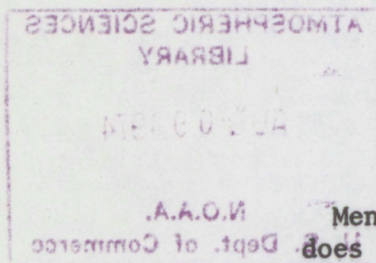
Mention of a commercial company or product
does not constitute an endorsement by the NOAA
National Environmental Satellite Service. Use
for publicity or advertising purposes of infor-
mation from this publication concerning propri-
etary products or the tests of such products is
not authorized.

TABLE OF CONTENTS

iii

ACKNOWLEDGEMENTS

1.0 Introduction

Part I of this report describes the data processing system developed to obtain various meteorological variables from infrared and microwave radiometric data obtained from the Nimbus-5 spacecraft. The meteorological parameters deduced from the radiance data include: (a) surface temperature, (b) vertical temperature profile, (c) precipitable water content, (d) total outgoing long-wave radiation flux, and (e) vertical cloud distribution. The data system enables the derivations to be made on a global basis independent of contemporary conventional data. Determinations are made with horizontal resolutions of 500 km and 150 km to satisfy the requirements for the large scale numerical forecast experiments and the fine-scale weather analysis-forecast studies being conducted as part of the Global Atmospheric Research Program (GARP). Part II of this report presents the significant results obtained from the Nimbus-5 data processing system.

The design of the sounding data processing system was completed prior to the launch of Nimbus-5 (December 11, 1972). Since the launch the processing system has undergone continual refinement to improve the accuracy of the meteorological determinations as well as to cope with unexpected pecularities of the Nimbus-5 radiance data (e.g., the erratic scan behavior of the ITPR, the spectral leaks of the SCR channels, and the incompatabilities of NEMS and ITPR data caused by their differences in spatial resolution). At the time of this writing, however, most of the goals of the Nimbus-5 data processing system have been met or exceeded. Only minor alterations and additions are needed to apply the data processing system to Nimbus-F for the quasi-real time generation of global data sets as part of the Data Systems Test (DST).

The Nimbus amalgamated sounding data processing system employs the most complete, from a physics point of view, meteorological data retrieval algorithms utilized to date. For example, in the derivation of vertical temperature profiles, the effects of cloudiness, terrain elevation, surface reflectance-emittance properties, and small-scale surface temperature inhomogeneities are taken into account. Also, the retrieval methods developed do not utilize contemporary conventional data, so that the determinations are independent and their accuracy is not biased by the conventional data network. (It is felt that the satellite sounding data to be utilized in the global experiment should have as little geographical bias as possible.) The retrieval system is flexible in that it automatically operates with any combinations of infrared and microwave observations available to obtain the best possible result.

2.0 The Observational Characteristics of the Nimbus-5 Sounding Experiments

The data processing system utilizes various data from four different
radiometric experiments aboard Nimbus-5: the Infrared Temperature Profile
Radiometer (ITPR), the Nimbus-E Microwave Spectrometer (NEMS), the Selec-
tive Chopper Radiometer (SCR) and the Temperature Humidity Infrared
Radiometer (THIR). As will be shown, certain data from each of these
experiments provides a unique contribution to the final result. Since
the engineering details of these experiments are given in the Nimbus-5
User's Guide (1972), only observational characteristics need be pre-
sented here.

2.1 ITPR

2.1.1 Experiment Description

The Nimbus-5 ITPR measures radiation in seven different
spectral intervals. Two of the spectral intervals are in the window
regions at 3.7 μm and 11 μm for the purpose of detecting clouds and
obtaining surface temperatures even when a partial cloud cover exists
in the instrument's field of view. There are four atmospheric tempera-
ture profiling channels in the 15-μm CO_2 band and a single water vapor
channel at 20 μm in the rotational water vapor absorption band. The
vertical weighting functions for the 4 CO_2 channels are shown in
figure 2-1.

The instrument has a linear spatial resolution of 35 km
and spatially scans in order to circumvent clouds and to obtain uniform
earth coverage. Figure 2-2 illustrates the ITPR scan geometry, as well as
that for NEMS and SCR which will be discussed later. As shown, the ITPR
samples 140 contiguous scan elements within three different grids, one
to the right, one at the center, and one to the left of the sub-satellite
track as the satellite moves along its orbit.

One novel feature of the ITPR is the simultaneous
measurement of the radiances in the 3.7-μm and 11-μm window regions
which enables the detection of clouds within the instrument's field
of view and the estimation of surface temperatures under partly cloudy
sky conditions. Since molecular absorption is small in the 3.7-μm and
11-μm window regions, these ITPR window channels sense only the radia-
tion from the earth's surface and any clouds within the instrument's
field of view. When sensing a uniform and opaque scene (e.g., the
earth's surface) they observe the same brightness temperatures. When
sensing a non-uniform scene (e.g., broken clouds),different brightness
temperatures are observed in the two window channels. This is because
of the vastly different radiance dependence upon scene temperature
for the two different wavelengths, a phenomenon described by Planck's
law. At 11 μm, the radiance is approximately proportional to
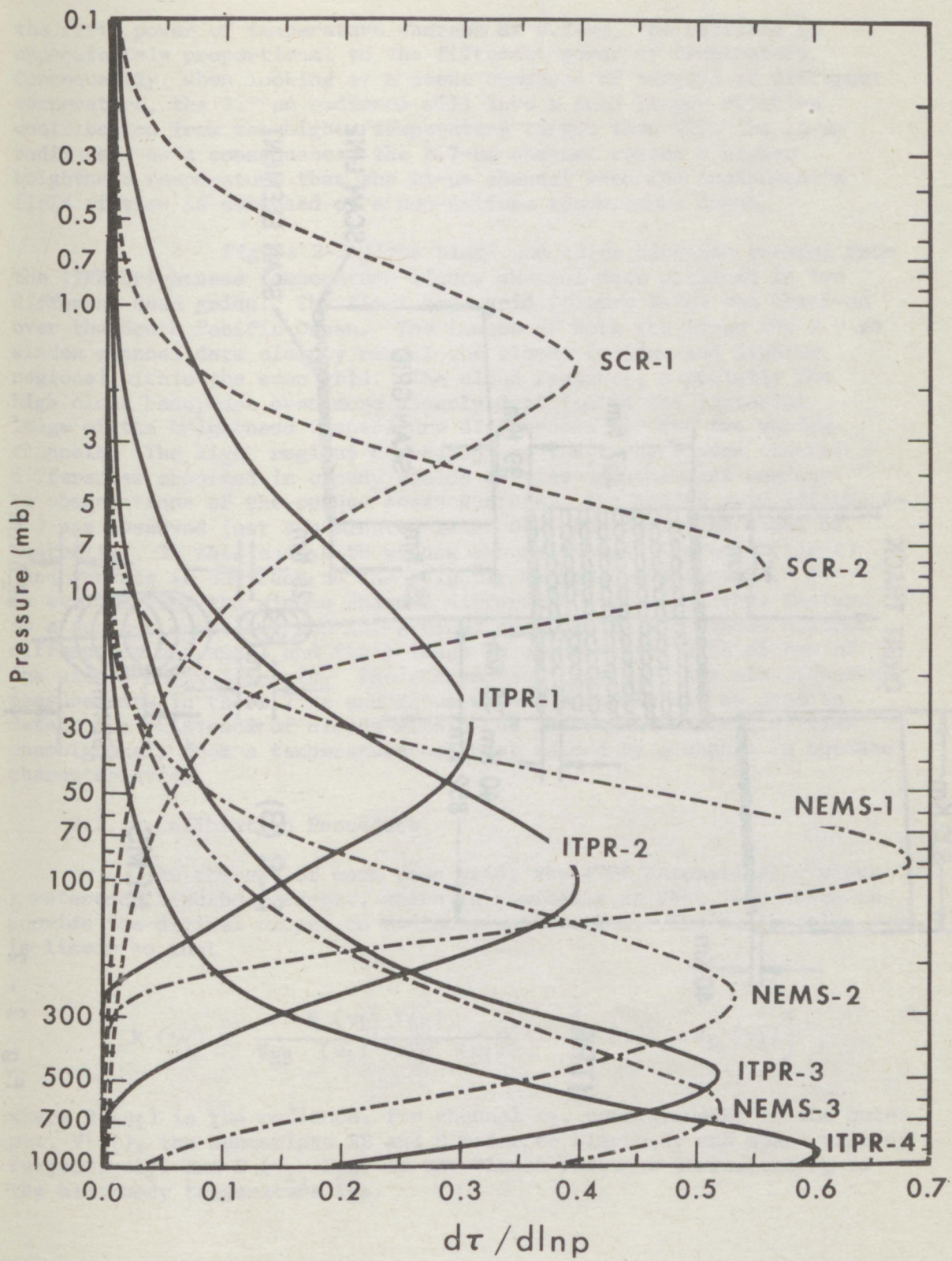
Fig. 2 - 1

NIMBUS-5 Sounder Scan Pattern
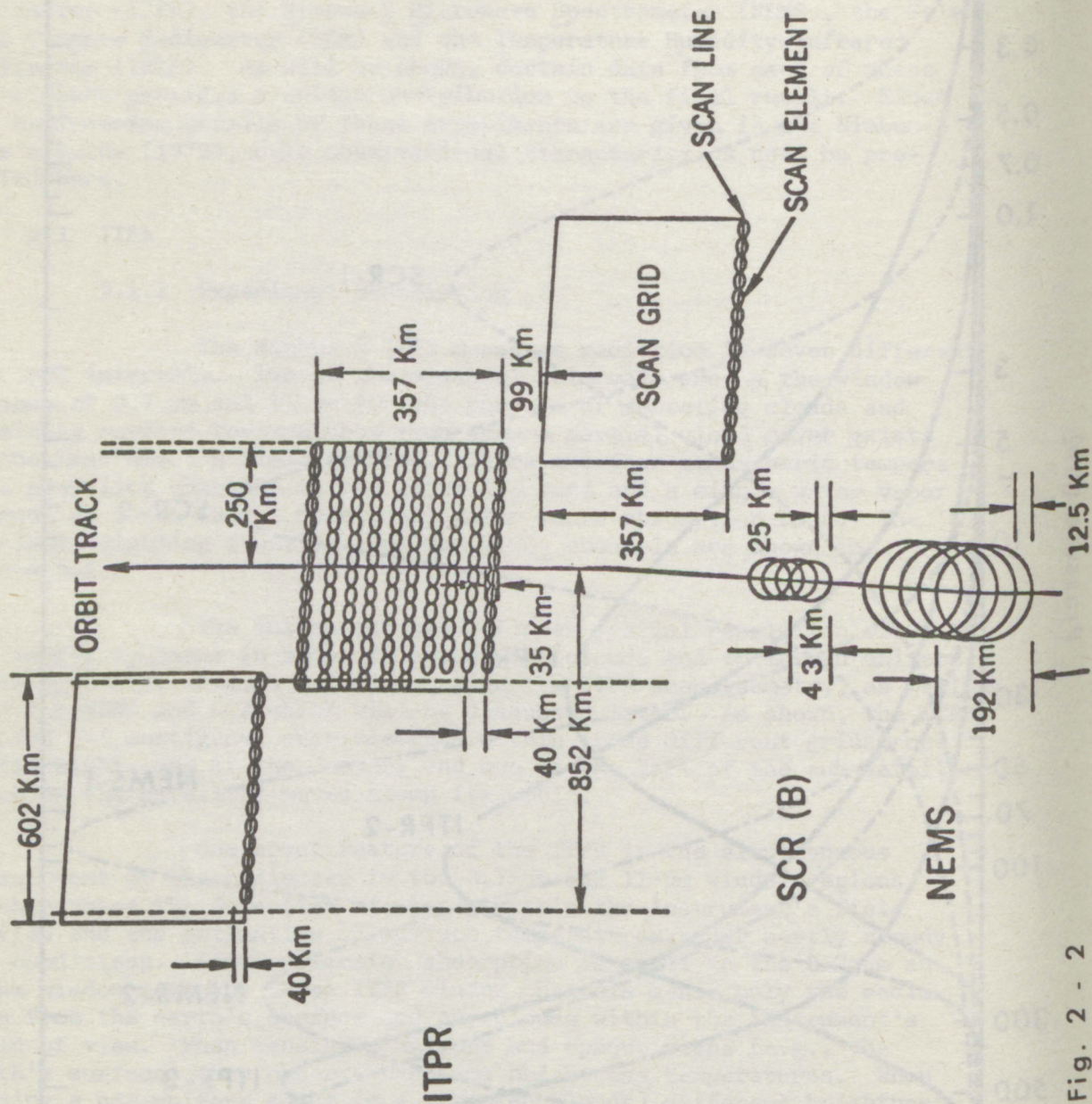
Fig. 2 - 2

the fifth power of temperature whereas at 3.7-µm, the radiance is
approximately proportional to the fifteenth power of temperature.
Consequently, when looking at a scene composed of targets of different
temperature, the 3.7-µm radiance will have a much larger relative
contribution from the higher temperature target than will the 11-µm
radiance. As a consequence, the 3.7-µm channel senses a higher
brightness temperature than the 11-µm channel when the instrument's
field of view is composed of a non-uniform temperature scene.

Figure 2-3 gives black and white pictures created from
the ITPR brightness temperature window channel data obtained in two
different scan grids. The first scan grid (figure 2-3a) was observed
over the South Pacific Ocean. The images of both the 11-µm and 3.7-µm
window channel data clearly reveal the clouds (colder and lighter
regions) within the scan grid. The cloud features, especially the
high cloud band, are even more clearly depicted in the pictorial
image of the brightness temperature differences for the two window
channels. The light regions correspond to the large window channel
differences observed in cloudy fields of view and the dark regions
to observations of the opaque ocean surface. The second grid (figure 2-
3b) was observed just two minutes later over the northeast coast of
Australia. In this case, both window channels sense the cold (light)
land surface in contrast to the slightly warmer ocean surface. It
is evident from the window channel difference image that this feature
is a surface coastline and not a cloud edge, since the window channel
differences are small and their image is uncorrelated with either of
the window channel images. These examples illustrate how simultaneous
measurements in the 3.7-µm and 11-µm window channels can be used to
detect the existence of clouds within the instrument's field of view
unambiguously from a temperature contrast caused by a change in surface
characteristics.

2.1.2 Calibration Procedure

At the end of each scan grid, the ITPR automatically views
a reference blackbody target, which is nominally at 24°C, and space to
provide the digital output to radiance calibration. The calibration
is linear so that

$$R(\nu_i) = \frac{B(\nu_i, T_{BB})}{V_{BB}(\nu_i) - V_S(\nu_i)} \left[V(\nu_i) - V_S(\nu_i)\right], \tag{1}$$

where $R(\nu_i)$ is the radiance, for channel ν_i, corresponding to the out-
put, $V(\nu_i)$, the subscripts BB and S refer to blackbody and space values,
respectively, and $B(\nu_i, T_{BB})$ is the Planck radiance corresponding to
the blackbody temperature T_{BB}.

NIMBUS 5   December 12, 1972

1247:28GMT

Ch.2—1 Diff.   Ch. 1   Ch. 2   Ch. 7

11.0—3.7μm   3.7μm   11.0μm   19.7μm
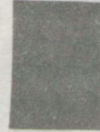
Ch. 3   Ch. 4   Ch. 5   Ch. 6

13.4μm   14.0μm   14.5μm   15.0μm

Fig. 2 - 3a

1248:48GMT

Ch.2—1 Diff.   Ch. 1   Ch. 2   Ch. 7

11.0—3.7μm   3.7μm   11.0μm   19.7μm
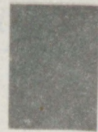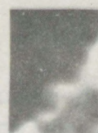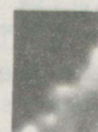
Ch. 3   Ch. 4   Ch. 5   Ch. 6
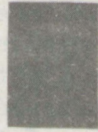
13.4μm   14.0μm   14.5μm   15.0μm

Fig. 2 - 3b

Grid Location:

159.7E   165.1E   19.2S

17.8S   165.1E

21.0S   22.4S

158.9E   164.4E

148.8E   154.2E   21.5S

19.7S   153.3E

22.8S   24.6S

147.9E   153.3E

Table 2-1 gives a listing of the ITPR data, for each channel, obtained during a sample calibration sequence. The three columns for each channel are the raw digital counts, the calibrated radiances ($mw/m^2 - sr - cm^{-1}$) and the equivalent blackbody temperatures (°K). As shown during the housing calibration, the instrument's output is exceptionally stable. However, a peculiarity, which has been noticed throughout the duration of the experiment exists in the space observations. In several channels (e.g. 1, 2, 3, and 7) there is a significant radiance signal when the scan mirror is in the space view position. This signal is diagnosed from the fact that the signal observed as the scan mirror moves out of this position towards earth is lower (a higher digital count value for sample 34) than is observed in the space position. It appears that channels 1, 2, 3, and 7 are the most significantly affected. These channels are at the top of the optical unit. It thus appears reasonable to assume that some material is hanging down from the spacecraft which partially obstructs the fields of view of the upper telescopes when viewing space.

Since channels 1 and 2 occupy the same telescope (i.e., have exactly the same field of view), it is possible to determine from their "space" signals the temperature of the radiating material and percentage of the field of view being obstructed. Assuming the obstructing material is a blackbody, the radiance measured in the space position is given by

$$R(\nu) = \alpha \, B\,(\nu,T) , \qquad (2)$$

where α is the fractional field of view obstruction and $B\,(\nu,T)$ is the Planck radiance. Since channels 1 and 2 occupy the same telescope it follows that

$$\frac{R(1)}{R(2)} = \frac{B(1,T)}{B(2,T)} , \qquad (3)$$

since α is the same for the two channels. It follows from (1) that

$$\frac{B(1,T)}{B(2,T)} = \frac{B(1,T_{BB})}{B(2,T_{BB})} \left[\frac{V_{BB}(2) - V_S(2)}{V_{BB}(1) - V_S(1)}\right] \left[\frac{V(1) - V_S(1)}{V(2) - V_S(2)}\right] , \qquad (4)$$

where V_S is the true space signal. Assuming the true space signal is obtained in sample 34 then the values in Table 2-1 yield

$$\frac{B(1,T)}{B(2,T)} = \frac{.576}{112.3} \left[\frac{155-765}{260-589}\right] \left[\frac{574-589}{741-765}\right] = 5.944 \times 10^{-3} \qquad (5)$$

Table 2 - 1   Counts, Radiances and Blackbody Temperatures for Each ITPR Channel during a Calibration Sequence

JUL DAY 2441916   YEAR 73   AUG 21   NIM DAY 233   HOUR 17   MIN 53   SEC 53   GRID NO. 0

ORBIT 3402   SOURCE 1   NIM FLAG 020010000   GRID CATEGORY 0   MAJ FRAME 0   LIMB DARK 0

LATITUDES FROM 35.0N TO 34.5N   LONGITUDES 999.00 TO 999.00

ITPR IS IN CALIBRATION

	CHAN 1	*	*	CHAN 2	*	*	CHAN 3	*	*	CHAN 4	*	*	CHAN 5	*	*	CHAN 6	*	*	CHAN 7
1	-562	0.000	0.0		0.0	0.0	-630	0.0	0.0	-573	0.0	0.0	-592	0.0	0.0	-587	0.0	0.0	-580	0.0	0.0
2	-570	0.000	0.0		0.0	0.0	-607	0.0	0.0	-595	0.0	0.0	-610	0.0	0.0	-605	0.0	0.0	-598	0.0	0.0
3	-911	0.000	0.0		0.0	0.0	-940	0.0	0.0	-933	0.0	0.0	-960	0.0	0.0	-953	0.0	0.0	-942	0.0	0.0
4	-579	0.000	0.0		0.0	0.0	-597	0.0	0.0	-596	0.0	0.0	-610	0.0	0.0	-605	0.0	0.0	-598	0.0	0.0
5																			-5	0.0	0.0
6	-341	0.000	0.0		0.0	0.0	-394	0.3	0.0	-395	0.3	0.0	-405	0.0	0.0	-401	0.0	0.0	-397	0.0	0.0
7	-562	0.000	0.0		0.0	0.0	-597	0.0	0.0	-579	0.0	0.0	-592	0.0	0.0	-587	0.0	0.0	-580	0.0	0.0
8	-575	0.000	0.0		0.0	0.0	-597	0.0	0.0	-595	0.0	0.0	-610	0.0	0.0	-605	0.0	0.0	-598	0.0	0.0
9	-911	0.000	0.0		0.0	0.0	-940	0.0	0.0	-933	0.0	0.0	-960	0.0	0.0	-953	0.0	0.0	-942	0.0	0.0
10	-579	0.000	0.0		0.0	0.0	-597	0.0	0.0	-596	0.0	0.0	-610	0.0	0.0	-605	0.0	0.0	-598	0.0	0.0
11	255	297.0	112.4		295.0	139	137.9	297.6	151	141.7	297.5	150	144.6	297.5	150	145.0	296.3	121	145.9	297.5
12	260	296.0	112.4		297.0	142	137.2	297.2	152	141.5	297.0	142	144.4	297.0	142	145.6	297.8	121	145.9	297.5
13	263	297.1	112.5		296.0	140	137.6	297.1	151	141.7	297.5	145	144.6	297.7	145	146.0	297.5	121	145.9	297.5
14	257	297.3	112.4		296.0	140	137.6	297.5	151	141.7	297.5	150	144.4	297.7	144	145.6	296.9	121	145.9	297.5
15	263	296.9	112.4		296.9	143	137.0	297.4	150	141.9	297.6	149	144.8	297.8	138	147.4	298.3	121	145.9	297.5
16	261	297.0	112.5		296.9	143	137.0	297.1	162	141.5	297.6	151	144.4	297.6	147	145.6	297.2	121	145.9	297.5
17	253	297.1	112.4		296.0	141	137.0	297.1	151	141.7	297.5	152	144.2	297.5	144	146.2	297.6	121	145.9	297.5
18	262	297.1	112.4		296.0	143	137.0	297.1	151	141.7	297.1	150	144.0	297.7	144	146.4	297.4	121	145.9	297.5
19	253	297.2	112.4		296.0	141	137.6	297.1	151	141.7	297.5	151	144.0	297.6	142	146.4	297.8	121	145.9	297.5
20	256	297.0	112.4		296.0	141	137.4	297.2	153	141.3	297.2	151	144.4	297.6	143	146.4	297.7	121	145.9	297.5
21	262	0.000	0.0		0.0	145	0.0	0.0	191	0.0	0.0	210	0.0	0.0	165	0.0	0.0	132	0.0	0.0
22	28	0.000	0.0		0.0	202	0.0	0.0	337	0.0	0.0	392	0.0	0.0	209	0.0	0.0	247	0.0	0.0
23	24	0.000	0.0		0.0	256	0.0	0.0	332	0.0	0.0	405	0.0	0.0	358	0.0	0.0	184	0.0	0.0
24	25	0.000	0.0		0.0	311	0.0	0.0	695	0.0	0.0	865	0.0	0.0	769	0.0	0.0	309	0.0	0.0
25	384	0.000	0.0		0.0	657	0.0	0.0	811	0.0	0.3	873	0.0	0.0	862	0.0	0.0	764	0.0	0.0
26	573	232.3	159.7		160.7	730	3.6	149.4	822	1.3	126.0	875	1.2	122.5	871	.6	111.1	837	2.4	112.5
27	572	234.0	163.7		163.7	783	2.9	144.5	821	1.3	123.2	877	.8	115.6	873	.2	100.1	836	2.4	113.9
28	577	224.9	168.9		168.8	780	3.6	148.4	823	1.0	123.2	878	.6	112.8	874	.2	84.4	837	2.4	112.5
29	581	203.8	163.7		160.7	783	2.5	141.0	823	1.0	123.2	877	.6	115.6	972	.4	106.9	837	2.4	112.5
30	572	234.4	167.7		163.9	783	2.9	144.5	323	1.3	123.2	878	.6	112.5	869	1.0	118.2	837	2.4	112.5
31	576	227.4	167.7		167.7	783	2.9	144.5	822	1.3	126.0	878	.6	112.5	870	.2	100.1	838	2.4	111.0
32	572	234.0	167.7		167.7	783	2.9	144.5	822	1.3	126.0	877	.8	115.6	870	.8	115.1	837	2.4	112.5
33	571	235.1	167.7		167.7	783	2.9	144.5	822	1.3	126.0	877	.8	115.6	855	1.9	127.2	838	2.2	111.0
34	539	0.000	0.0		0.0	793	.6	123.7	825	.6	126.0	878	.6	112.9	867	1.4	123.1	845	.8	96.1
35	413	0.000	0.0		0.0	597	0.0	0.0	656	0.0	0.0	877	1.9	115.0	660	0.0	0.0	579	0.0	0.0
36	-116	0.000	0.0		0.0	345	0.0	0.0	528	0.0	0.0	546	0.0	0.0	576	0.0	0.0	312	0.0	0.0
37	-186	0.000	0.0		0.0	292	0.0	0.0	501	0.0	0.0	649	0.0	0.0	575	0.0	0.0	236	0.0	0.0
38	-105	0.000	0.0		0.0	299	0.0	0.0	498	0.0	0.0	651	0.0	0.0	574	0.0	0.0	264	0.0	0.0
39	-140	0.000	0.0		0.0	323	0.0	0.0	499	0.0	0.0	651	0.0	0.0	580	0.0	0.0	326	0.0	0.0
40	-148	0.000	0.0		0.0	323	0.0	0.0	505	0.0	0.0	651	0.0	0.0	581	0.0	0.0	327	0.0	0.0

ITPR INTERNAL TEMPERATURES (CELSIUS)

38.2	38.7	37.8	37.8	39.0	37.8	23.9	24.2	24.2	24.0	24.0	25.0	17.6	39.9	31.3
42.6	14.3	37.6	38.0	37.8	38.0	21.6	15.1	19.9	9.5	12.3	25.0	37.5100.0	38.6	15.3
38.2	38.7	37.8	37.9	39.0	38.0	29.2	24.2	23.9	24.0	12.9	28.5	17.7	40.0	32.3
42.6	15.0	37.7	37.6	37.8	38.0	29.3	15.1	21.6	9.5	12.2	28.5	37.5100.0	37.5	15.2
285		513	241	296	385	241	901	365	DIGTL VERIF 0707.3					

NIMBUS ENGINEERING DATA

DIGTL VERIF 0707.3

Figure 2-4 gives the ratio B (1,T)/B (2,T) as a function of temperature. It can be seen from figure 2-4 that the temperature of the obstruction is 29°C. It follows from (2) that the percentage obstruction

$$\alpha = \frac{R(2)}{B(2,29°C)} = \frac{112.6}{121.4} \left[\frac{741-765}{155-765}\right] = 3.6\% \qquad (6)$$

Since portions of the spacecraft are also at 29°C, the calculated values support the assumption that part of the spacecraft (or an attached cable or piece of insulation) is probably contaminating the ITPR's space view. As a result, the instrument output signal obtained in sample 34 as the instrument's scan mirror sweeps down toward earth was assumed to be the "true" space signal and used to calibrate the ITPR data.

2.2 NEMS

2.2.1 Experiment Description

The NEMS experiment was developed primarily to sense the atmospheric temperature profile even through clouds. This is accomplished by detecting the thermal radiation at three frequencies around the 60 GHz oxygen resonance. Simultaneous measurement of the radiation (brightness temperature) is accomplished using three separate microwave radiometer receivers, each having its own antenna and calibration network.

To obtain a set of nearly independent radiation measurements, the frequencies of 53.65, 54.90 and 58.80 GHz were chosen, resulting in a set of weighting functions which peak at approximately 650, 250 and 80 mb, respectively (figure 2-1). By linearly combining the radiation measurements of these frequencies, the vertical temperature profile is constructed.

As shown in figure 2-2, the instrument has a horizontal spatial resolution of 100 n. mi. Although clouds are generally present within the field of view, the oxygen channels are generally insensitive to the clouds. Clouds do not alter the 54.90- and 58.80-GHz brightness temperatures and only infrequently affect the lower-peaking channel at 53.65 GHz, where a maximum attenuation of 3°K has been observed. This result correlates with theoretical considerations, which show less than a 3°K attenuation by a nimbostratus type cloud having 0.10 g/cm^2 of liquid water. Clouds having larger liquid water content generally do not fill the entire 100 n. mi. field of view so that their effects are smaller.
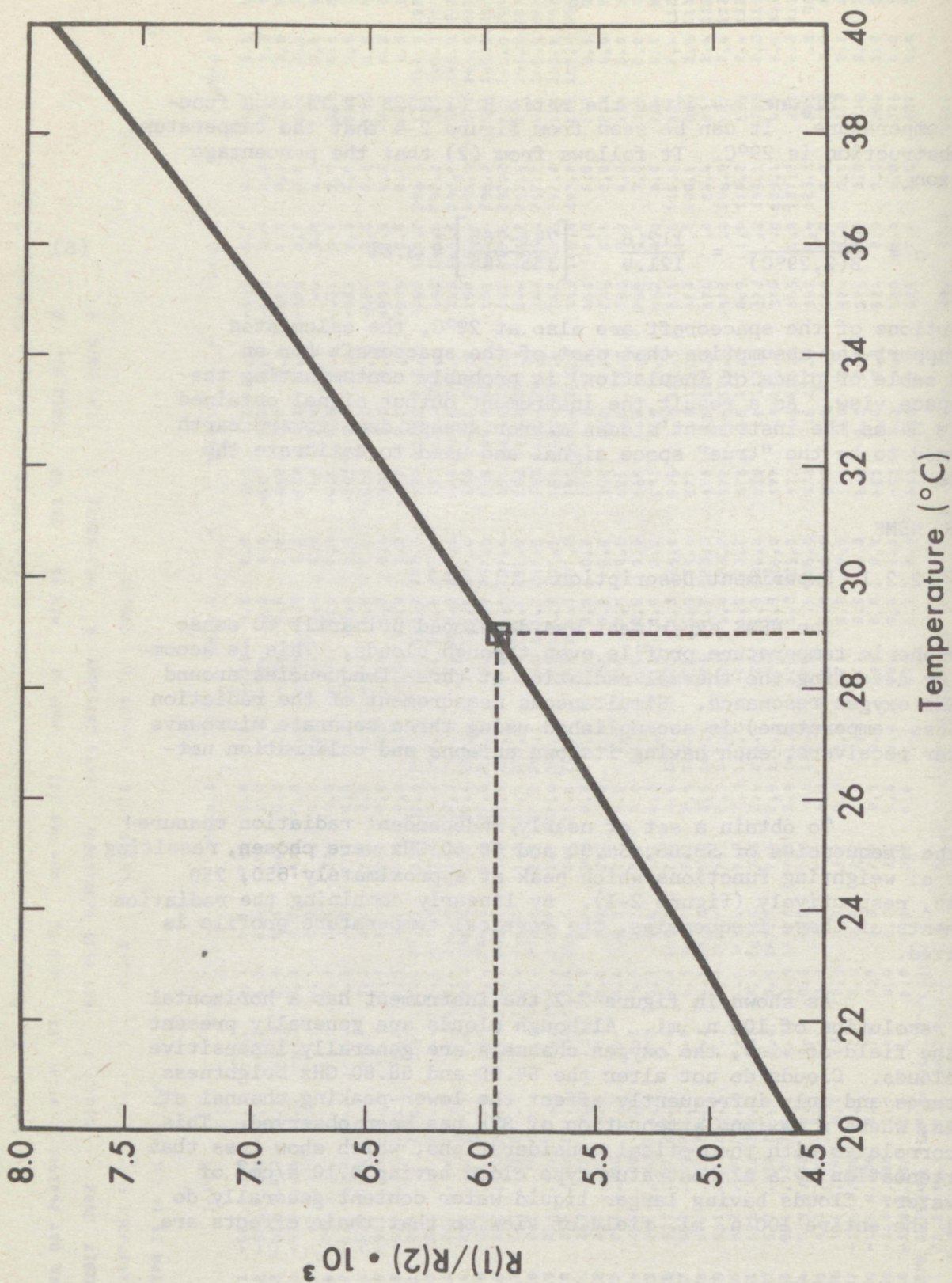
Fig. 2 - 4

Although the 53.65-GHz channel has a weighting function which peaks at about 650 mb, there is some radiation detected by the earth's surface. The surface radiation variation is about 2°K for sea surface and 4°K over land. This variation is approximately accounted for by using nominal sea surface and land emissivities, and reduces the variations to within 1°K.

Instrument noise is a major source of error in the retrieval of vertical temperature profiles derived from measured brightness temperatures. The NEMS measurements are noise limited to within 0.3°K by using a 1.9 second integration time and a band pass of 250 MHz in the R.F. section.

2.2.2 Calibration Procedure

The NEMS instrument consists of 5 separate Dicke type radiometers, each having its own earth viewing antenna. The 5 channels are individually calibrated by switching the input from the antenna position to two "blackbody" temperature sources (cold and warm loads), and linearly relating the output channel response to the monitored input temperatures. Insertion losses in the antenna feed, input waveguide sections, and ferrite switch act as thermal sources (whose temperatures are monitored), and are subtracted out in the calibration procedure. Also included in the instrument's calibration procedure are any variations due to drifts in power supply voltage and crystal mixer currents.

The cold load used in calibration is a space cooled radiator which maintains a temperature of about 217°K with, on the average, less than a 1 percent deviation from its mean value during an orbit. The warm load is maintained at the spacecraft's ambient temperature of about 296°K with the same percent deviation as for the cold load. These two calibration temperatures generally lie outside the range of atmospheric and surface radiation detected by the 5 channels, and enable calibration throughout the instrument's dynamic range.

The instrument is recalibrated after every 224 seconds of earth data to minimize any changes due to variations in power supply voltage, crystal current, and calibration load temperatures. Thus, every 224 seconds a new gain and intercept are computed for the NEMS calibration.

The NEMS instrument normally operates in automatic sequence where the signal (earth viewing) antenna is input to the instrument for 14 VIP*frames, followed by 1 VIP frame of calibration load (cold) and one of base load (warm). This 16 VIP frame sequence is then repeated as long as the instrument is in the normal operating

---

*Versatile Information Processor

mode. During the 14 VIP frames when the signal antenna is input to the instrument, a 100-n. mi. spot is viewed at nadir with measurements of microwave radiation intensities at five frequencies every two seconds.

2.3 SCR

2.3.1 Experiment Description

The Nimbus 5 Selective Chopper Radiometer (SCR) is designed to measure the radiance arising from the earth and atmosphere in 16 discrete spectral intervals. Eight of the intervals (the A and B channels) are centered within the carbon dioxide bands at a wavelength of about 15 µm. These are the primary temperature sounding channels, and give weighting functions with peaks almost uniformly distributed in height from the surface of the earth to a height of about 42 km.

The instrument carries an 11.0-µm window channel (channel C4) and two short wave window channels (channels D3, D4). As a group, these channels effectively determine the earth's surface temperature even in the presence of substantial cloud cover. The short wave window channels (D3, D4) have been chosen to have close response to water vapor, but differ in their response to liquid water or ice. Channels C1 and C2 also show close response for water vapor, but very different response for ice. This pair of channels was designed to detect the presence of cirrus clouds, and to derive some of their physical properties.

Channels D1, D2 (2.69 and 2.62 µm) are in regions of strong atmospheric absorption by carbon dioxide and water vapor, respectively. During daytime they respond to reflected solar radiation from clouds when the cloud tops are above the highly absorbing levels of the lower atmosphere.

The final channel, C3, is centered at 18.3 µm. It is intended to detect emission by water vapor in the short wave wing of the pure rotation band. Table 2-2 summarizes the spectral response characteristics of the SCR.

The four B channels all employ the same multi-layer filter centered at 14.96 µm. This is the wavelength of the main Q branch of the carbon dioxide ν_2 band, which is very strong, but also very narrow spectrally. The weighting function obtained with the filter alone is peaked at about 25 km, and has a half bandwidth (altitude difference between the points at which the weighting function is half its maximum value) of about 25 km. In order to provide weighting functions with narrow half bandwidths and which peak at altitudes in the

TABLE 2-2

Channel Designation	Center cm^{-1}	Width at Half Transmission cm^{-1}	Filter Type	Path Length mm	Pressure CO_2 mb	Total Pressure Including He mb
A1	668.5	9.0	DHW			
A2	688.5	9.0	DHW			
A3	707.4	9.3	DHW			
A4	726.5	12.6	DHW			
B1	668.2	3.4	FP	3	0	13
B2	668.2	3.4	FP	3	40	49
B3	668.2	3.4	FP	3	95	103
B4	668.2	3.4	FP	3	310	325
C1	110*		MESH			
C2	202	18	2nd Order FP MESH			
C3	536.4	13.3	DHW			
C4	859	89	DHW			
D1	3710	72	DHW			
D2	3805	100	DHW			
D3	4260(*10%)					
D4	2817	50	DHW			

* Edge Filter: Number is position of edge.

25 to 42-km range, each B channel has an additional filter which is simply a small carbon dioxide filled cell. For channel B1, the cell is empty. The cell for channel B4 contains the maximum amount of carbon dioxide. Weighting functions for the B channels (also A) are shown in figure 2-5. The weighting functions for differences (e.g., B1-B2) correspond to the difference between the radiances received at the detector after transmission through B1 and B2 separately. The projected fields-of-view have been shown in figure 2-2.

2.3.2 Calibration Procedure

Radiative calibration of the instrument is accomplished by rotating the source selector mirror to view either space or an on-board calibration target at ambient temperature. The source temperature is measured by three independent thermistors, each capable of an accuracy of ± 0.25°K.

NIMBUS-5 Preliminary Weighting Functions

February 7, 1973
C. D. Rogers

A1
B1
B2
B3

B1—B2(=S2)

B2—B3

B3—B4(=S1)
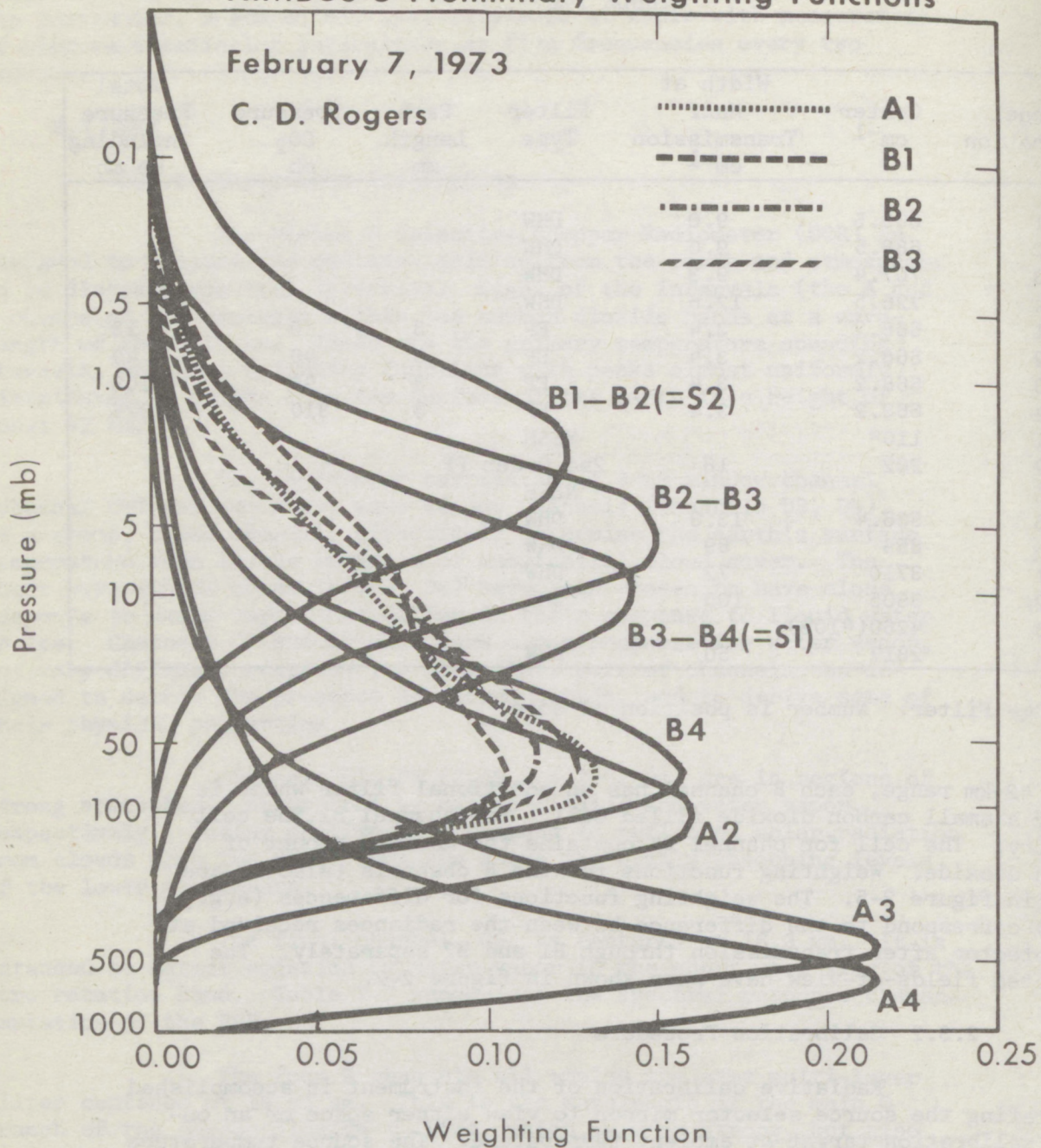
B4

A2

A3

A4

Pressure (mb)

Weighting Function

Fig. 2 - 5

The pyroelectric detector responsivity is temperature dependent. For this reason, the temperatures of the detector unit shrouds are all measured to an accuracy of about ± 0.25°K, and appropriate correction for shroud temperature is made during ground-based processing of the radiometer data.

In the amalgamation of data from the SCR with the NEMS and ITPR, only the upper (difference) B channels of the SCR have been considered. Of the three possibilities, two are currently being studied (i.e., B1-B2 and B3-B4). Their weighting functions are shown in figure 2-1. However, SCR calibrated radiances for all channels are being archived for research purposes.

It should be noted that the procedures described here are those in use at the NESS. They are not identical to those employed by the experimenters in England.

The form of the output from the SCR instrument radiometric channels is a series of samples along a voltage ramp which rises linearly with time. The intensity of the chopped radiation flux incident on the detector is proportional to the slope of the ramp. Five samples at intervals of 200 ms are digitized on board the spacecraft and appear after decoding on the ground as an integer count between 0 and 1023. Offset ramps are generated on the spacecraft and are added onto the signal ramp. The offsets are different in earth and space views, and shall be denoted here by EZ and EZO respectively.

A small local emission is always included in the measured radiance. This is caused partly by the emissivity of the optics between the source and the chopper, and also by the emissivity of objects on the spacecraft seen in the extreme wings of the angular response of the instrument. We shall call these stray radiances r_e, r_s and r_b for the earth, space and internal source views, respectively.

Letting

    RE = Earth radiance
    RB = Internal source radiance (a quantity known through the
         measured source temperature)
    EA = Ramp slope in earth view
    BB = Ramp slope in internal source view
    SP = Ramp slope in space view

and with the assumption that the space radiance is zero, the three equations describing the three possible source selector mirror positions are

$$
\left.
\begin{aligned}
(RE + r_e)\, G &= EA - EZ \\[4pt]
r_s\, G &= SP - EZO \\[4pt]
(RB + r_b)\, G &= BB - EZ
\end{aligned}
\right\}
\qquad (7)
$$

where G is the gain of the radiometer (and would be constant in an ideal system).

By careful design of the apertures in the instrument, the terms r_e, r_s, and r_b were rendered almost equal. From equation (1) we find

$$\left[RE + (r_e - r_s)\right] G = (EA - EZ) - (SP - EZO) \tag{8}$$

$$\left[RB + (r_b - r_s)\right] G = (BB - EZ) - (SP - EZO) \tag{9}$$

Equations (8) and (9) represent the basic calibration equations of the radiometer. During a calibration sequence of nine VIP frames (every 128 major frames), EZ, BB, EZO, SP and again EZ are measured in order. From equation (9) the gain G is then defined, and may be used to define the earth radiance through equation (8).

In practice the gain G is a function both of time and of the temperature of the "detector housing shroud," T_S, of the channel under consideration. Since the temperature dependence is small, and in any case should be unrelated with the time dependence of the gain, we may separate the variables by writing

$$G(t, T_S) = x(t)\, y(T_S) \tag{10}$$

During a calibration G is measured at the prevailing T_S. In the interval to the next acceptable calibration the gain is given by the current T_S ($=T_{SC}$) as

$$G(t, T_{SC}) = x(t)\, y(T_{SC})$$
$$= G(t, T_S)\cdot y(T_{SC})/y(T_S) \tag{11}$$

The function $y(T_S)$ was initially determined in thermal vacuum tests before the satellite was launched and has since been updated from the in-orbit data.

A similar temperature dependence arose with EZ and EZO, and was found to be best correlated with the temperature (T_3) of the thermistor located closest to the zener diode thought to be causing the effect. A similar correction scheme to that for G was used.

Although EZO is also dependent on T_3, it was not necessary to correct EZO, since the quantity always occurs in the calibration equations 8 and 9 as the difference (SP-EZO). It was established in thermal vacuum tests of the radiometer that this quantity is temperature-independent.

The short wave D channels are highly sensitive to sunlight. For this reason it is necessary to reduce the gain of the D channel amplifier when the instrument is observing the sunlit earth. The reduction factors are set by high stability resistors in the amplifier. The D channels are therefore calibrated in the "high amplifier gain" mode; this calibration data is applied to measurements of earth radiance made in either gain mode.

The A and B channels (a total of 8 temperature sounding channels positioned in the 15-μm band of carbon dioxide) all show substantial spectral leakage. Spectral leakage is defined as transmission in a part of the spectrum for which zero transmission had been intended, and which significantly affects the interpretation of the radiance data.

The A channels exhibit spectral leakage at several percent of the intended equivalent width of the filters; for the B channels, the effect is an order of magnitude higher.

The investigators at Oxford University have proposed an empirical correction method for spectral leakage, which involves the strong correlation between calculated leakage radiance and the radiance measured in channel C4. This procedure is now used in the NESS analysis.

For the B-difference channels, there is a built-in resistance to the effect of spectral leakage. The B-difference radiance formed from the radiance observed in channels B1 and B2 (for example) is proportional to the difference in the flux incident on the detector when cell B1 is replaced by cell B2. Since the leakage radiance is mostly outside the spectral regions of carbon dioxide absorption, the leakage flux incident on the detector is almost the same in both cases. The fact that the spectral properties of the cell windows are closely matched ensures that the residual leakage in the B-difference channel is small. In practice, the individual B channels are corrected with the C4 radiance; the difference radiances are then formed as a linear function of the corrected individual radiances:

$$B_{nm} = \lambda_{nm} \; B_n - (\lambda_{nm} - 1) \; B_m \tag{12}$$

The $\lambda(nm)$ are purely functions of the transmission of the carbon dioxide cells

$$\lambda_{nm} = \tau_n / \; (\tau_n - \tau_m) \tag{13}$$

The D channels are all sensitive to sunlight. During daytime calibrations, sunlight is usually scattered into the detector optics, rendering such calibrations useless. On these channels, therefore, only calibrations performed in the earth's umbra are accepted.

A further problem has been the (infrequent) incidence of "moonshine" into the space viewing part. This occurs every month and invalidates the calibration involved over a period of about 2 days. This problem has been overcome by rejecting all space view signals which fall outside pre-set limits.

2.4 THIR

2.4.1 Experiment Description

The THIR is a high resolution scanning radiometer with two channels, one in the 10.5- to 12.5-μm (11.5 μm) window region, the other in the 6.5- to 7.0-μm (6.7 μm) water vapor band. In the Nimbus-5 sounding data processing system, only the 11.5-μm window measurements are utilized.

The radiometer consists of an optical system (comprising a scan mirror, a telescope, and a dichroic beam-splitter) and an electronics module. Incoming radiant energy is detected by means of germanium-immersed thermistor bolometers.

The instrument's field of view and scan geometry are such that essentially full coverage of the earth is obtained. However, in order to simplify the THIR data handling, the sounding data processing system does not make use of the full resolution THIR observations. The THIR swath is divided into six segments, containing equal numbers of earth views. In each segment, the lowest voltage (corresponding to the highest scene brightness temperature) is extracted from the observations in two swaths. Statistical filtering is applied to prevent the inclusion of noise spikes. This processing is done at NASA; the sampled data is then relayed to the sounding data processing center along with the VIP data for the same orbits.

2.4.2 Calibration Procedure

The THIR detectors view, in sequence, the in-flight blackbody calibration target (part of the housing), outer space, earth, space, and again the calibration target. The space and housing views are used in the in-flight calibration of the data, along with the housing temperature, which is monitored by thermistors and telemetered to the ground stations. The THIR output signals are converted to scene radiances using the in-flight calibration data in an identical fashion as the ITPR calibration discussed earlier.

3.0 Atmospheric Transmission Functions

3.1 ITPR

3.1.1 CO_2 and H_2O Channels

Due to the excessive computer time required for "exact" computations by spectral integration of atmospheric transmission in the infrared; simplified band models were developed which permitted rapid computations for the ITPR spectral intervals. The details of these models are given by Davis (1972). Briefly, analytical representations of the atmospheric transmittance for the ITPR channels in select spectral intervals of the rotational band of water vapor and the 15 μm band of carbon dioxide were designed in terms of universal functions of absorber amount, pressure and temperature. Spectral averages of theoretical homogeneous - path transmittances, available by line-computations by R. Drayson (University of Michigan) and H. Bolle (University of Munich) were used as input data. Appropriate coefficients for converting actual non-homogeneous optical paths into equivalent homogeneous paths were derived concurrently with the parameters of each analytical representation. The derived analytical formula and coefficients for computing the atmospheric transmission for the ITPR H_2O and CO_2 channels are also given by Davis (1972) and thus need not be repeated here.

3.1.2 Window Channels (3.7 μm and 11 μm)

The transmission functions for the 3.7-μm and 11-μm window channel regions are assumed to have the following generally accepted exponential forms (McClatchey, 1970):

for the 11 μm window channel;

$$\tau_{Total} = \tau_{H_2O, Lines} \cdot \tau_{H_2O \, Cont.},$$

and for the 3.7-μm window channel;

$$\tau_{Total} = \tau_{H_2O, Lines} \cdot \tau_{CO_2 \, Cont.} \cdot \tau_{N_2 \, Cont.} \cdot \tau_{H_2O \, Cont.}$$

In the above expressions,

$$\tau_{H_2O \, Lines} = \exp \left\{ - \beta \left[\frac{1}{g} \int_o^P PW \left(\frac{T_o}{T} \right)^{1/2} dP \right]^{1/2} \right\} \tag{14}$$

$$\tau_{H_2O \, Cont.} = \exp \left\{ - \frac{k}{0.622g} \int_o^P PW^2 \left(\frac{296}{T} \right)^5 dP \right\} \tag{15}$$

$$\tau_{CO_2 \text{ Cont.}} = \exp \left\{ - C_c \int_0^P \left(\frac{P}{P_o}\right)^{1.75} \left(\frac{T_o}{T}\right) dP \right\} \tag{16}$$

$$\tau_{N_2 \text{ Cont.}} = \exp \left\{ - C_n \int_0^P \left(\frac{P}{P_o}\right)^2 \left(\frac{T_o}{T}\right) dP \right\} \tag{17}$$

where g is the acceleration due to gravity, P is pressure (P_o = 1000 mb), W is water vapor mixing ratio. T is temperature (T_o = 273°K), and the mixing ratios of CO_2 and N_2 (C_c and C_n) are assumed to be constant.

The constants used in these expressions are derived from McClatchey's data and given in the table below:

Channel	β	K	C_c	C_n
3.7 μm	0.035	6	0.33×10^{-4}	0.28×10^{-4}
11 μm	0.05	10	0	0

Experimental vertification of the window channel transmission functions had been obtained at Jackass Flats, Nevada in November of 1972. The transmission measurements were conducted with a spacecraft prototype of the ITPR by viewing the sun as a function of air mass (solar zenith angle). As may be seen in figure 3-1, the adopted models yield transmission values which are generally within 1% of the observational data.

3.2 NEMS

The atmospheric absorption of microwave radiation for clear atmospheric conditions is due to the molecular oxygen and water vapor constituents. Both absorption mechanisms have been treated by Van Vleck in 1945 and comprise the basis for the NEMS transmission functions. The analytical expressions for the oxygen and water vapor transmission functions contained in the work of Barrett and Chung (1962) and Meeks and Lilley (1963) are employed in our calculations of those functions.

3.3 SCR

This description of SCR transmittances is limited to the B channels, since the other channels were not considered in the joint ITPR/NEMS/SCR system.

Jackass Flats, Nevada
November 12, 1972

○ Observed
3.7μm Transmission

△ Observed
11.0μm Transmission

ITPR 3.7μm
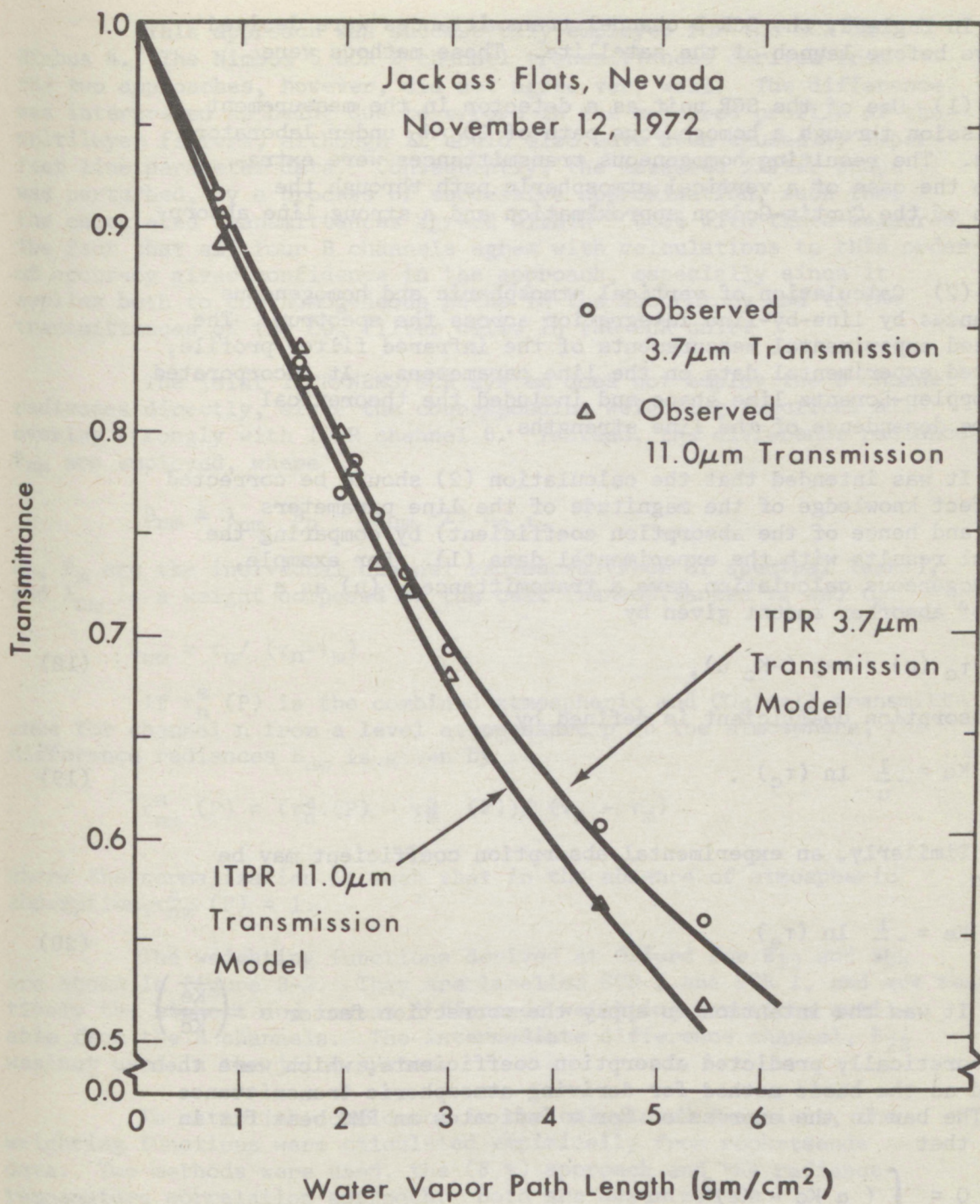Transmission
Model

ITPR 11.0μm
Transmission
Model

Fig. 3 - 1

In England, the SCR B channel transmittances were derived in two ways before launch of the satellite. These methods were

(1) Use of the SCR unit as a detector in the measurement of transmission through a homogeneous path of CO_2/N_2 under laboratory conditions. The resulting homogeneous transmittances were extrapolated to the case of a vertical atmospheric path through the assumption of the Curtis-Godson approximation and a strong line absorption model.

(2) Calculation of vertical atmospheric and homogeneous transmittances by line-by-line integration across the spectrum. The process used experimental measurements of the infrared filter profile, and selected experimental data on the line parameters. It incorporated a mixed Doppler-Lorentz line shape and included the theoretical temperature dependence of the line strengths.

It was intended that the calculation (2) should be corrected for imperfect knowledge of the magnitude of the line parameters employed (and hence of the absorption coefficient) by comparing the theoretical results with the experimental data (1). For example, if the homogeneous calculation gave a transmittance τ (u) as a function of absorber amount given by

$$\tau_c \ (u) = \exp \ (-K_c \ u), \tag{18}$$

then an absorption coefficient is defined by

$$Kc = -\frac{1}{u} \ \ln \ (\tau_c) . \tag{19}$$

Similarly, an experimental absorption coefficient may be defined as

$$Ke = -\frac{1}{u} \ \ln \ (\tau_e) \tag{20}$$

It was the intention to apply the correction factor $\alpha = \left(\overline{\frac{Ke}{Kc}}\right)$

to all theoretically predicted absorption coefficients, which were then to be used as the basic method for deriving atmospheric transmittance curves. The bar in the expression for α indicates an RMS best fit in the sense that

$$Q = \int \ (\ \alpha \ Kc \ - \ Ke)^2 \ du \tag{21}$$

was minimized.

This approach was successfully employed for the SCR on Nimbus 4. The Nimbus 5 SCR B-channel transmittances derived from the two approaches, however, did not agree very well. The difference was interpreted as being due to errors in the measured profile of the multilayer filters, although it could also have been caused by imperfect line parameter data. Consequently, the measured filter shape was perturbed, by a process of successive approximation, such that the calculated transmittances agreed within 0.5% with those measured. The fact that all four B channels agree with calculations to this order of accuracy gives confidence in the approach, especially since it applies both to the homogeneous paths in the laboratory and to the transmittances of the CO_2 filter cells in the SCR unit.

The joint ITPR/NEMS/SCR system does not employ the B channel radiances directly, since the corresponding weighting functions all overlap strongly with ITPR channel 6. Instead, the difference radiances B_{nm} are employed, where

$$B_{nm} = \lambda_{nm} \; B_n - (\lambda_{nm} - 1) \; B_m \; , \tag{22}$$

B_n, B_m are the individual channel radiances (free of spectral leaks), and λ_{nm} is a weight composed of the cell transmittances τ_n and τ_m:

$$\lambda_{nm} = \tau_n / \; (\tau_n - \tau_m) \tag{23}$$

If τ_n^a (P) is the combined atmospheric and CO_2 cell transmittance for channel n from a level at pressure p in the atmosphere, the difference radiances B_{nm} is given by

$$\tau_{nm}^a \; (P) = (\tau_n^a \; (P) - \tau_m^a \; (P))/ \; (\tau_n - \tau_m) \tag{24}$$

where the normalization is such that in the absence of atmospheric absorption, τ_{nm}^a (P) = 1.

The weighting functions derived at Oxford for B_{12} and B_{34} are shown in figure 3-2. They are labelled SCR 2 and SCR 1, and are respectively the highest and lowest difference weighting functions available from the B channels. The intermediate difference channel, B_{23} was not used in the joint system.

To establish confidence in the calculated functions, the weighting functions were calculated empirically from rocketsonde data. Two methods were used, the (β, γ) approach and the radiance-temperature correlation approach. Both are described in section 3.4. Results from the two empirical approaches are shown in figure 3-2, and were derived from over 50 nearly simultaneous rocket/satellite data sets. The criteria for near simultaneity were a latitude-longitude window of ± 4 degrees and a time window of ± 2 hours.
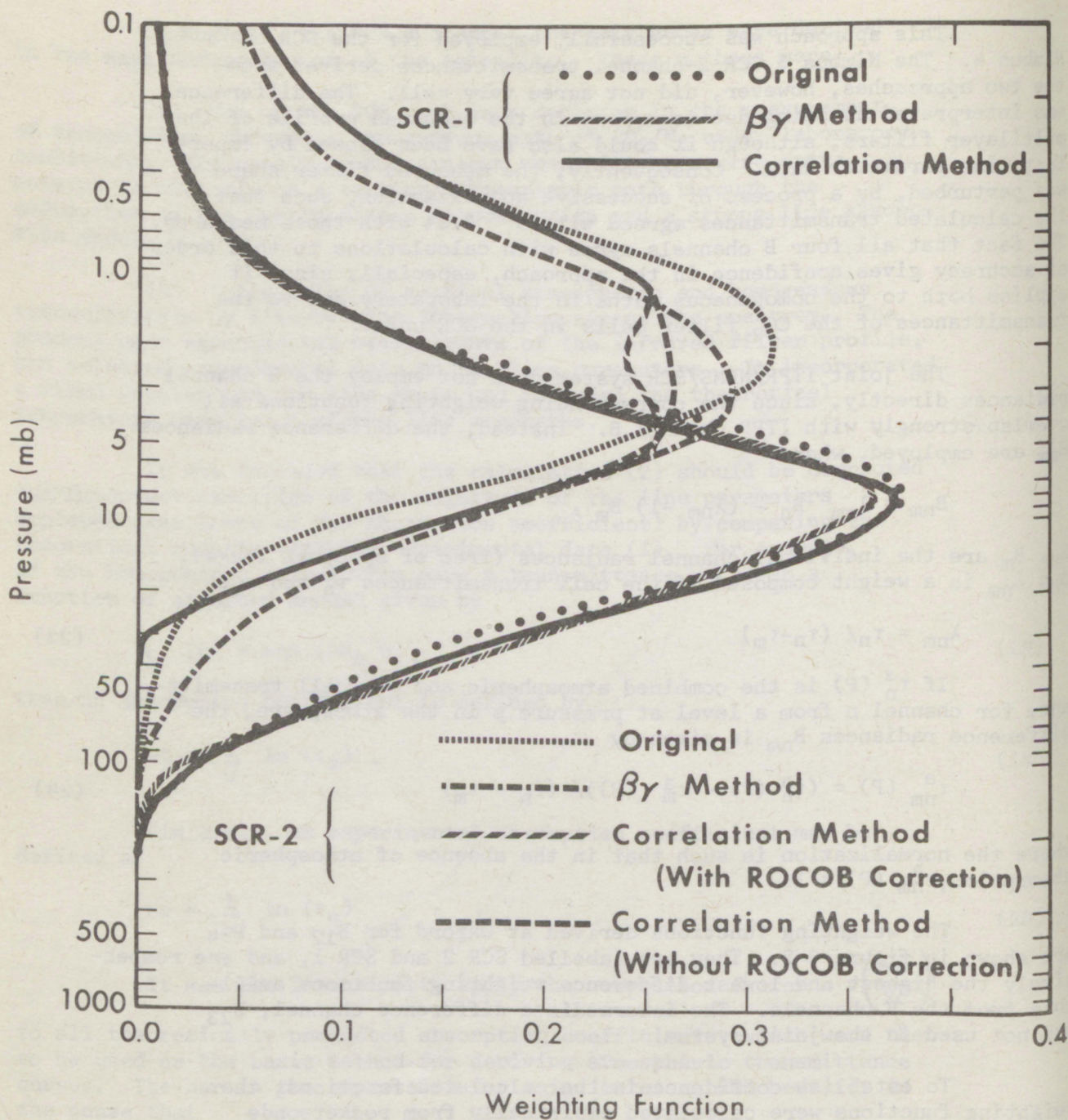
Fig. 3 - 2

The rocket temperature profiles were corrected for dynamical heating and other effects through a standard correction as a function of height.

As a quality check on the data, measured radiances were plotted as a function of calculated radiances, where the calculated radiances were derived from the corrected rocket temperature and the current weighting function. Points which deviated from the best-fit straight line by more than a reasonable amount (judged by eye to be about 1.5 times the RMS of the main body of points) were removed from the sample. Weights were applied to the points remaining such that all measured radiances were approximately equally weighted in the final calculation.

The empirically calculated functions of figure 3-2 agree well for the SCR 1 channel. Both prefer a slight lowering of the weighting function, with little change in shape. The (β,γ) approach is very limited as far as shape changes are concerned, since such changes are contained in the single variable γ. This is to be contrasted with the correlation approach in which the shape changes contain many more independent variables. This difference between the two methods is illustrated in the results for the SCR 2 channel. The (β,γ) approach prefers a lowered weighting function of similar shape to the original. The correlation approach prefers substantial change of shape with a smaller downward movement of the peak of the weighting function.

Another reason for differences between the two approaches is the different sensitivity to noise in the measurements of radiance and of atmospheric temperature. This may account for a substantial part of the behavior of the solutions for SCR 2, since the noise level of the SCR 2 radiances is about twice that of SCR 1, and the rocket-measured temperature profile needs substantial correction above the 1-mb level. To establish which of the SCR 1, SCR 2 weighting functions are more appropriate requires their comparison under operational conditions over time periods of at least several weeks. This has been done for the original as well as the (β,γ) solutions, and the results are presented later in this report.

3.4 Empirical Adjustments to Transmittance Functions

3.4.1 General

As a part of the Nimbus-5 data processing, "coincident" radiosonde and satellite observations have been collected and stored on a history tape. The matched observations serve not only to evaluate temperature determinations but also to obtain estimates of instrumental bias error and empirical transmission function adjustment factors, at least for the more transparent channels. Unfortunately, the limited altitude of radiosonde soundings precludes the use of the history tape

to determine adjustments to the more opaque channels (e.g. SCR-1, SCR-2, ITPR-5, ITPR-6, and NEMS-3). However, for these channels a limited sample of coincident radiosonde-rocketsonde and satellite observations has been obtained with the cooperation of the National Weather Service and Cooperative Meteorological Rocket Network. In order to determine empirical adjustments of theory, it is assumed that the true transmittance function τ is given by

$$\tau = \hat{\tau}^{\gamma} \tag{25}$$

where $\hat{\tau}$ is the theoretically estimated function, and γ is an empirically derived constant. Furthermore, the true radiance is assumed to be given by

$$R = R_m - \beta \tag{26}$$

where R_m is the measured radiance with bias error β. (The bias error β is presumed to exist because of uncertainties in the on-board calibration sources.) It follows that

$$R_m = R(\gamma) + \beta \tag{27}$$

where $R(\gamma)$ is the radiance calculated with the true value of γ. To solve for β and γ it is assumed that $R(\gamma)$ can be expressed by a first order Taylor expansion about some initial estimate γ_0;

$$R(\gamma) = R(\gamma_0) + \frac{\partial R(\gamma)}{\partial \gamma_0} (\gamma - \gamma_0) \tag{28}$$

Substituting eq (28) into eq (27) yields

$$R_m - R(\gamma_0) = \beta_0 + (\gamma - \gamma_0) \frac{\partial R(\gamma_0)}{\partial \gamma} \tag{29}$$

From a sample of matched radiosonde and satellite observations the left-hand side of eq (29) is determined for each pair. Also, for each pair the derivative is approximated by

$$\frac{\partial R(\gamma_0)}{\partial \gamma} = \frac{R(\gamma_0 + 0.1\,\gamma_0) - R(\gamma_0 - 0.1\,\gamma_0)}{0.2\gamma_0} \tag{30}$$

Then from the sample it is straightforward to determine the constants β and $(\gamma - \gamma_0)$ by linear regression. The solution is iterated (i.e., the new value of γ replaces γ_0 in eq (29) and eq (30) in order to account for the non-linearity between R and γ until $(\gamma_n - \gamma_{n-1})/\gamma_{n-1} < .001$, where n refers to the nth iteration.

Matched satellite-radiosonde observations collected on the history tape are subject to three conditions:

(a) The radiosonde must occur within a 2 degree latitude box about the Nimbus sounding location (the centroid of the clear area of an ITPR sounding grid).

(b) The radiosonde must have reached the 100-mb level or higher.

(c) The radiosonde must be within six hours of the Nimbus overpass.

To be considered in a sample for adjusting the transmittance functions of the various sounding channels, somewhat stricter tolerances are imposed:

(d) The radiosonde must have reached the 30-mb level or higher.

(e) The sounding must be within three hours of the radiosonde launch.

(f) The maximum temperature discrepancy between satellite determination and radiosonde must not exceed 15°C.

(g) The sounding must have resulted from "clear-column" radiances.

(h) The horizontal temperature gradient as measured by sub-grid (75 n. mi. scale) departures from the full grid (250 n. mi.) average retrieval must not exceed 2°C at any level up to 100 mb.

(i) The difference between the satellite measured surface temperature and the radiosonde surface temperature must not exceed 10°C.

(j) The difference between calculated and observed radiances for ITPR channels must not exceed 5 percent of the observed radiance.

The collection of adequate data for correcting the transmittance functions of the stratospheric sounding channels was very difficult. After considerable effort a sample of slightly more than 50 coincident satellite, radiosonde/rocketsonde observations were obtained for the period January through April 1973. Since these were obtained manually, no specific spatial window was imposed but soundings in areas with large horizontal gradients were avoided unless the match-up was very close. Only those rocketsondes which agreed with and over-lapped the support rawinsonde and which attained an altitude of 0.3 mb

were considered. A generally accepted dynamic temperature correction
was applied. Final quality control of the sample was achieved by
plotting computed vs. observed radiances and subjectively excluding
any pair which deviated markedly from the general trend.

The quadrature calculation of a radiance from the
radiosonde temperature profile as necessary for the left hand side
of eq (29) requires that the profile extend to 0.2 mb. For the opaque
channel sample this causes no difficulty. In those few cases when
the highest level measured by the rocketsonde was 0.3 mb, the 0.2 mb
value was extrapolated. For the tropospheric channel sample, however,
additional temperature levels must be extrapolated from at least 10 mb
and often 30 mb. These additional levels are computed by regression,
using as independent variables the highest three available mandatory
level temperatures and the radiances measured by channels ITPR-5,
ITPR-6, and SCR-1, SCR-2 (if available). The regression coefficients
are determined from a standard set of 1200 radiosonde/rocketsonde temp-
erature profiles (see appendix) with their computed radiances obtained
from the standard transmittances adjusted by the factors obtained with
the opaque channel sample. The procedure for obtaining the amalgamated
set of transmittance adjustments is shown schematically in figure 3-3.
The final transmittance adjustments can be taken from the transparent
channel sample (so that all channels are compatible) if it is assumed
that the information of the opaque sample is passed through the
regression temperature extrapolation.

The adjustment factors determined from a radiosonde
sample collected from January-April, 1973, are given in table 3-1.

TABLE 3-1

January - April, 1973, Sample Adjustment Factors

Channel	Beta	Gamma
ITPR-3	0.03	0.993
ITPR-4	-0.88	0.986
ITPR-5	1.54	1.495
ITPR-6	3.36	1.024
ITPR-7	1.35	0.756
NEMS-1	3.15	1.236
NEMS-2	-2.52	1.183
NEMS-3	-4.83	1.253
SCR-1	-0.70	1.025
SCR-2	-2.04	0.779

Compute transmittance adjustment factors for
ITPR-5, ITPR-6, NEMS-3, SCR-1, SCR-2
from Radiosonde/Rocketsonde sample

Compute regression coefficients
to predict temperatures at high levels.

Extend quadrature levels of Radiosonde
sample by regression up to 0.2 mb.

Compute transmittance adjustment factors
for all channels from Radiosonde samples

Fig. 3 - 3

One striking feature noted in the table is the large biases, β, which occur with some of the channels when γ is close to unity. For NEMS these are attributable to our use of antenna as opposed to brightness temperatures. (The conversion of antenna temperatures to brightness temperatures requries side lobe contribution corrections which are about the same magnitude of our derived β corrections.) For ITPR-6 the bias is unexplained. Extensive experimentation with the shape of the transmittance function has failed to remove the bias. This is discussed further in section 3.4.2.

A second striking feature in the tables is the large departure of γ from unity for several of the channels. Large deviations are basically undesirable since they imply one of the following: a) the theoretical transmittance function is seriously in error; b) the channel is measuring a layer insensitive to raising or lowering the transmittance function; c) the radiosonde/rocketsonde temperature measurements are not representative of the radiance measurement. For SCR 2 a strong case can be made for the latter especially as a considerable portion of the transmittance function lies above the last quadrature level at 0.2 mb. For NEMS-3 and ITPR-5 the area of greatest suspicion is the second. Computations of the standard deviation and mean difference between measured and calculated radiances as γ is varied from 0.6 to 1.3 reveal that, for NEMS-3 and especially ITPR-5, the minimum in the standard deviation (which essentially determines the correct γ) is very ill-defined. This can be attributed to the fact that the channels are sensing on both sides of the tropopause so that raising or lowering the transmittance function does not materially affect the emitted energy.

In summary, the γ values derived here indicate that theoretical transmittance computations are accurate for all the ITPR CO_2 channels, except for possibly channel 5. On the other hand the theoretical computations for the NEMS oxygen channels are systematically in error. The consistent γ > 1 values indicate the theoretical computations over estimate the transmission of the atmosphere in the 50-60 GHz region. By far the largest discrepancy (deviation of γ from unity) exists for the ITPR 20-μm H_2O channel. The empirically derived γ value indicates that atmospheric water vapor is considerably more transparent to 20-μm radiation than is predictable from theoretical computations. This result has been independently verified by atmospheric transmission function estimates from vertical profile radiance measurements, conducted with a prototype ITPR aboard the NASA CV-990 aircraft, made beneath the Nimbus-5 satellite (Smith, Wydick, Howell, and Pellegrino, 1974). The error in the theoretical computations for this spectral region appears to be due to uncertainties of the continuum coefficients (the e-type and p-type) for this spectral region.

3.4.2 Adjustments to the ITPR Q Branch Channel 6

The original (pre-launch) weighting function for channel 6 is shown in figure 3-4. This function was derived by Davis (1972). As described earlier, his approach employs a combination of random and regular transmission functions to represent the transmission of homogeneous paths. The extrapolation to the condition of atmospheric near-vertical paths is through the Curtis-Godson approximation.

The retrieved temperature profiles from the ITPR-NEMS-SCR system in the early months of 1973 showed significant disagreement with radiosonde and rocket measurements of the temperature profile in the range covered by the original weighting function. In addition, the channel 6 radiances conflicted with those of the SCR 1 channel, whose weighting function overlaps substantially with that of channel 6. The new weighting function (fig. 3-4) gives improved agreement with rocket-based measurements of temperature. The conflict with the SCR 1 radiance is substantially reduced, and should be further resolved with minor modification of the weighting function of either channel.

The technique depends on the correlation between the radiance emitted through the top of the atmosphere with the atmospheric temperature at any pressure level in the atmosphere. A standard correlation function of atmospheric pressure, $Q(p)$, was set up, correlating the measured radiance with rocketsonde observed temperatures for a set of nearly simultaneous satellite-rocket observations. Similar functions $S_n(P)$ were calculated for n models of the channel 6 atmospheric transmission function. The transmission function which produced the highest correlation between $S_n(P)$ and $Q(P)$ was selected as the empirical best fit.

The details of the method are as follows. A set of n atmospheric transmittance functions, $\tau_n(P)$ was calculated through line-by-line integration using the computer program of Drayson. Each transmittance function in the set was calculated from a channel 6 spectral profile within the range of experimental error of the spectral measurements. A set of m rocket-measured temperature profiles, $T_m(P)$, were collected. The corresponding satellite measurements of radiance, R_m, were also noted. Let the correlation function between R_m and $T_m(P)$ be $Q(P)$. This function, at each pressure level P in the atmosphere, is the correlation coefficient between the measured (satellite) radiances and the measured (rocketsonde) temperatures. Similar functions, $S_n(P)$, were calculated for the correlation between calculated radiance (for each $\tau_n(P)$) and measured (rocketsonde) temperature. The calculated radiance is given by

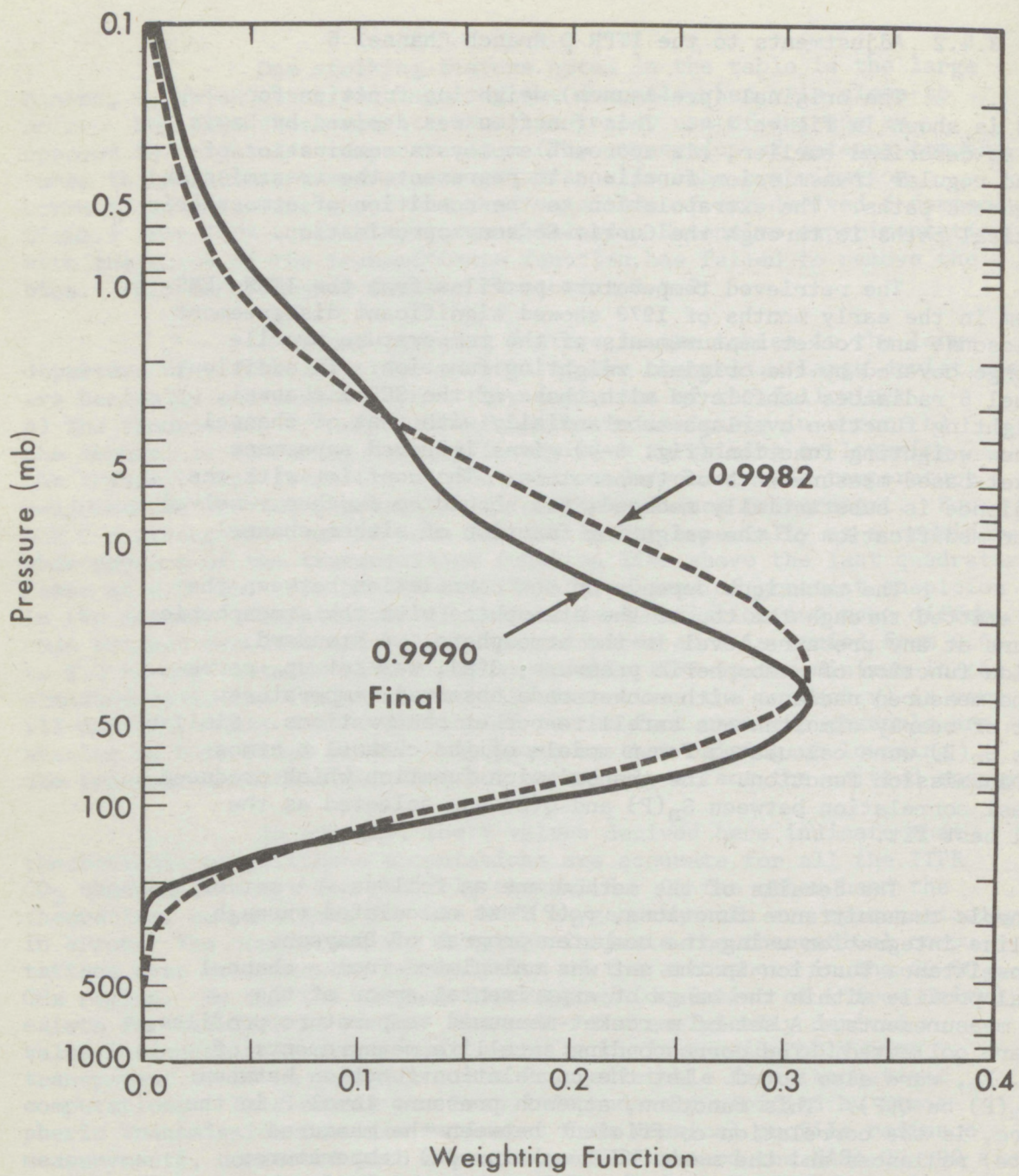$$RC_{m,n} = \int_{P_s}^{O} B(\nu_o, T_m(P)) \frac{d\tau_n(P)}{dp} \, dp \qquad (31)$$

Fig. 3 - 4

where B represents the Planck function at the center ν_o of the filter. P_S represents surface pressure; the boundary term due to surface emission is zero for channel 6, since $\tau(P_S)$ is zero. Equation (31) was approximated for the purposes of this calculation by a sum over the 25 standard ITPR pressure levels. The calculation was simplified by the fact that for channel 6 the $\tau_n(P)$ are virtually independent of temperature profile.

The correlation coefficients x_n were then found between $Q(p)$ and $S_n(p)$. That $\tau_n'(p)$ which had maximum x_n was selected as the best empirical transmittance function of the original set. To further improve the empirical fit, a set of 100 transmission functions was calculated from $\tau_n'(p)$ by the addition of a perturbation term

$$\Delta\tau = a \exp(-b\, p^2)$$

where a was random within a range $\pm a_o$ and $\log_e(b)$ was random within a range ℓ_1 to ℓ_2. This perturbation function has the same general shape as the original transmittance function $\tau_n'(p)$. The constants ℓ_1 and ℓ_2 were chosen to be 0.0 and 5.0, which confines the main effect of the perturbation to the range 0.5 to 20 mb. a_o was initially $\pm .05$. On selection of that $\tau_n''(p)$ from the range n'' = 1 to 100 which gave the highest x_n, a further set of 100 $\tau_n(p)$ was generated, with a_o multiplied by the factor 0.7. A total of 4 similar iterations completed the optimization.

Figure 3-4 shows the result for a relatively small sample of 28 atmospheric profiles. In figure 3-5, several weighting functions are shown together with the corresponding x_n to illustrate the sensitivity of the method. Large departures from the best fit are readily detected, but there is not a high sensitivity (with this sample) to small changes from best fit. The result shown in figure 3-4 is dependent on the atmospheric profile sample size. A 56-sounding sample set analysis showed a more pronounced secondary peak in the 2- to 5-mb range than that of figure 3-4. The sample size dependence is probably a result of the errors present in the temperature and radiance measurements, and the dependence should reduce as the sample size increases. Results will be presented in Part II of this report for a sample size of about 100 profiles.
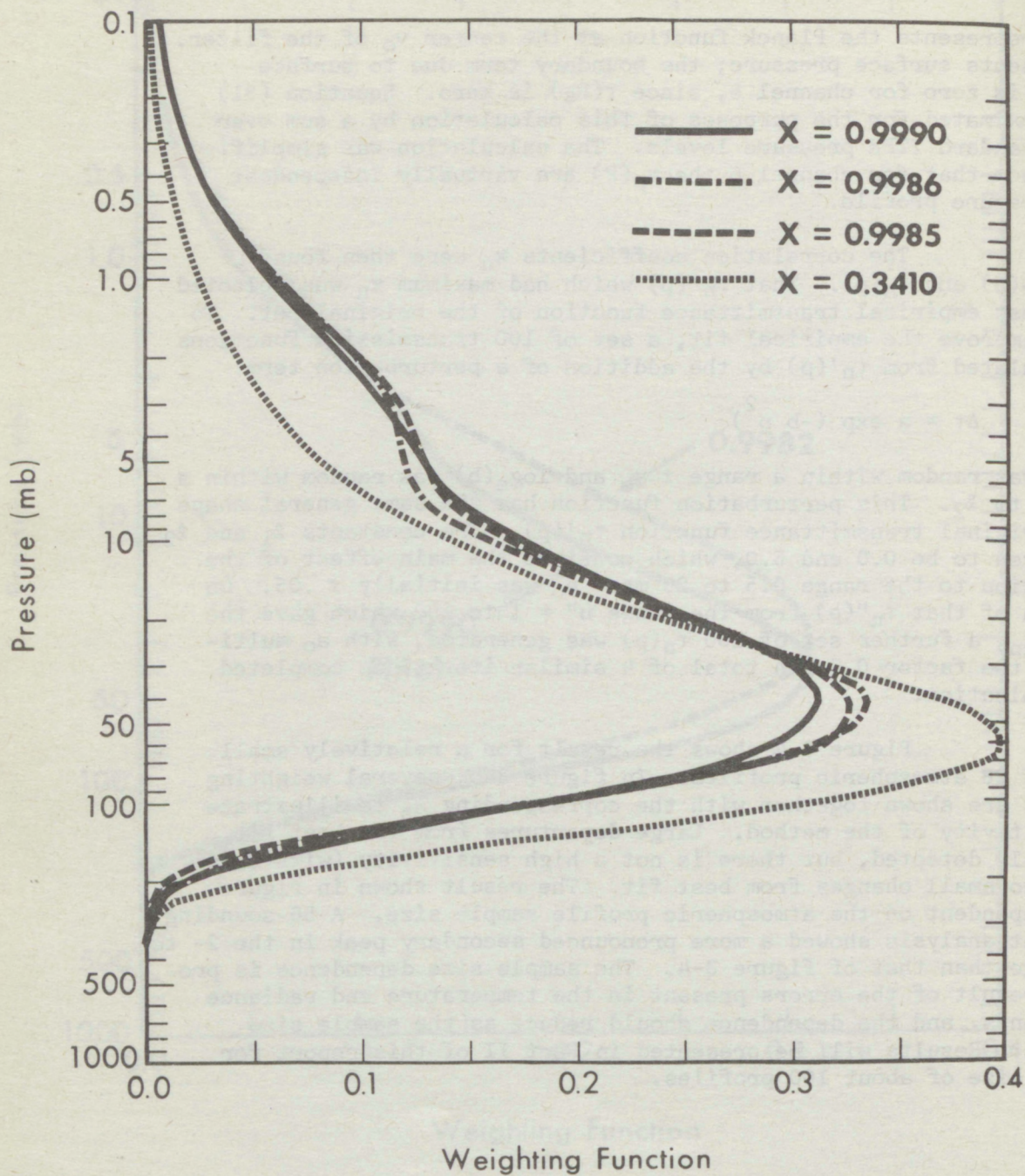
Weighting Function

Fig. 3 - 5

4.0 Determination of Sounding Radiances

4.1 Surface Temperature and Clear-Column Radiance Computation Methods

This section describes the procedure used to specify surface temperature and clear column radiances from the Nimbus-5 ITPR measurements. Simultaneous 3.7-μm and 11-μm window observations are utilized to filter erroneous clear-column radiance determinations due to varying cloud properties (i.e., heights, opacities, etc.) as well as to determine the surface temperatures. Numerous "valid" determinations are averaged in order to reduce the cloud-induced noise to a tolerable level for accurate temperature retrievals down to the earth's surface.

4.1.1 Preliminary Data Processing

4.1.1.1 Angular Correction Model for ITPR Radiance Measurements

The ITPR measures the spatial distribution of upwelling radiance by viewing 20 different nadir angles. Before the data can be used to compute atmospheric parameters, it is necessary to account for the radiance variations of the observations due solely to variations in the nadir angle of the observation.

We desire corrections which will normalize the radiance observed at nadir angle θ to the value which would have been observed at nadir angle 0°. The vector of corrections $\vec{R}'(\theta)$, in which each vector element denotes a different measurement frequency, is given by

$$\vec{R}'(\theta) = \vec{R}(0) - \vec{R}(\theta) = [\underline{W}(0) - \underline{W}(\theta)] \cdot \vec{B} = \underline{W}'(\theta)\,\vec{B} \tag{33}$$

where $W'(\theta)$ is the matrix of transmittance (weighting) functions (an element for each frequency and level) and $\vec{B}$ is a vector of Planck radiances (an element for each level). Assuming a linear relationship between the B profile and the radiance measurements; i.e.,

$$\vec{B} = \underline{A}(\theta) \cdot \vec{R}(\theta) \tag{34}$$

where $\underline{A}(\theta)$ is a regression matrix. It then follows that

$$\vec{R}'(0) = \underline{W}'(\theta)\ \underline{A}(\theta)\ \vec{R}(\theta) \tag{35}$$

or

$$\vec{R}'(0) = \underline{C}(\theta)\,\vec{R}(\theta). \tag{36}$$

Equation (36) states that the correction for angle can be estimated from a linear combination of the radiances. Consequently, given a statistical sample of radiances (in practice synthetic ones are used) the coefficients (i.e., the elements of $\underline{C}$) can be estimated by linear regression. The final model for the angular correction to the radiance in the ith spectral interval at the jth angle is

$$R'_{i,j} = C_{i,j,o} + \sum_{k=2}^{7} C_{i,j,k}\ R_{j,k} \quad \begin{array}{l} i=1,2,\ldots,7 \\ j=1,2,\ldots,20 \end{array} \tag{37}$$

where k denotes the radiance channel number. (In applying the coeffi-
cients of equation (37), the radiances are normalized to the ITPR
reference frequency of 714.8 cm^{-1}.)

For the ITPR window channels, the regression
procedure is used to normalize the radiance values to the radiance
observed for zero molecular absorption at nadir angle zero. Conse-
quently, the derived regression equations are used to correct the
window channel observations for all molecular absorption as well as
angular dependencies.

The standard errors (mw/m^2-sr-cm^{-1}), explained
variances, and coefficients determined from a statistical sample of
2040 atmospheres (120 different soundings in which clouds were assumed
to exist at the 200-, 300-, 500-, and 700-mb levels in addition to the
cloudless case) are given in table 7-2. The standard error of the radi-
ance measurements was assumed to be 0.15 for channels 2-7 and 0.003 for
channel 1 in generating the regression matrices. As may be seen, the
standard error of the limb correction regression is well below the
measurement noise level, even for the largest zenith angle of 42.5°.
Finally, figures 4-1, 4-2, 4-3, and 4-4 show the angular corrections for
the seven ITPR channels resulting from an application of the angular
correction regression model to statistically independent tropical and
polar model temperature profiles for cloudless and high cloud situations.
As may be seen, the prediction of the vertically propagating radiance
from off-nadir observations is near perfect in all cases. As a conse-
quence, this approach is used to correct the 3.7-µm and 11-µm channels
for molecular absorption and to normalize all the ITPR radiance observa-
tions with respect to zero nadir angle to facilitate accurate computations
of clear-column radiance.

4.1.1.2 Modeling of Reflected Solar Radiation for ITPR Channel 1 (3.7-µm Window)

In the processing of ITPR 3.7-µm channel
data, it is necessary to consider the limits of surface reflected solar
radiation under a cloudless atmospheric condition. Neglecting atmos-
pheric scattering processes, the solar radiation transfer can be
summarized by the diagram below.

15N (Clear)

Ch. 3
Ch. 4
Ch. 5
Ch. 6
Ch. 7

- - - - $R(0) - R(\theta)$
⊙ ⊙ ⊙ $R(0) - R(0)$

ΔR

θ

Fig. 4 - 1

15N Cloudy (Cloud P = 200 mb)

Ch. 3

Ch. 4

Ch. 5

Ch. 6

Legend:
- - - - R (0) − R (θ)
⊙ ⊙ ⊙ R (0) − R (0)

Ch. 7

θ

Fig. 4 - 2

75N (July) Clear

Ch. 3

Ch. 4

CH. 4

Ch. 5

Ch. 6

— — — R (0) − R (θ)

⊙ ⊙ ⊙ R (0) − R (0)

Ch. 7

ΔR

θ

0   10   20   30   40

Fig. 4 - 3

75N (July)   Cloudy (Cloud P. = 300 mb)

Ch. 3

Ch. 4

Ch. 5

Ch. 6

R (0) − R (ℓ)

⊙ ⊙ ⊙   R (0) − R (0)

Ch. 7

ΔR

θ
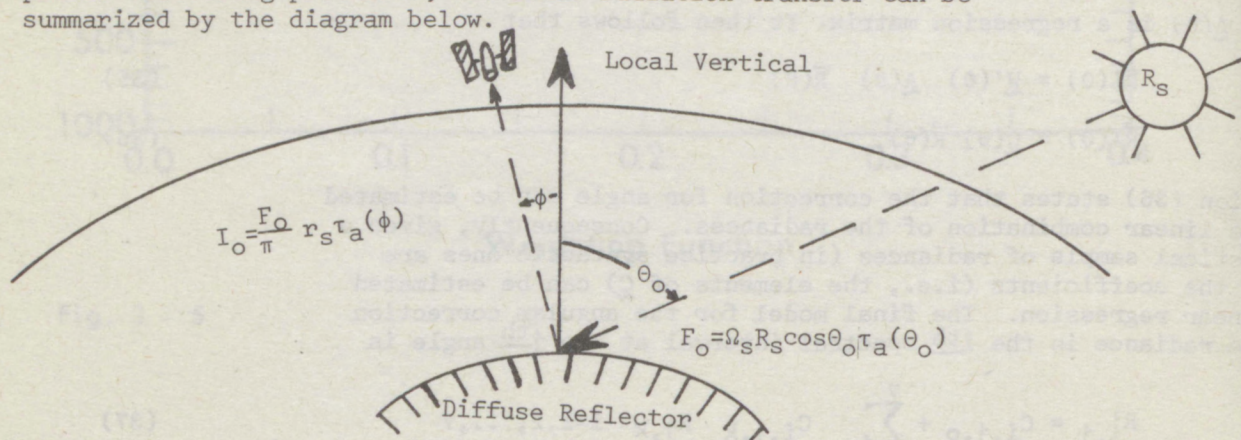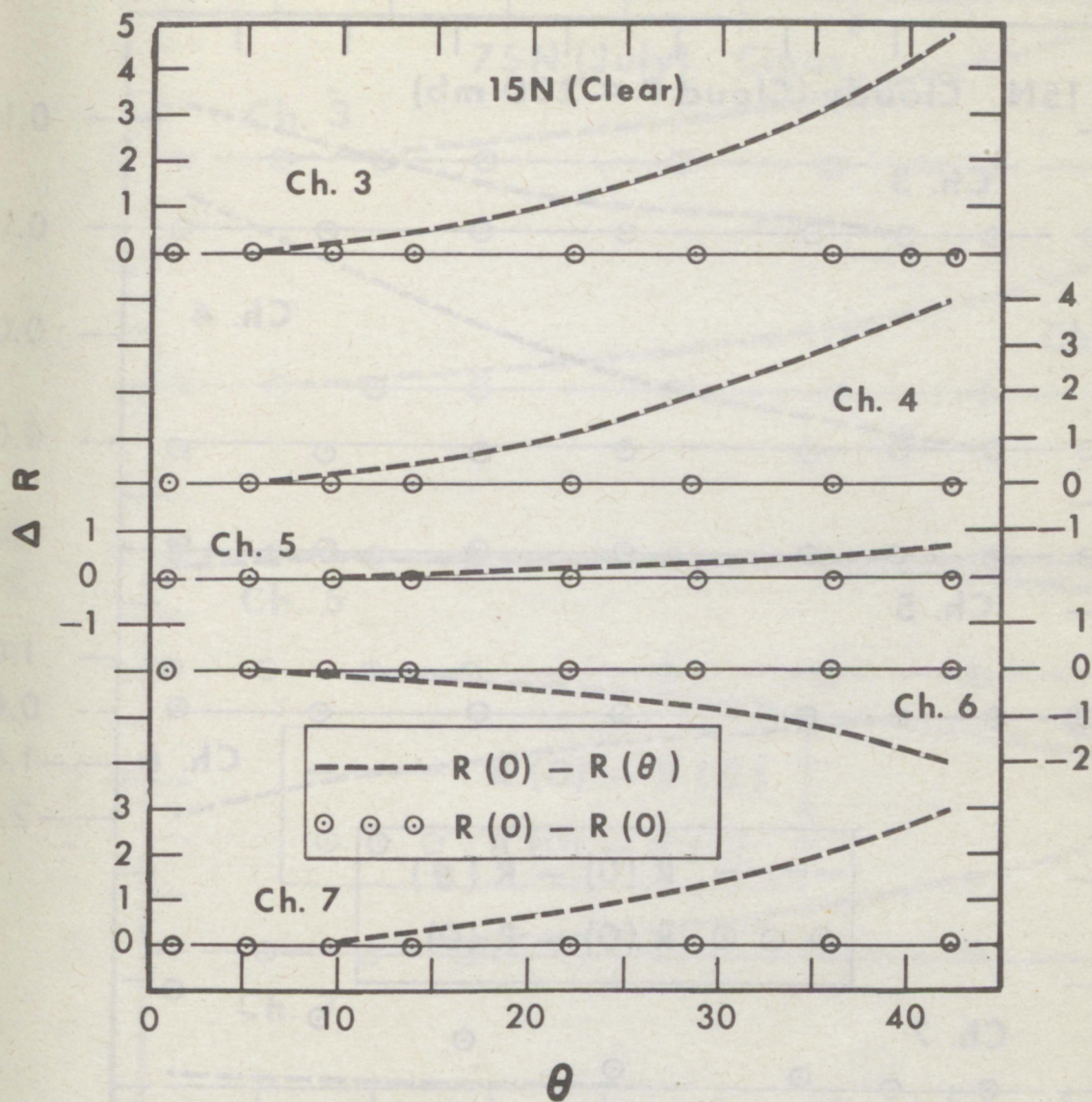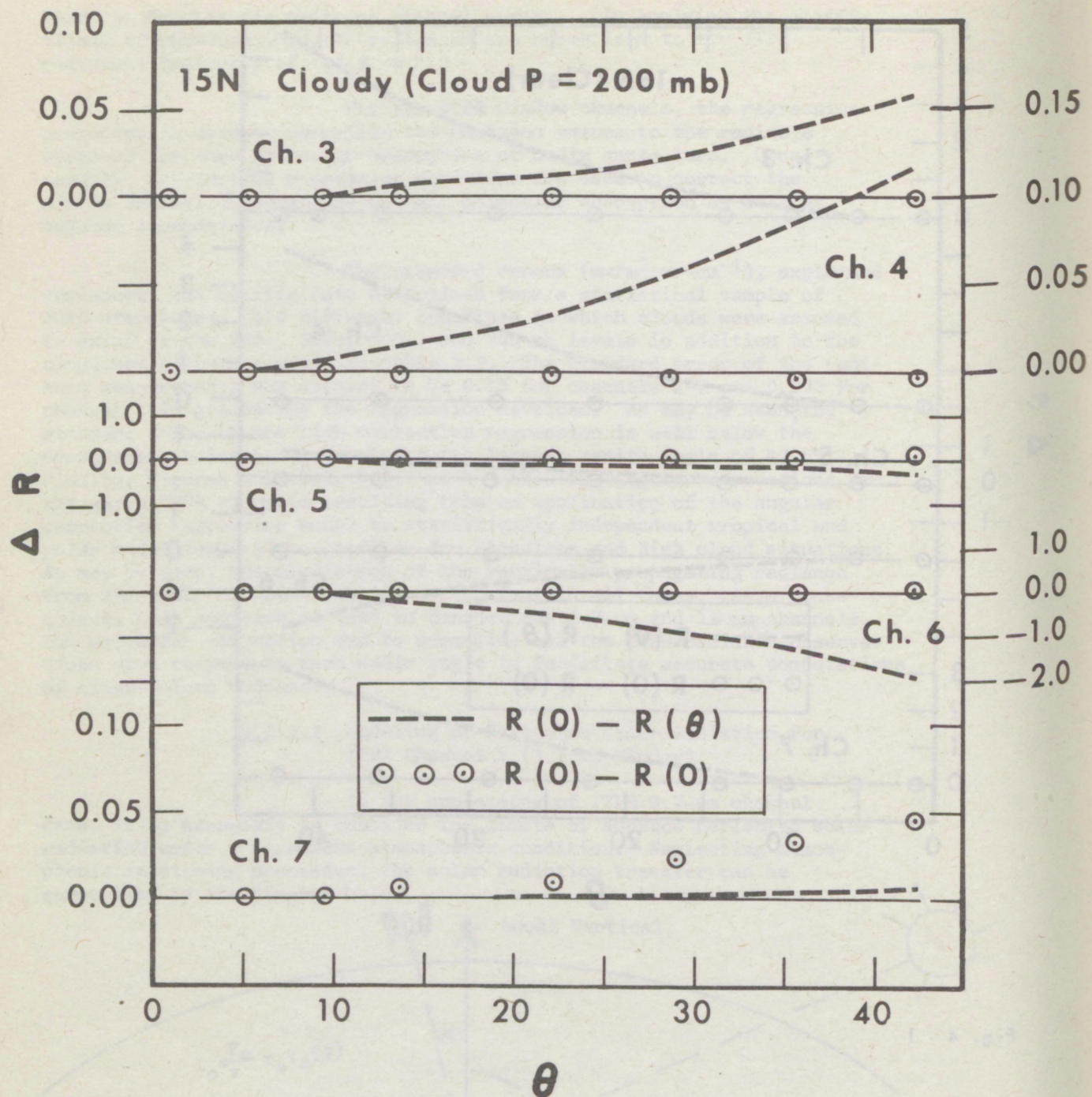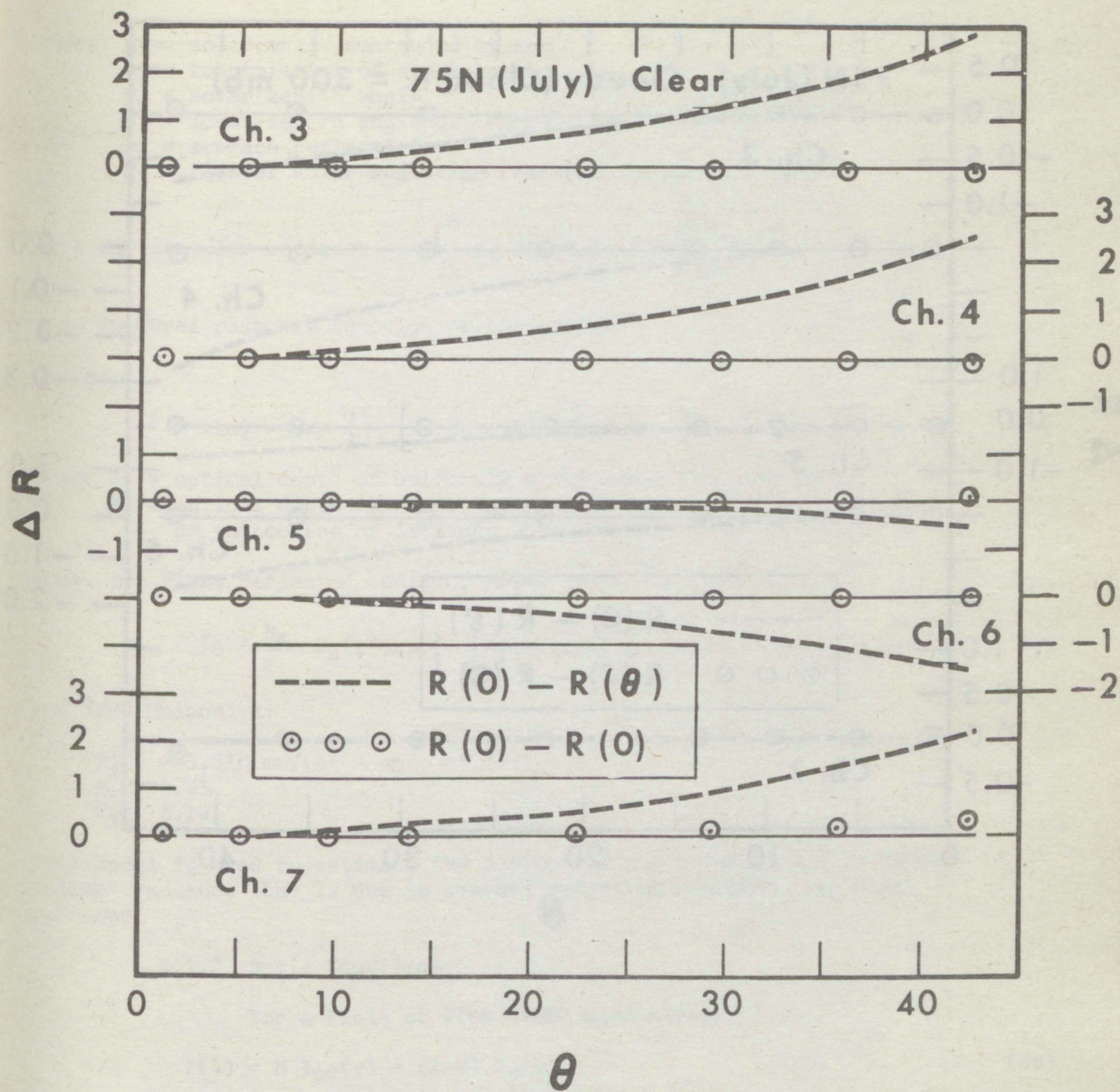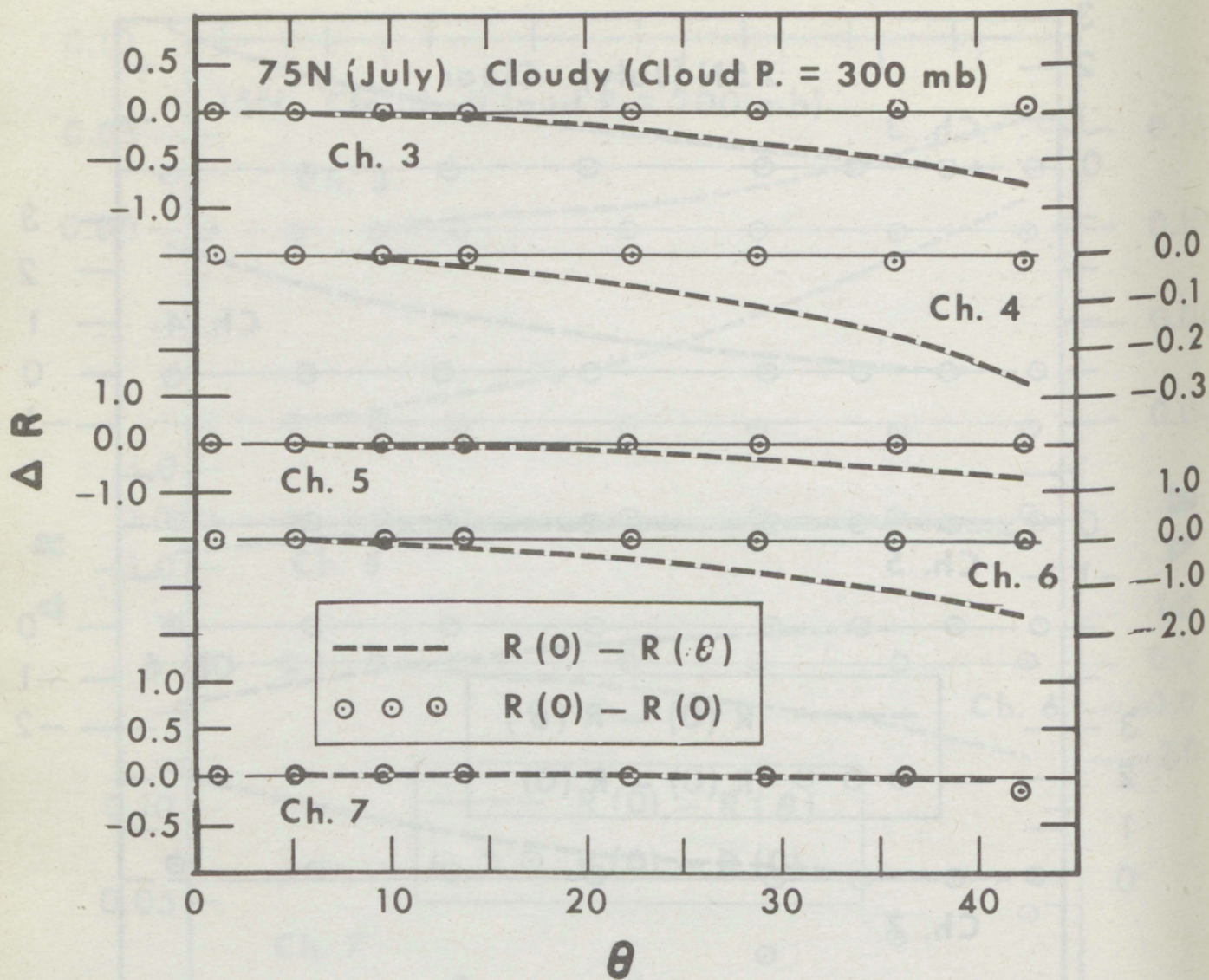
Fig. 4 - 4

where; Ω_S = solid angle subtended by sun

τ_a = transmission of atmosphere

Θ_o = solar zenith angle

ϕ = local zenith angle of emerging ray

r_s = surface reflectivity

F_o = flux of solar radiation reaching the earth's surface

$$R_S = \text{Direct solar radiance} = \int_0^\infty \phi_\nu \, B[\nu, T_S(\nu)] \, d \left/ \int_0^\infty \phi_\nu \, d\nu \right.$$

ϕ_ν = Spectral response function of the channel

Assume;

$$\tau(\alpha) = \exp \left\{ - \left[K_1 + K_2 \cos(\text{lat}) \right] \sec \alpha \right\} \tag{38}$$

where K_1 = optical depth of uniformly mixed gases (CO_2 and N_2O)

K_2 = optical depth of water vapor which is modelled as a function of the cosine of latitude

Thus, the final reflected sunlight model takes the form

$$I_O = \frac{R_S}{\pi} \, \Omega_S(t) \exp \left\{ - \left[K_1 + K_2 \cos(L) \right] \left[\sec\theta_o + \sec\phi \right] \right\} r_S \cos\theta_o \tag{39}$$

For ITPR Channel-1:

R_S = 243,310 mw/(m^2 - sr - cm^{-1})

K_1 = 0.05

K_2 = 0.14

This model is used to estimate the portion of the observed 3.7-μm "clear-column" radiance that is due to surface reflected sunlight (see next section).

4.1.2 Basic Equations

For a Field of View (FOV) with clouds,

$$I(\nu) = N \, I_{cd}(\nu) + (1-N) \, I_c(\nu), \tag{40}$$

where $I(\nu)$ is the observation, N is the fraction of the field covered by clouds, $I_{cd}(\nu)$ is the average radiance from the cloud covered portions of the field of view, and I_c is the average radiance from cloud free portions of the field. Assuming a field of view sufficiently small (e.g., 15 n. mi. for ITPR) so that no more than a single layer of clouds exist in the field,

$$I_{cd}(\nu)=I_u(\nu,p_c,0)+r_c(\nu)I_d(\nu,p_c,0)\tau(\nu,p_c,0)+\tau_c(\nu)I_u(\nu,p_c,p_s)\tau(\nu,p_c,0) \qquad (41)$$

where p_c is the pressure of the cloud layer, and r_c, ε_c, and τ_c are the reflectivity, emissivity, and transmissivity of the clouds, respectively, and are related to each other by Kirchoff's law ($\tau_c+\varepsilon_c+r_c=1.0$). The term $I_u(\nu,p_c,0)$ is the upward radiance emitted at the frequency ν by the cloud and the atmosphere above the cloud. $I_d(\nu,p_c,0)$ is the downward component of the radiance at the cloud level. $I_u(\nu,p_c,p_s)$ is the upward component of the radiance at the cloud base, and $\tau(\nu,p_c,0)$ is the transmittance of the atmosphere between the cloud pressure level p_c and the top of the atmosphere $p=0$. In writing eq (41) it is assumed that the cloud has infinitesimal thickness such that its pressure is some effective value.

The clear column radiance $I_c(\nu)$ is given by

$$I_c(\nu) = I_u(\nu,p_s,0) + r_s(\nu)\, I_d(\nu,p_s,0)\tau(\nu,p_s,0) \qquad (42)$$

where p_s is the surface pressure, r_s and ε_s are the surface reflectivity and surface emissivity ($r_s+\varepsilon_s=1.0$), the term $I_u(\nu,p_s,0)$ is the upward radiance emitted by the surface and atmosphere, $I_d(\nu,p_s,0)$ is the downward component of radiance at the surface, and $\tau(\nu,p_s,0)$ is the transmittance of the atmosphere.

It is noted that equation (40) holds for spectral regions where reflected sunlight contributes to the outgoing radiance as long as the clouds do not cast any shadows over the cloudless air columns.

For spectral absorption bands beyond 6 μm (e.g., the 15-μm CO_2 and 20-μm H_2O channels) the earth and cloud reflected sky and solar radiation is negligible compared to the infrared emission, and the earth's surface can be assumed to be a blackbody (i.e., $\varepsilon_s(\nu)=1.0$). Thus for the cloud components

$$I_u(\nu,p_c,0)=\int_0^{p_c} B[\nu,T(p)]\, \frac{d\tau(\nu,0p)}{dp}\, dp + B[\nu,T(p_c)]\, \varepsilon_c(\nu)\tau(\nu,p_c,0), \qquad (43)$$

$$r_c(\nu)\, I_d(\nu,p_c,0)\tau(\nu,p_c,0) = 0, \text{ and} \qquad (44)$$

$$I_u(\nu,p_c,p_s) = \int_{p_c}^{p_s} B[\nu,T(p)]\, \frac{d\tau(\nu,p_c,p)}{dp}\, dp + B[\nu,T(p_s)]\tau(\nu,p_c,p_s). \qquad (45)$$

And for the clear components,

$$I_u(\nu,p_s,0)=\int_0^{p_s} B[\nu,T(p)]\, \frac{d\tau(\nu,0,p)}{dp}\, dp + B[\nu,T(p_s)]\tau(\nu,0,p_s), \text{ and} \qquad (46)$$

$$r_s(\nu) \, I_d(\nu,p_S,0)\tau(\nu,p_S,0) = 0. \tag{47}$$

For atmospheric window regions, the atmospheric transmittance is near unity. However, the reflected cloud and surface components of solar radiation for the short wavelength window regions $\lambda < 4.0$ μm cannot be neglected. Also, at 11 μm the surface emissivity is near unity for most surfaces. Denoting short wavelength window regions as W_S and long wavelength window regions as W_L, then

$$\tau(W_S,p_1,p_2) = \tau(W_L,p_1,p_2) = 1.0, \tag{48}$$

$$I_u(W_S,p_C,0) = B\left[W_S,T(p_C)\right] \varepsilon_C (W_S,p_C), \tag{49a}$$

$$I_u(W_L,p_C,0) = B\left[W_L,T(p_C)\right] \varepsilon_C (W_L,p_C), \tag{49b}$$

$$I_d(W_S,p_C,0) = I_0(W_S) \, \mu_0, \tag{50a}$$

$$I_d(W_L,p_C,0) = 0 , \tag{50b}$$

$$I_u(W_S,p_C,p_S) = I_0(W_S) \, \mu_0 \, \tau_C \, (W_S)r_s(W_S) + \varepsilon_s(W_S) \, B\left[W_S,T(p_S)\right], \tag{51a}$$

$$I_u(W_L,p_C,p_S) = B\left[W_L,T(p_S)\right], \tag{51b}$$

$$I_u(W_S,p_S,0) = \varepsilon_s(W_S) \, B\left[W_S,T(p_S)\right], \tag{52a}$$

$$I_u(W_L,p_S,0) = B\left[W_L,T(p_S)\right], \tag{52b}$$

$$I_d(W_S,p_S,0) = I_0(W_S) \, \mu_0, \tag{53a}$$

$$I_d(W_L,p_S,0) = 0, \text{ and} \tag{53b}$$

$$I_0(W) = \frac{B[W,T^S]}{\pi} \, \Omega_S, \tag{54}$$

where T^S is the brightness temperature of the sun, Ω_S is the solid angle subtended by the sun, and μ_0 is $\cos(\theta)$, where θ is the solar zenith angle for $\theta < 90$, and zero for night conditions ($\theta > 90$). Substituting eq (48)-(51) into (41) and (42), equation (40) for the window regions becomes

$$I(W_S) = \varepsilon_s(W_S) \, B\left[W_S,T(p_S)\right] + r_s(W_S)I_0(W_S)\mu_0$$

$$+ N \left\{ B\left[W_S,T(p_C)\right] \varepsilon_C(W_S,p_C) + \left[r_c(W_S)r_s(W_S)\right] \, I_0(W_S)\mu_0 \right. \tag{55}$$

$$\left. - 1-\tau_C(W_S) \, \varepsilon_s(W_S) \, B\left[W_S,T(p_S)\right] + \tau_C^2 \, (W_S)r_s(W_S)I_0(W_S)\mu_0 \right\}, \text{ and}$$

$$I(W_L) = B\left[W_L,T(p_S)\right] + N\left\{B\left[W_L,T(p_C)\right] \varepsilon_C(W_L,p_C)\right.$$

$$\left. + \left[1-\tau_C(W_L)\right] B\left[W_L,T(p_S)\right]\right\}. \tag{56}$$

4.1.3 Surface Temperature Guess Generation

The specification of clear-column radiances and consequent temperature and moisture profiles to the Earth's surface requires knowledge of the Earth's surface temperature.

In the Nimbus-5 data processing, an initial estimate of the surface temperature is obtained from the 24-hour old day or night NIMBUS-derived surface temperature analysis (see section 6). This surface temperature estimate, denoted as $T_o^{(1)}(p_S)$, will be considered to be within an error α of the actual surface temperature. α is itself a function of temperature, varying from 2°C at 270°K or below, to 7°C at 330°K or above.

In addition, within each NIMBUS data grid, as shown in figure 4-5, are sixty-four 11-μm window radiance maxima provided by the THIR 4 n. mi. resolution radiometer. A second estimate of the surface temperature $T_o^{(2)}(p_S)$ is derived from the average of all THIR radiances within a grid, which, after being corrected for molecular absorption, have associated brightness temperatures which are within 2.0°C of the maximum THIR brightness temperature observed within the grid.

If $T_o^{(2)}(p_S) \geq T_o^{(1)}(p_S) - \alpha$°C, then $T_o^{(2)}(p_S)$ is adopted as the final surface temperature guess, $T_o(p_S)$, and is assumed to be within an error β, of $\pm$ 2.0°C of the actual surface temperature at any location within the grid. If $T_o^{(2)}(p_S) < T_o^{(1)}(p_S) - 4$°C then $T_o^{(1)}(p_S)$ is adopted as the final surface guess, $T_o(p_S)$, and is assumed to be within an error, β, of $\pm$ α of the actual surface temperature at any location within the scan grid.

4.1.4 Surface Reflectivity, Surface Temperature and Clear Column Radiance Retrieval (From Sounder Data) Equations

(a) Surface Reflectivity Equation

Before the surface temperature can be retrieved from the 3.7-μm and 11.0-μm window observations when broken clouds exist within the FOV, the surface reflectivity must be known. This, when possible, is obtained from any cloudless ITPR fields of view within the scan grid. It follows from (55) and (56) that, if no clouds exist within the field of view,

$$I(W_S) = I_C(W_S) = \varepsilon_S B\left[W_S,T(p_S)\right] + r_S(W_S)I_o(W_S)\mu_o, \text{ and} \tag{57}$$

Radiance Measurement Distribution in Grids 1 thru 5

NIMBUS - E
Orbital Track

135 n. m.

5

4

53.6 n. m

3

193 n. m.

2

1

325 n. m.

Location Range

Chan. B (6 per grid) (40 n.m.)

SCR F.O.V. - 2,3,4

Chan. A,C,D { (15 n.m.) (16 per grid) }

THIR F.O.V. (4 n.m.) (64/every grid)

ITPR F.O.V. (15 n.m.) (140 per grid - 1, 3, 5)

2 NEMS FOV's (108n.m.) (2 per grid - 2, 3, 4)
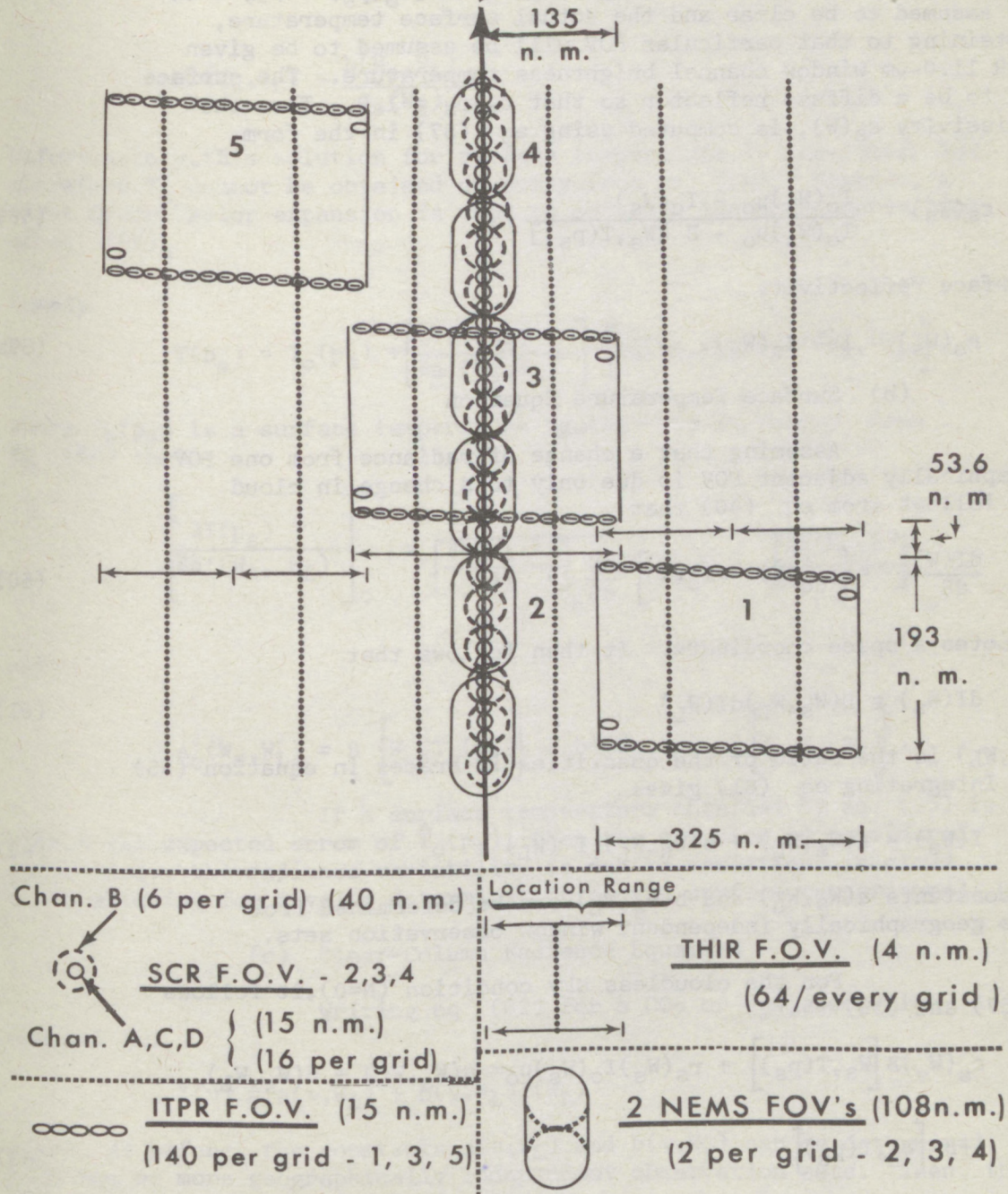
Fig. 4 - 5

$$I(W_L) = I_c(W_L) = B\left[W_L, T(p_S)\right] . \tag{58}$$

Thus, if the 11.0-μm window channel brightness temperature (after making appropriate molecular corrections) is greater than $[T_o(p_S) - \beta]$, then the FOV is assumed to be clear and the actual surface temperature, $T(p_S)$, pertaining to that particular FOV will be assumed to be given by the ITPR 11.0-μm window channel brightness temperature. The surface is assumed to be a diffuse reflector so that $\varepsilon_S + r_S = 1.0$. Then the surface emissivity $\varepsilon_S(W)$, is computed using eq (57) in the form

$$\varepsilon_S(W_S) = \frac{I_o(W_S)\mu_o - I_c(W_S)}{I_o(W_S)\mu_o - B\left[W_S, T(p_S)\right]} , \tag{59a}$$

and the surface reflectivity

$$r_S(W_S) = 1 - \varepsilon_S(W_S). \tag{59b}$$

(b) Surface Temperature Equation

Assuming that a change of radiance from one FOV to a geographically adjacent FOV is due only to a change in cloud amount, it follows from eq (40) that

$$\frac{dI(W)}{dS} = \left[I_{cd}(W) - I_c(W)\right]\frac{dN}{dS} , \tag{60}$$

where S denotes a space coordinate. It then follows that

$$dI(W_S) = D(W_S, W_L)dI(W_L) \tag{61}$$

where $D(W_S, W_L)$ is the ratio of the quantities in braces in equation (55) and (56). Integrating eq (61) gives

$$I(W_S) = a(W_S, W_L) + b(W_S, W_L) I(W_L) \tag{62}$$

where the constants $a(W_S, W_L)$ and $b(W_S, W_L)$ can be determined from two or more geographically independent window observation sets.

For the cloudless sky condition (N=0), it follows from eq (57) and (58) that

$$\varepsilon_S(W_S)B\left[W_S, T(p_S)\right] + r_S(W_S)I_o(W_S)\mu_o = a(W_S, W_L) + b(W_S, W_L)$$

$$+B\left[W_L, T(p_S)\right] \tag{63}$$

or

$$B\left[W_S, T(p_S)\right] = a'(W_S, W_L) + b'(W_S, W_L) B\left[W_L, T(p_S)\right] \tag{64}$$

with

$$a'(W_S,W_L) = \frac{a(W_S,W_L) - r_S(W_S)I_O(W_S)\mu_O}{\varepsilon_S(W_S)} \quad \text{and}$$

$$b'(W_S,W_L) = \frac{b(W_S,W_L)}{\varepsilon_S(W_S)} .$$

Unfortunately, this solution for surface temperature is non-linear and, therefore, T_S cannot be obtained directly from eq (64). However, a first order Taylor expansion is used to obtain a linear approximation of eq (64),

namely

$$T(p_S) = T_O(p_S) + \left[\frac{\partial T(p_S)}{\partial a'(W_S,W_L)}\right] \left[a'_O(W_S,W_L) - a'(W_S, W_L)\right], \tag{65}$$

where $T_O(p_S)$ is a surface temperature "guess" and it follows from eq (64) that

$$\left[\frac{\partial T(p_S)}{\partial a'(W_S, W_L)}\right]_O = \left[\frac{\partial B(W_S,T)}{\partial T}\right]_O \frac{1}{-b'(W_S,W_L)} \left[\frac{\partial B(W_L,T)}{\partial T}\right]_O$$

and

$$a'_O(W_S,W_L) = B\left[W_S,T_O(p_S)\right] - b'(W_S,W_L) \; B\left[W_L,T_O(p_S)\right] .$$

If a surface temperature obtained by eq (65) is within the expected error of $T_O(p_S)$, then the solution is considered valid (i.e., the radiance variability is due to variations in cloud cover allowing for a valid determination of the surface temperature).

(c) Clear-Column Radiance Equation

Writing eq (62) for a CO_2 or H_2O absorption channel (ν),

$$I(\nu) = a(\nu,W_L) + b(\nu,W_L)I(W_L) \tag{66}$$

where, as before, the constants $a(\nu,W_L)$ and $b(\nu,W_L)$ can be determined from two or more geographically independent observation sets. Then, the clear column radiance, $I_C(\nu)$, is given by

$$I_c(\nu) = a(\nu,W_L) + b(\nu,W_L)I_c(W_L) \, , \tag{67}$$

where $I_c(W_L)$ is specified by eq (58) from the surface temperature.

In practice an alternate form is used which is derived from eq (40) by considering the ratio of the radiances measured in two FOV's, say FOV i and j. Assuming the cloud and clear air radiance is the same for both FOV's (i.e., any variations is due only to variations in cloud amount),

$$\frac{I_i(\nu) - I_{i,j}^c(\nu)}{I_j(\nu) - I_{i,j}^c(\nu)} = \frac{N_i}{N_j} = N^*_{i,j} \, . \tag{68}$$

It follows from eq (68) that

$$I_{i,j}^c(\nu) = \frac{I_i(\nu) - N^*_{i,j} I_j(\nu)}{(1 - N^*_{i,j})} \, . \tag{69}$$

In applying eq (68) and (69), the ith FOV is taken as that having the maximum longwave window channel radiance. Then using the long wavelength window channel to define $N^*_{i,j}$,

$$N^*_{i,j} = \frac{I_i(W_L) - I_{i,j}^c(W_L)}{I_j(W_L) - I_{i,j}^c(W_L)} \, , \tag{70}$$

the clear-column radiance is obtained using eq (69)

4.1.5 Filtering Observation Pairs Having Different Cloud Properties

The above solutions for surface temperature and clear-column radiance are valid only if the variation of radiance from one field of view to another is due to a variation in the fractional cloud coverage and not due to variations in the cloud properties (e.g., height, opacity, etc.). Such variations in cloud properties can be detected from an erroneous solution for the clear-column radiance of the shortwave window channel.

It follows from eq (57) that, for a diffusely reflecting surface ($r_s = 1-\varepsilon_s$),

$$I_c(W_s) = B\left[W_s, T(p_s)\right] + r_s\left\{I_0(W_s)\mu_0 - B\left[W_s, T(p_s)\right]\right\} \tag{71}$$

Therefore the maximum possible clear-column radiance, $I_c^{max}(W_S)$, is given by

$$B\left[W_S,T(p_S)+\beta\right]+r_s^{max}\left\{I_O(W_S)\mu_O-B\left[W_S,T(p_S)+\beta\right]\right\} \quad (72a)$$

$$B\left[W_S,T(p_S)+\beta\right]+r_s^{min}\left\{I_O(W_S)\mu_O-B\left[W_S,T(p_S)+\beta\right]\right\} \quad (72b)$$

$I_c^{max}(W_S)$ = greatest of

$$B\left[W_S,T(p_S)-\beta\right]+r_s^{max}\left\{I_O(W_S)\mu_O-B\left[W_S,T(p_S)-\beta\right]\right\} \quad (73a)$$

$$B\left[W_S,T(p_S)-\beta\right]+r_s^{min}\left\{I_O(W_S)\mu_O-B\left[W_S,T(p_S)-\beta\right]\right\} \quad (73b)$$

and the minimum possible clear column radiance, $I_c^{min}(W_S)$ is given by

$$I_c^{min}(W_S) = \text{smallest of } 72a - 73b .$$

Using eq (69) and (70) to compute $I_{i,j}^c(W_S)$, the cloud properties are considered to be the same in elements i, and j, if

$$I_c^{min} - \frac{2\ \sigma\varepsilon}{(1-N^*)} \leq I_{i,j}^c(W_S) \leq I_c^{max}(W_S) + \frac{2\ \sigma\varepsilon}{(1-N^*)} \quad (74)$$

where the term added (subtracted) to I_c^{max} (I_c^{min}) is the expected 2σ error of $I_{i,j}^c(W_S)$

If condition (74) does not hold then the solutions of equations (65), (67), and (69) are considered invalid.

4.1.6 Detecting Clear and Overcast Air Columns

(a) From Multi-Channel Window Observations

For a cloudless sky or an overcast cloud condition, it follows from eq (58) and (59) that

$$\hat{T}(p_S) = B^{-1}\left[I(W_L)\right], \quad (75)$$

where B^{-1} refers to the inverse Planck function, or

$$\hat{T}(p_S) = B^{-1}\left[\frac{I(W_S) - r_s(W_S)I_O(W_S)\mu_O}{\varepsilon_s}\right] \quad (76)$$

where the s subscript refers to either the cloud or earth's surface.

At night, $I_O(W_S)\mu_O = 0$, if

$$\Delta T^* = \left\{ B^{-1} \left[I(W_L) \right] - B^{-1} \left[\frac{I(W_S)}{\varepsilon_S} \right] \right\} < 2\rho , \tag{77}$$

where ρ is the expected difference due to instrumental error, the FOV is either cloudfree or completely filled with an opaque cloud ($\tau_c = 0$), with an emissivity near that of the surface. These two conditions are differentiated by comparing the $B^{-1}[I(W_L)]$ with $T_0(p_S)$, the estimated surface temperature. If

$$\text{(a)} \qquad B^{-1} \left[I(W_L) \right] > T_0(p_S) - \beta \tag{78a}$$

the FOV is considered to be clear; if

$$\text{(b)} \qquad B^{-1} \left[I(W_L) \right] < T_0(p_S) - \beta \tag{78b}$$

the FOV is considered to be overcast.

If

$$\Delta T^* > 3\rho , \tag{79}$$

the FOV is considered to be composed of broken or mixed clouds.

During the day, $I_0(W_S)\mu_0 > 0$, we can solve for r_S using eq (59).

If

$$r_S(W_S) \leq r_S^{max}(W_S) \tag{80}$$

where $r_S^{max}(W_S)$ is the maximum expected value of the surface reflectivity and if condition (78a) holds, the element is considered cloudless. During the day no differentiation between overcast and broken cloud conditions can be made for an individual FOV from only the window observations.

(b) From Multi-FOV Observations

From an array of observations, it is possible to determine whether or not a particular H_2O or CO_2 channel radiance is affected by any clouds within the FOV's making up the geographical observation array.

I. If the channel is unaffected by cloud, then

$$\text{(1)} \quad \text{Var} \left[I(\upsilon) \right] \approx \sigma_\varepsilon^2 + \sigma_T^2$$

and

$$\text{(2)} \quad \text{Var} \left[I(W) \right] \gg \sigma_\varepsilon^2 + \sigma_T^2 \tag{81}$$

or

$$\text{(3)} \quad \overline{I}(W) \approx B \left[W, T_0(p_S) \right] ,$$

where the bar denotes the average value and $\sigma_T{}^2$ is the expected variance due to surface or atmospheric temperature variations.

II. If the channel is <u>affected by cloud</u>, then

$$(1) \quad \text{Var} \left[I(\nu)\right] \gg \sigma_\epsilon{}^2 + \sigma_\tau{}^2 . \tag{82}$$

III. If

$$(1) \quad \text{Var} \left[I(\nu)\right] \approx \sigma_\epsilon{}^2 + \sigma_\tau{}^2$$

and

$$(2) \quad \text{Var} \left[I(W)\right] \approx \sigma_\epsilon{}^2 + \sigma_\tau{}^2 \tag{83}$$

and

$$(3) \quad \widetilde{I}(W) < B \left[W, T_0(p_S)\right]$$

Then an overcast exists, but it cannot be said whether or not $I(\nu)$ is affected by the cloud.

4.2 Computational Procedures for Nimbus-5 ITPR Data

4.2.1 Definition of Grid Values of $T(p_S)$, $r_S(W_S)$, and $\epsilon_S(W_S)$

Steps:

(1) Specify grid average surface temperatures, $T_0(p_S)$, from clear-column THIR window data as discussed above in Section 3.

(2) Find the element for which the difference in brightness temperature between the 3.7-μm and 11.0-μm channels is minimum. If this minimum difference is greater than $15°K$, then it is assumed that no clear FOV's exist. If the minimum difference is less than $15°K$, proceed as follows. From all elements at which the 3.7-μm to 11.0-μm brightness temperature difference is no greater than the minimum difference plus $1°C$, find the maximum 11.0-μm brightness temperature, Tmax. Then average all values $\geq$ Tmax -4. If this grid average is greater than $[T_0(p_S)-8]$, replace the surface temperature estimate obtained in step (1) with this grid average clear-column ITPR 11.0 μm window channel brightness temperature value.

(3) Compute $r_S(W_S)$ and $\epsilon_S(W_S)$ from the grid average clear-column 3.7-μm ITPR data, defined in step (2), using equations (59). Let $r_S{}^{max} = r_S + 0.10\, r_S$ and $r_S{}^{min}=0$.

Options:

(1) If no clear-column THIR data exist then we let $T_O(p_S)$ be given by the day-old surface temperature analysis.

(2) If no ITPR clear-columns exist we assume

$$r_s = 0.02 \text{ and } \varepsilon_s = 0.98$$

4.2.2 Definition of Spatial Radiance Sets for Clear-Column Radiance Computations

The ITPR major grids are partitioned into 12 sub-grids, as shown in figure 4-6a, for the purpose of calculating surface temperatures and clear-column radiances using spatially independent radiance observations. Figure 4-6b shows the configuration of the 36 spatially independent and adjacent ITPR observation sets to be used for the ITPR sub-grid computations. When the ITPR is in the nadir mode, each of 36 FOV's is paired with one 10-FOV's removed along the sub-orbital track. This is the minimum separation that provides spatial independence.

Also in figure 4-5 are shown the distribution of SCR and NEMS observations that correspond (in terms of time) with the ITPR grid data. The selection and sampling of SCR and NEMS data are described in sections 4.3 and 4.4, respectively.

4.2.3 Specification of ITPR Sub-Grid Values of $T(p_S)$, $r_S(W_S)$, and $\varepsilon_S(W_S)$

Steps:

(1) Average all THIR clear-column window data in sub-grid region which are greater than $[T_O(p_S)-\beta]$, where $T_O(p_S)$ is the sub-grid average surface temperature estimate obtained from the day-old analysis.

(2) Same procedure as employed for grid, 4.2.1 (2).

(3) Compute sub-grid values of $r_S(W_S)$ and $\varepsilon_S(W_S)$ from clear-column ITPR 3.7-µm window data in sub-grid using equations (59). Define r_s^{min} and r_s^{max} for the sub-grid as $r_s^{min} = 0$, $r_s^{max} = r + 0.10 \ r_S$.

Options

(1) If no clear-column THIR data exist, then we let $T_O(p_S)$ for the sub-grid be given by the day-old analysis.

ITPR Clear Column Radiance Sub-Grid Display

(1,14) — (1,11) — (1,8) — (1,7) — (1,4) — (1,1)

(4,14) — (4,11) — (4,8) — (4,7) — (4,4) — (4,1)

(7,14) — (7,11) — (7,8) — (7,7) — (7,4) — (7,1)

(10,14) — (10,11) — (10,8) — (10,7) — (10,4) — (10,1)

Center Line

Fig. 4 - 6a

(4, 4)

(7, 4)

(4, 1)

(7, 1)
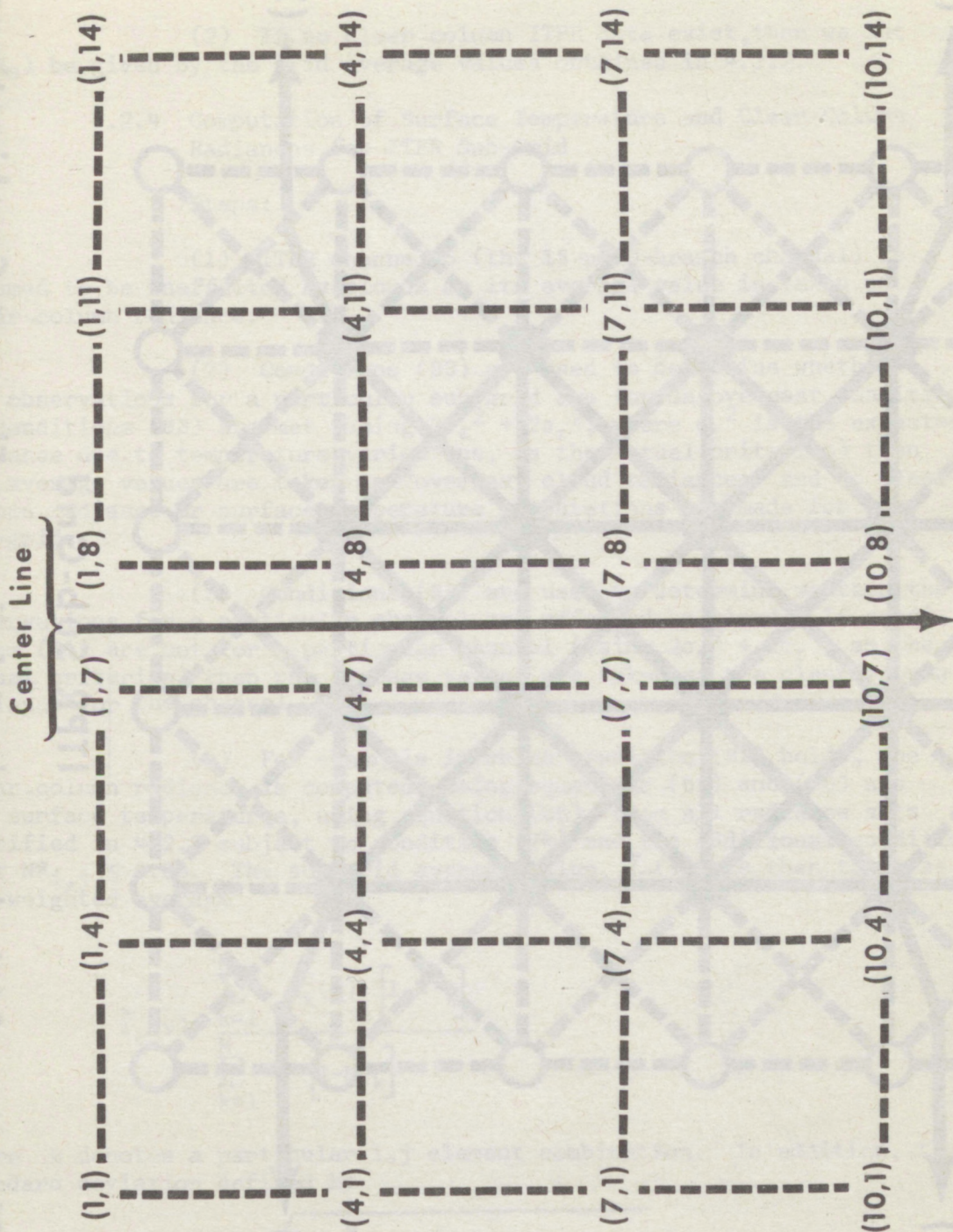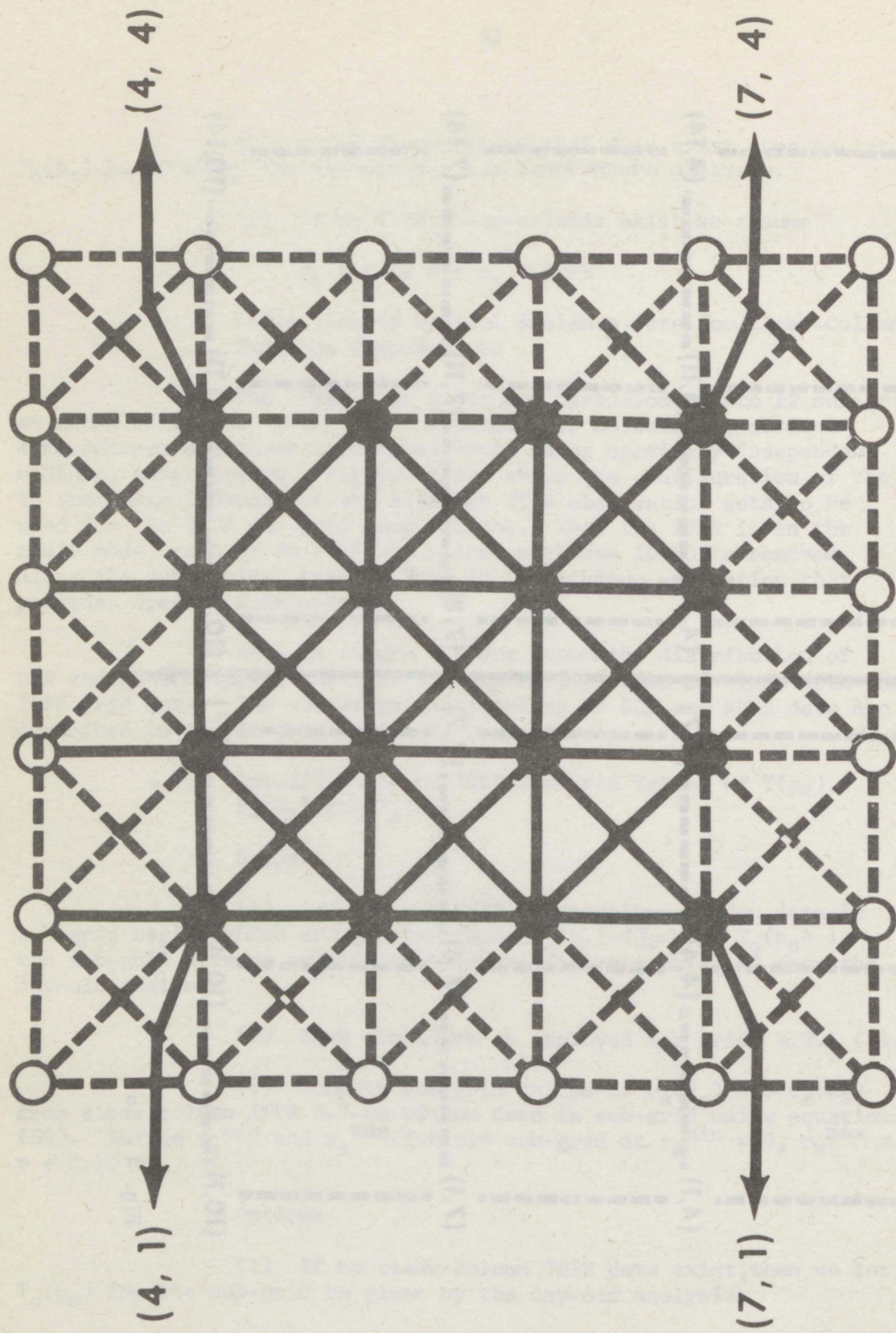
ITPR Sub-Grid

Showing 36 Independent Adjacent Element Combinations

Fig. 4 - 6b

(2) If no clear-column ITPR data exist,then we let $r_S(W_S)$ be given by the grid average values obtained in 4.2.1.

4.2.4 Computation of Surface Temperature and Clear-Column Radiances for ITPR Sub-Grid

Steps:

(1) ITPR channel 6 (the 15-μm Q-branch channel) is assumed to be unaffected by clouds so its average value is taken as clear-column radiance.

(2) Conditions (83) are used to determine whether the observations for a particular sub-grid are for an overcast condition. If conditions (83) are met (using $2\sigma_\epsilon^2 + 2\sigma_\tau^2$, where σ_τ^2 is the expected variance due to temperature variations, as the actual criterion) then the average values are taken as "overcast cloud radiances" and no clear-column radiance or surface temperature computations are made for the sub-grid.

(3) Conditions (81) are used to determine whether the observations for a particular channel are affected by cloud. If conditions (81) are met for a particular channel (using $2\sigma_\epsilon^2 + 2\sigma_\tau^2$, as the actual criterion) then the average values are taken as the clear-column radiance for the channel.

(4) For channels in which condition (82) holds, the clear-column radiance is computed, using equations (69) and (70) and the surface temperatures, using equation (65), from all radiance sets specified in 4.2.2 subject to condition (74) and the additional condition that $N^*_{i,j} \leq 0.86$. The sub-grid average value, $\tilde{I}_c(\nu)$, is then taken as the weighted average

$$\tilde{I}_c(\nu) = \frac{\sum_{k=1}^{M} I_k^c(\nu)\left[1-N^*_k\right]}{\sum_{k=1}^{M}\left[1-N^*_k\right]} \tag{84}$$

where k denotes a particular i,j element combination. In addition, the standard deviation defined by

$$\sigma\left[I_c(\nu)\right] = \sqrt{\frac{1}{M}\sum_{k=1}^{M}\left[I_k^c(\nu)-\tilde{I}_c(\nu)\right]^2} \tag{85}$$

is obtained. All $I_k^c(\nu)$ values which depart from $\tilde{I}_c(\nu)$ by more than 1.5 $\sigma(I_c)$ are filtered from the sample and a final weighted average is

obtained from the filtered data set. The standard deviation is again obtained and used to specify the expected error of the determination, $\varepsilon[I_c(\nu)]$, assuming that

$$\varepsilon\left[I_c(\nu)\right] = \frac{\sigma\left[I_c(\nu)\right]}{\sqrt{N}} , \qquad (86)$$

where $\sigma(I_c)$ is for the filtered data set, and N is the product of the total number of spatially independent observations times the ratio of the final number of determinations over the total number possible.

An analogous averaging procedure is used for the surface temperature determinations.

(5) If neither conditions (81) or (82) hold, the radiance set corresponding to the maximum channel 2 radiance value is taken as "clearest broken cloud radiances" and no clear-column radiance or surface temperature computations are made for the sub-grid.

(6) The ITPR grid average values, $\overline{\overline{I}}_c(\nu)$, are then obtained by

$$\overline{\overline{I}}_c(\nu) = \frac{\displaystyle\sum_{\ell=1}^{L} \overline{I}_c(\nu) \ast W_\ell(\nu)}{\displaystyle\sum_{\ell=1}^{L} W_\ell(\nu)} , \qquad (87)$$

where L is the number of sub-grid clear column radiances obtained, and the weight, $W_\ell(\nu)$, is defined by

$$W_\ell(\nu) = \frac{M_\ell}{\varepsilon_\ell\left[\overline{I}_c(\nu)\right]} . \qquad (88)$$

The expected error, $\varepsilon[\overline{\overline{I}}_c(\nu)]$, of the grid average value is assumed to be given by

$$\varepsilon\left[\overline{\overline{I}}_c(\nu)\right] = \frac{\displaystyle\sum_{\ell=1}^{L} \sigma_\ell\left[\overline{I}_c(\nu)\right] M_\ell}{\sqrt{N} \displaystyle\sum_{\ell=1}^{L} M_\ell} . \qquad (89)$$

where N is for the entire grid.

4.3 Construction of Stratospheric Difference Channels for SCR

As depicted in figure 4-5, section 4.2.2, there are 16 SCR B-channel FOV's in the 64 seconds (four major frames) that correspond to an ITPR grid. At each of the 16 locations, two difference radiances are calculated (channels S1 and S2) from the four B-channel radiances using the weighting procedure described in section 3.3. These 16 measurements are then averaged, and one-sigma filtering is performed to eliminate noise spikes. The resulting single "observation" (two radiance values) is then output along with the corresponding (in time) ITPR and NEMS data. These values are not used directly in the re- trieval of temperature profiles, but serve as input to a global objective analysis routine (see section 6).

4.4 Sampling of NEMS Observations

Again referring to figure 4-5, section 4.1.3, we note that the four-major-frame ITPR grid structure encompasses 32 NEMS FOV's. Although simple averaging of all available FOV's in the four-major- frame ensemble has been found to be sufficient in the case of the SCR stratospheric difference channels (section 4.3), this procedure proved unsatisfactory with respect to NEMS.

The ITPR sub-grids (section 4.2.2) are arranged in three rows of four each. Suppose that the clear-column radiance computations (section 4.2.4) yield reliable results for some, but not all, of the 12 sub-grids. Full-grid clear-column radiances are obtained by weighted averaging of the "good" sub-grids. If a straight average of NEMS measurements is amalgamated with such a radiance set in the temperature- retrieval process (section 5.1), the result may be degraded by incom- patibility between the two radiative estimates of atmospheric properties, since they are, in effect, sampling different (horizontal) regions.

In order to obtain NEMS "observations" more nearly consistent, in the sense of spatial coverage, with ITPR full-grid clear-column radiance estimates, the following procedure was devised, and is successfully employed in routine processing.

The 32 NEMS FOV's are divided into three groups, correspond- ing to the three rows of ITPR sub-grids. In each group, the measure- ments are averaged and screened with a one-sigma filter. In constructing the single "full-grid" observation, each group average is weighted by the number of "good" ITPR sub-grids in the corresponding row. Thus the NEMS and ITPR "sounding radiances" are nominally representative of the same horizontal region of the atmosphere.

5.0 Retrieval Methods

In this section, the procedures developed for determination of meteoro-
logical parameters from the "sounding radiances" obtained using the
techniques of section 4 are described. These parameters are the vertical
temperature profile, $T(p)$ - section 5.1; vertical profile of mixing ratio,
$w(p)$, total precipitable water, W, and liquid water, Q - section 5.2; the
vertical distribution of cloud amount, $A(p)$ - section 5.3; and total out-
going longwave 5- to 25- μm radiation flux, F - section 5.4.

5.1 Temperature Profile

5.1.1 Inversion Algorithm

The algorithm employed in the inversion of the radiative
transfer equation (RTE) to obtain atmospheric temperature from radiance
measurements is a hybrid of regression and the minimum information solu-
tions. The regression solution is used to specify a "first guess" for
the minimum information retrieval. The mathematical basis for these
techniques and their application to remote sounding have been discussed
in considerable detail in the recent literature (e.g., Smith, Woolf, and
Jacob, 1970; Smith, Woolf, and Fleming, 1972; and Fritz et. al., 1973).
Therefore, only those aspects pertinent to the Nimbus-5 amalgamation (of
information from different sensors) problem need be presented here.

As part of the linearization entailed in the development
of the minimum information solution, it is necessary to normalize the
radiative measurements. When the sensing channels are in a fairly
narrow spectral region - such as the 15-μm CO_2 band, as in the case of
the SIRS-B experiment on Nimbus-4 - it is sufficient to normalize to
a nominal frequency near the center of the band (Smith et. al., 1972).
In the present Nimbus-5 situation, we wish to combine infrared radiances
(ITPR) with microwave brightness temperature (NEMS) measurements in
vastly different spectral regions. Thus, a more complicated normali-
zation procedure is required. Employing the first order Taylor expansion
we define relative radiances, R_j, whose magnitudes are similar for all
wavelengths. For the infrared,

$$R_j = \frac{I_j - I^\circ_j}{I_j} = \sum_{i=1}^{N} (T_i - T^\circ_i) \left\{ \frac{1}{I_j} \frac{\partial B^\circ_{ij}}{\partial T^\circ_i} \Delta\tau_{ij} \right\} \tag{90}$$

and for the microwave (where Brightness Temp = Constant x Radiance)

$$R_j = \frac{BT_j - BT^\circ_j}{BT_j} = \sum_{i=1}^{N} (T_i, T^\circ_i) \left\{ \frac{1}{BT_j} \Delta\tau_{ij} \right\} \text{ and} \tag{91}$$

$$\left(\frac{\partial B^\circ}{\partial T^\circ} \right) = \frac{C_2\nu}{T^{\circ 2}} \left[\frac{B^\circ \exp(C_2\nu/T^\circ)}{\exp(C_2\nu/T^\circ - 1)} \right] = K \left(\frac{B}{\nu T} \right)^2 \exp\left[-\frac{C_2\nu}{T^\circ} \right] , \tag{92}$$

where $K = C_2/C_1 = 120836.13$; B is Planck radiance; BT is brightness temperature; subscript i denotes level, j channel; and the superscript zero denotes initial-guess quantities (generation of guess temperature profiles is described in section 5.1.2, following).

In matrix form,

$$\vec{R} = \delta T \underset{\sim}{W} \quad , \tag{93}$$

where the elements W_{ij} of $\underset{\sim}{W}$ are

$$W_{ij} = \frac{1}{I_j} \frac{\partial B_{ij}}{\partial T^\circ_i} \Delta\tau_{ij} \quad \text{(infrared)} \tag{94a}$$

and

$$W_{ij} = \frac{1}{BT_j} \Delta\tau_{ij} \quad \text{(microwave)} . \tag{94b}$$

The minimum information solution is then the "conditioned inverse" of eq (93)(see Smith et. al., 1972),

$$\vec{\delta T} = (\underset{\sim}{W}^T \underset{\sim}{W} + \vec{\gamma} \, \underset{\sim}{I})^{-1} \, \underset{\sim}{W}^T \vec{R} \tag{95a}$$

or

$$\vec{\delta T} = \underset{\sim}{C} \, \vec{R} \quad , \tag{95b}$$

where $\underset{\sim}{I}$ is the identity matrix and γ is a vector Lagrangian multiplier.

The "error matrix" $\vec{\gamma} \, \underset{\sim}{I}$ serves to condition the matrix $\underset{\sim}{W}^T \underset{\sim}{W}$ for inversion.

$$\vec{\gamma} = \frac{\sigma\epsilon^2(\vec{R_i})}{\sigma\epsilon^2(\vec{\delta T_i})} \tag{96}$$

where $\sigma\epsilon^2(\quad)$ is the expected error of the particular quantity.

$$\sigma\epsilon(R_j) = \frac{\sigma\epsilon(I_j)}{I_j} \quad \text{(infrared)} \tag{97a}$$

and

$$\sigma\epsilon(R_j) = \frac{\sigma\epsilon(BT_j)}{BT_j} \quad \text{(microwave)} \tag{97b}$$

$$\sigma\epsilon(\delta T_i) = 5^\circ C \quad . \tag{97c}$$

The above formulation is particularly convenient when various combinations of radiative measurements are employed. (See section 5.1.4). In determining the coefficient matrix $\underset{\sim}{C}$, eq 95, , we can readily zero the coefficient for any channel simply by specifying a very large "error" for that channel. A value of 10^6, for example, for any diagonal element insures a value of zero in the corresponding diagonal element of the inverse matrix, and therefore in the elements of $\underset{\sim}{C}$ for that channel.

5.1.2 First Guess

The first guess temperature profile for the minimum information solution is obtained by applying to the sounding radiances a set of regression coefficients appropriate to the particular combination of channels being employed. These regression coefficients are obtained through radiance synthesis, using a fixed data base of radiosonde/rocketsonde temperature profiles (see Appendix, Section 7.1). Infrared radiances and microwave brightness temperatures are calculated from these profiles - 400 in each of three latitude bands (60-90 N and S, 30-60 N and S, 30N-30S) spanning all seasons - by radiative transfer, using the transmittance functions described in section 3. Normally distributed errors, with RMS levels equal to the nominal noise equivalent radiance in each channel, are applied to simulate expected instrumental deviations. Infrared radiances are converted to brightness temperatures, to render them spectrally compatible with the microwave data. Then, multiple linear regression is performed with the "observed" brightness temperatures as predictors (x) and the original in situ atmospheric temperatures as predictands (y).

In matrix notation,

$$\tilde{y} = \tilde{x}\underset{\sim}{A} , \tag{98}$$

where $\tilde{x}$ is a vector of brightness temperatures, and $\tilde{y}$ the corresponding temperature-profile vector; extending eq (98) to the ensemble of data (400 samples in a latitude band) yields the matrix relationship

$$\underset{\sim}{Y} = \underset{\sim}{X} \underset{\sim}{A} \tag{99}$$

where $\underset{\sim}{X}$ is an nxm matrix of n observations in m channels, $\underset{\sim}{Y}$ is an nxℓ matrix of n observations at ℓ levels, and A is the desired mxℓ coefficient matrix. The least-squares solution to eq (99) is straightforward, being

$$\underset{\sim}{A} = (\underset{\sim}{X}^T\underset{\sim}{X})^{-1} \underset{\sim}{X}^T\underset{\sim}{Y} . \tag{100a}$$

Now the matrix of radiance observations $\underset{\sim}{X}$ are expressed in terms of their true values plus a random error component, as

$$\underset{\sim}{X} = \underset{\sim}{x} + \underset{\sim}{E} \tag{100b}$$

Substituting eq (100b) into eq (100a), noting the fact that the errors of radiance are uncorrelated with the temperature profiles (i.e., $\underset{\sim}{E}^T\underset{\sim}{Y}=0$), yields

$$\underset{\sim}{A} = (\underset{\sim}{X}^T\underset{\sim}{X} + \underset{\sim}{E}^T\underset{\sim}{E})^{-1}\ \underset{\sim}{X}^T\underset{\sim}{Y} \ . \tag{100c}$$

Applying the reasonable constraint that errors be uncorrelated between channels (X's), than $\underset{\sim}{E}^T\underset{\sim}{E}$ is a diagonal matrix, $\underset{\sim}{E}^T\underset{\sim}{E} = \tilde{k}\ \underset{\sim}{I}$ where $k_{jj} = \sigma_\epsilon^2[BT_j]$ and $\underset{\sim}{I}$ is the identity matrix, such that

$$\underset{\sim}{A} = (\underset{\sim}{X}^T\underset{\sim}{X} + k\underset{\sim}{I})^{-1}\ \underset{\sim}{X}^T\underset{\sim}{Y} \tag{100d}$$

Equation (100d) is identical (in matrix form) to eq (95a). We use this feature in much the same way: namely, to zero the coefficients of various channels, simply by making the appropriate element(s) of $\tilde{k}$ very large, say 10^6.

5.1.3 Terrain Effects

Implicit in the retrieval model is the assumption that the base of the atmosphere is at the 1000-mb level. Over regions of the earth where the terrain intrudes appreciably into the atmosphere, this assumption no longer holds, and it is necessary to account for the reduced vertical extent of the atmosphere in performing the requisite radiative transfer calculations.

An auxiliary data set, consisting of the elevations above sea level of the earth's surface on a one-degree latitude by one-degree longitude grid, is used to specify the surface pressure for the retrieval program. If the retrieval location is found to have a non-zero elevation, the surface pressure is estimated by the hydrostatic equation;

$$P_{sfc} = 1000\ \exp\left\{-Z_{sfc}\bigg/\frac{RT_{sfc}}{g}\right\} \tag{101}$$

where Z_{sfc} is the terrain elevation, T_{sfc} is the surface (skin) temperature obtained in the course of clear-column radiance determination, R is the gas constant, and g is the acceleration due to gravity. If $P_{sfc} > 1000$ mb, the terrain is ignored (i.e., P_{sfc} is assumed equal to 1000 mb); otherwise, P_{sfc} is replaced by the nearest retrieval model level (e.g., 920 mb, 850 mb, or 700 mb).

In all subsequent radiative transfer calculations relating to this location, the downward integration of the RTE is terminated at P_{sfc}, and the boundary term, I_B, is changed from

$$I_B = B(T_{sfc}, \nu) \cdot \tau(0, p_0) \tag{102a}$$

to

$$I_B = B(T_{sfc}, \nu) \cdot \tau(0, p_{sfc}), \tag{102b}$$

where B is Planck radiance (infrared) or brightness temperature (microwave), and $\tau(0,p)$ is the total transmission from the "top" of the atmosphere (p=0) to pressure p.

5.1.4 Solutions for "Non Clear-Column Radiance" Conditions

For situations where no reliable "clear-column" radiances could be derived (which are flagged as being "overcast" or "unreliable"), an attempt is made to correct the radiances for cloud effects using the established procedures used for SIRS-A and SIRS-B data processing (Smith, Woolf, and Jacob, 1970). In this case, the clear-column radiance is given by the relation

$$I_c(\nu) = I_m(\nu) + A \left[B(T_S)\tau(p_S) - B(T_c)\tau(p_c) - \int_{P_c}^{P_S} B(T) \frac{d\tau(o,p)}{dp} dp \right], \tag{103}$$

where the c subscript denotes the cloud level and A is the amount of cloudiness. The quantity in brackets must be evaluated using a "guess" temperature profile which is usually obtained from regression relations employing the surface temperature and the cloud unaffected radiances from stratospheric channels 5 and 6. If NEMS data are available, the regression solution obtained from the NEMS oxygen channel radiances and surface temperature is used to compute the cloud correction term. The cloud pressure, p_c, and amount, A, are specified by the technique given in section 5.3. Having corrected the radiances for cloud contamination, the temperature (and moisture) retrieval proceeds as described earlier for the clear-column radiance case. However, since it is known that the retrieval below the cloud level is heavily biased towards the initial guess as a result of this cloud correction procedure (Smith, Woolf, and Fleming, 1972), the profiles are set equal to "missing" flag values at all levels below the inferred cloud level.

5.1.5 Channel Combinations

There are three basic channel combinations employed in the retrieval of temperature profiles in the Nimbus-5 sounding system:

(1) ITPR + SCR;

(2) NEMS + SCR; and

(3) ITPR + NEMS + SCR.

There are several variations on this basic "theme" which bring the number of combinations in use to a total of twelve. Note that SCR is considered "present" in all three basic sets; this is by virtue of the objective analysis applied to the SCR difference channels, providing global grid-point fields of stratospheric radiance. However, when the SCR is in calibration, no data can be provided to the analysis routine, and grid-points in the vicinity of the calibration region will be unchanged in value from the 24-hour old "guess" field. Therefore, SCR is considered unavailable when in calibration; this constraint raises the number of "basic" channel combinations to six.

The six additional sets involve various reductions in the number of ITPR channels used, based on considerations of the reliability of clear-column radiance determinations. For example: if the ITPR grid is deemed overcast, only the stratospheric channels (5 and 6) are employed with the surface temperature to generate the "first guess" profile. Note that all channels are still used in the subsequent "minimum information" solution.

When the ITPR is scanning to the left or right of the orbital track, or when the NEMS is in calibration, the latter is not available, and only channel combination (1), or a variation of the type described in the immediately preceding paragraph, is employed. Otherwise (ITPR center grid or nadir mode), the three basic combinations, or variations thereof, are utilized. However, if either solution (1) or solution (2) fails any of the consistency checks described in the next section, solution (3) is not attempted.

5.1.6 Consistency Checks

Several internal consistency checks are applied in the course of obtaining temperature profiles. If any of the following conditions are met, the retrieval is tagged unsatisfactory:

(1) Difference between retrieved 1000-mb temperature and surface temperature greater than 5 degrees (this eliminates retrievals over hot land surfaces, where our handling of boundary effects is of uncertain reliability);

(2) Difference between the regression solution and the subsequent minimum information retrieval greater than 5 degrees at any level up to 100 mb;

(3) Difference between the observed brightness temperature in NEMS channel 3 (53.65 GHz), and that computed from the ITPR + SCR (or ITPR only) solution, greater than 3 degrees. (This test is not applied over elevated terrain, since that NEMS channel becomes sensitive to surface emissivity);

(4) RMS deviation between observed radiances and those calculated from the retrieved profile greater than the expected instrumental noise, for the channels actually employed in the particular solution; or

(5) Retrieved profile superadiabatic between any two levels up to 100 mb.

As mentioned in the preceding section, failure of any consistency check for a type one (ITPR + SCR or ITPR) or type two (NEMS + SCR or NEMS) solution precludes any attempt at the type three retrieval (ITPR + NEMS + SCR or ITPR + NEMS) for that set of radiances.

5.1.7 ITPR Sub-Grid

As described in section 4.2.4, surface temperatures and clear-column radiances are obtained on a so-called sub-grid scale from ITPR observations. Temperature profiles up to the 100-mb level are retrieved from these data, using minor modifications of the full-grid retrieval procedure. The minimum information solution is applied directly. The full-grid clear-column radiances and the temperature profiles obtained from them are taken as "guess" values. The selection of channels used for clear-column cases is in accordance with the following criteria:

Let $\Delta I(\nu) = \left| I(\nu)_{full} - I(\nu)_{sub} \right|$; then

(i) if $\Delta I(899) < 5$, use all four CO_2 channels;

(ii) if $\Delta I(899) \geqslant 5$, but $\Delta I(747) < 4$, use the 714, 690, and 668 cm-1 channels;

(iii) if $\Delta I(899) \geqslant 5$, $\Delta I(747) \geqslant 4$, but $\Delta I(714) < 3$, use the 690 and 668 cm^{-1} channels;

(iv) if $\Delta I(899) \geqslant 5$, $\Delta I(747) \geqslant 4$, and $\Delta I(714) \geqslant 3$, do not attempt a sub-grid retrieval.

The purpose of the above criteria is to eliminate sub-grid retrievals for cases when noisey sub-grid radiances exist. Sub-grid retrievals are output in the form of $\delta T(p)$, the direct result of the solution. In order to obtain the temperature profile at a sub-grid location, the full grid retrieval is employed as a "guess", to which the δT's are added at each level.

The above applies only to sub-grids for which clear-column radiances have been obtained. For sub-grids in which the radiances have been flagged as overcast or unreliable, the following "reclamation" process is attempted. Provided either (a) the ITPR full grid radiances are clear, or (b) a full grid retrieval has been made with the use of NEMS data (so that the full grid solution can be assumed to be free of cloud contamination), an algorithm similar to that described in section 5.1.4 is applied to correct sub-grid radiances for cloud contamination. The temperature retrieval then proceeds as described previously. As in the non clear-column radiance full grid case, the sub-grid profile is set equal to the "missing" flag values at all levels below the inferred cloud level.

5.2 Atmospheric Water Substance

5.2.1 From ITPR

The retrieval of atmospheric water vapor information from full grid ITPR clear-column radiances is performed in two steps. First, a guess profile of mixing ratio from 1000 to 150 mb is obtained by application of regression equations, which are generated in the same manner as those for specifying temperature (section 5.1.2). This regression solution employs all ITPR channels except the $3.7\text{-}\mu m$ window.

Next, an initial guess radiance is calculated for the $20\text{-}\mu m$ water vapor channel, using the guess mixing ratio profile in the radiative transfer model. Then, the total water vapor mass is adjusted through an iterative solution (Smith, 1970) in which the difference between observed and calculated $20\ \mu m$ radiance is reduced to the nominal noise level. The iterative solution is

$$u^{n+1}(p) = u^n(p) \left\{ 1 + \left[\frac{I(\nu) - \hat{I}^n(\nu)}{\int_o^{p_s} u^n(p)\ \frac{\partial \tau(p)}{\partial u^n(p)}\ \frac{\partial B}{\partial p}\ dp} \right] \right\} , \qquad (104)$$

where it is assumed that the ratio of the actual path length profile $u(p)$ to the initial profile $u'(p)$ is a constant. The superscript denotes the iterative step.

The shape of the mixing ratio profile $w(p) = g \partial u^{(p)}/\partial p$ remains essentially as specified in the initial regression solution. The final value of the total precipitable water, $W(=u(p_S))$, is output along with the mixing ratio profile.

5.2.2 Determination of Atmospheric Water Content From Nimbus-5 NEMS Measurements

The brightness temperature, $T_B(\nu)$, measured by NEMS is related to the surface temperature, T_S, surface emissivity, $\epsilon_S(\nu)$, and atmospheric transmittance, $\tau(\nu)$, by the approximate radiative transfer solution (Grody, 1974).

$$T_B(\nu) = T_S \left[\alpha - \beta\tau^2 (1-\epsilon_S) \right] \tag{105}$$

$$\left.\begin{aligned} \alpha &= 0.860 + 0.270\tau - 0.134\tau^2 \\ \beta\tau^2 &= 0.023 - 0.020\tau + 0.999\tau^2 \end{aligned}\right\} \nu = 22.235 \text{ GHz}$$

$$\left.\begin{aligned} \alpha &= 0.845 + 0.304\tau - 0.151\tau^2 \\ \beta\tau^2 &= 0.020 - 0.011\tau + 0.990\tau^2 \end{aligned}\right\} \nu = 31.40 \text{ GHz} \quad,$$

where the RMS deviations in α and $\beta\tau^2$ are within 0.5 percent of the exact radiative transfer solution for $\tau > 0.35$. These values were obtained using a total of 330 simulations, which included one clear and four cloudy atmospheric models. The cloud models consist of two types of nimbo-stratus with water densities of 0.15 and 0.30 g/m^3 extending from 900 to 650 mb. and two cumulonimbus clouds having water densities of 0.45 and 0.60 g/m^3 extending from 850 to 450 mb.

In general, the transmittance is written as the product of the cloud liquid water, $\tau_{cl}(\nu)$, water vapor, $\tau_{H_2O}(\nu)$, and oxygen, $\tau_{O_2}(\nu)$, transmittances:

$$\tau(\nu) = \tau_{cl}(\nu) \cdot \left[\tau_{H_2O}(\nu) \cdot \tau_{O_2}(\nu) \right] , \tag{106}$$

where the bracketed term has a NEMS frequency dependence given by

$$\tau_{H_2O}(31) \cdot \tau_{O_2}(31) = 0.6753 + 0.3120 \, \tau_{H_2O}(22) \cdot \tau_{O_2}(22) \tag{107}$$

which was determined using atmospheric simulations and found to be accurate to within 1 percent (RMS).

The frequency dispersion associated with the cloud transmittance is given in the Rayleigh limit,

$$\tau_{cl}(\nu) = \epsilon - k\nu^2 Q , \tag{108}$$

where ν is the frequency in GHz, Q is the cloud liquid water in g/cm^2 and k is a parameter which depends on the mean cloud temperature, T_{cl}.

Here $\qquad K = 1.11 \times 10^{\left[0.0122(291-T_{cl}) - 3\right]}$. $\qquad\qquad$ (109)

An approximately linear relationship exists between the precipitable water content, W, and the water vapor transmittance at 22.235 GHz:

$$W(g/cm^2) = 18.114 \left[1-1.042\tau_{H_2O}(22) \cdot \tau_{O_2}(22)\right] , \qquad (110)$$

where the above equation was obtained using atmospheric simulations and found to result in less than a 10 percent RMS error.

Before applying equations (105) - (110) for computing liquid and precipitable water from brightness temperature measurements, it is necessary to have knowledge of the surface temperature, emissivity and mean cloud temperature. Since the determination of transmittance from brightness temperatures is most accurate for low emissivity surfaces (see eq 105), the procedure is applied only to measurements over sea surfaces, as opposed to higher emissivity land surfaces. The sea surface temperature is obtained from Nimbus-5 ITPR measurements and the emissivity is approximately given by the equations for a smooth sea surface:

$$\left.\begin{array}{l} \varepsilon_S(31) \cdot T_S = 130.5°K \\ \\ \varepsilon_S(22) \cdot T_S = 121.5°K \end{array}\right\} \qquad (111)$$

where equation (111) is a reasonable approximation for winds less than 10 m/sec. In the liquid water computations we consider a mean cloud temperature of about 260°K, so that $k \simeq 2.5 \times 10^{-3}$ (eq 109).

The computations proceed as follows:

(1) From brightness temperatures at 22.235 and 31.40 GHz, together with the ITPR-derived surface temperature, we compute the total atmospheric transmittance at the two frequencies using equations (105) and (111).

(2) Applying equations (106), (107), and (108), the liquid water and water vapor-oxygen transmittance terms are computed from the total transmittances.

(3) Employing the relationships (108), (109), and (110), the precipitable and liquid water contents are computed using the results of step (2).

5.3 Cloud Height Distribution

5.3.1 Theory

The radiance measured over a partly cloudy air column is given by

$$I = NI_{cd} + (1-N) I_c ,$$ (112)

where I is the measured radiance, I_{cd} is the radiance from the cloud covered portion, I_c is the radiance from the clear portion, and N is the fractional cloud coverage.

The cloud radiance is given by

$$I_{cd} = \varepsilon I_{Bcd} + (1-\varepsilon) I_c ,$$ (113)

where ε is the emissivity of the cloud and

$$I_{Bcd} = B(p_c)\tau(p_c) - \int_o^{P_c} B(p) \frac{d\tau(p)}{dp} dp$$ (114)

$$I_c = B(p_o)\tau(p_o) - \int_o^{P_o} B(p) \frac{d\tau(p)}{dp} dp .$$ (115)

Substituting eq (113), (114), and (115) into (112) yields after integration by parts

$$I_c - I_{Bcd} = \int_{P_c}^{P_o} \tau(p) \frac{dB(p)}{dp} dp$$ (116)

and

$$I - I_c = N\varepsilon \left[I_{Bcd} - I_c \right] .$$ (117)

We consider two frequencies, ν_1 and ν_2, where the radiances are sensitive to cloud and the cloud emissivity can be assumed to be equal (e.g., the 714 cm^{-1} and 747 cm^{-1} CO_2 channels). It follows from eq (116) and (117) that

$$\gamma(\nu_1,\nu_2) \equiv \overbrace{\frac{I(\nu_1)-I_c(\nu_1)}{I(\nu_2)-I_c(\nu_2)}}^{\text{Observed}} = \overbrace{\frac{\int_{p'_c}^{P_o} \tau(\nu_1,p) \frac{dB(\nu_1,p)}{dp} dp}{\int_{p'_c}^{P_o} \tau(\nu_2,p) \frac{dB(\nu_2,p)}{dp} dp}}^{\text{Calculated}} = R(\nu_1,\nu_2,p_c') .$$ (118)

Thus, given the temperature profile, $R(\nu_1, \nu_2, p_c')$ can be calculated. The cloud pressure for any given ITPR grid element is then given by that p_c' value in which

$$|\gamma(\nu_1, \nu_2) - R(\nu_1, \nu_2, p_c')| = \text{Minimum.} \tag{119}$$

The effective cloud amount $A(=N\varepsilon)$ can be obtained using the highly transparent CO_2 channel in equation (117), i.e.,

$$A = \frac{I_c(\nu_c) - I(\nu_c)}{I_c(\nu_c) - I_{Bcd}(\nu_c, p_c)}, \tag{120}$$

where $\nu_c = 747$ cm^{-1}.

5.3.2 Computational Procedure

After the full-grid temperature profile has been retrieved, clear-air radiances (I_c), "black-cloud" radiances (I_{Bcd}), and the ratios $R(\nu_1, \nu_2, p_c')$ for two channel cmbinations ($\nu_1, \nu_2 = 714, 747$ cm^{-1}; $\nu_1, \nu_2 = 747, 899$ cm^{-1}) are calculated. For each of the 140 ITPR scan elements, the quantities $\gamma(\nu_1, \nu_2)$ - the left hand side of eq (118) - are computed for the two channel combinations using observed radiances. If $I(899) > [I_c(899)-2]$, then the element is assumed to be clear. Otherwise, a search for a "minimum" (eq 119) is performed, using the upper pair of channels (714, 747) first. If a level of minimum is found, and the associated cloud amount (eq 120) is reasonable (between 0 and 1), the cloud determination is accepted if $p_c < 700$ mb (i.e., the cloud is higher in altitude than the 700 mb level). Should p_c be greater than 700 mb the search-for-minimum is performed again, using γ and R for the lower pair of channels (747, 899). If $p_c > 700$ mb then the result of this second pass is accepted; however, if the lower pair of channels yields $p_c < 700$, then the result obtained in the first pass is retained. If an acceptable minimum is not found on either pass, the scan element is flagged as having "non-determinable" cloud pressure and amount.

When this process has been applied to all 140 scan elements, the results are summarized in the form of a histogram, giving the grid-average percent cloud cover at each pressure level:

$$A_t(p_i) = \frac{1}{M} \sum_{j=1}^{J(p_i)} A_j(p_i), \tag{121}$$

where $J(p_i)$ is the number of elements with cloud at pressure p_i, and M is the total number of "good" elements ($M \leq 140$). The 1000-mb level is used to accumulate the total percent determined to be clear. A sample distribution is shown below:

Pressure =	1000	920	850	700	500	400	300	250	200	150	100
Amount =	25	0	0	5	20	5	0	0	25	15	5

This distribution is interpreted as follows; the ITPR grid area has
a total cloud cover of 75% (i.e., 25% clear) with 30% middle clouds
whose tops are near 500 mb and 40% high cloud with tops in the vicinity
of 200 mb.

5.4   Total Outgoing Long-Wave Flux

Winston et al. (1972) demonstrated the feasibility of
specifying, to a high degree of relative accuracy, the total out-
going longwave (5-25 μm) radiative flux by statistical regression
from infrared sounder data. The 15 μm CO_2 and 11 μm window channels
of the Nimbus-3 SIRS-A instrument (Wark and Hilleary, 1969) were
employed in that study. The same procedure has been applied to Nimbus-5,
using the 11 μm window, 15 μm CO_2, and 20 μm H_2O channels of ITPR.
Radiances in these channels were calculated by radiative transfer from
100 radiosonde profiles for which flux computations have been made (Wark
et. al., 1962). Clouds were treated as blackbodies in both the flux
and radiance computations. Stepwise multiple regression analysis was
then performed on the data, treating the calculated radiances as
predictors and longwave flux as the predictand.

Individual correlations of the ITPR radiances with longwave
flux are as follows:

Channel No.	2	3	4	5	6	7
$\nu(cm^{-1})$	899	747	713.8	689.5	668.3	507.4
r	0.986	0.994	0.945	0.028	0.257	0.967

As pointed out by Winston et al., tropospheric temperature,
water vapor, and clouds are the primary modulators of the total out-
going flux; this accounts for the high correlations exhibited by
channels 2, 3, 4, and 7. Channel 5 has maximum sensitivity near the
tropopause, and therefore has little relation, in a statistical sense,
to the flux. The stratospheric channel (6) has a relatively low,
but nevertheless significant, correlation.

The results of the stepwise regression analysis are given
in Table 5-1, which is self-explanatory. The values of C_o and SE
for step zero are the sample mean and standard deviation, respectively,
of longwave flux.

TABLE 5-1

Results of Stepwise Multiple Regression Analysis

ITPR Channel Coefficients

Step No.	C_0	C_2	C_3	C_4	C_5	C_6	C_7	SE	EV
0	482.7	0	0	0	0	0	0	84.0	0
1	61.1	0	5.49	0	0	0	0	9.3	98.7
2	105.4	1.04	3.94	0	0	0	0	8.1	99.1
3	65.9	1.17	3.75	0	0.91	0	0	6.8	99.3
4	36.4	1.67	1.93	0	0.92	0	1.35	6.1	99.5
5	38.8	1.69	1.82	0	0.42	0.41	1.38	6.0	99.5
6	24.3	2.03	0.61	0.92	0.13	0.47	1.77	5.9	99.5

SE = Standard Error, ly/day
EV = Explained Variance, percent

Values of total outgoing longwave flux are calculated routinely on the ITPR full-grid scale by means of the equation

$$F = C_0 + \sum_{i=2}^{7} C_i I_i,$$

where F is flux in ly/day, $C_0 - C_7$ are the values obtained for step 6 (Table 5-1), and $I_2 - I_7$ are grid averaged values of observed (not derived clear-column) radiance in standard units (mw/m^2 - sr-cm^{-1}).

6.0   Objective Analysis

6.1   Introduction

An objective analysis system was designed as an integral part of the Nimbus-5 processing system to provide analyzed fields on a spherical grid with a horizontal resolution meeting the GARP specifications (5 degree longitude wide x 4 degree latitude). Analyses listed below are provided for three purposes:

(1) Surface temperature analyses are used to aid in the discrimination of cloud free areas and clear column radiances for the ITPR. Two global analyses are processed to provide local noon or local midnite estimates of the temperature.

(2) Radiance analyses are used to estimate the radiance which would be obtained by the SCR instrument at the off-nadir positions where no SCR measurements are made. The analysis values for the SCR 1 and SCR 2 radiances are used with the measured ITPR radiance in determining the temperature structure.

(3) Constant pressure temperature analysis are performed at twenty pressure levels (1000 to 1 mb) to aid in quality control of the temperature determinations as well as to provide a "level 3" data archive of the Nimbus-5 measurements.

The analysis program was designed to be flexible enough to be readily adaptable to the three purposes stated above. It is basically a Successive Approximation Technique (SAT) whereby the gridpoints of an initial guess field are modified by the neighboring data in 4 scans over the field. This system can be used for computing grid-point values for any initially specified meteorological quantity with observations, but it has been specifically tailored to temperature observations as obtained by a polar-orbiting satellite. A brief summary of the theory and numerical techniques is given in section 6.2.

The computer programs and their use are described in section 6.3. A generalized flow diagram of the modules comprising the system is included. The actual programs are listed in section 6.3. Results obtained with the program are given in Part II of this report.

6.2   Numerical Techniques

6.2.1   Neighboring Report Discrimination

The basic vehicle for changing the initial estimate at a gridpoint is a discrepancy indicated by neighboring observation. It

is therefore necessary to know which observations influence each gridpoints. Because the SAT technique involves 4 scans over the entire field, it is economical to pre-process and save the neighbors for each gridpoint. To do this an observation subscript array is ordered from northernmost to southernmost. Then for each gridpoint, a search is made among those reports between the limits of five grid-lengths north or south of the gridpoint. Of these, all that are not more than five gridlengths (20 degree latitude) in total distance from the gridpoint are ordered from closest to furthest. Finally, up to 5 neighbors are selected according to the following rules:

(1) The nearest in each quadrant about the gridpoint is selected.

(2) The nearest of the remaining irrespective of quadrant is selected.

(These rules are designed to promote isotropy in the corrections to the initial gridpoint estimates, since experiments have shown that isotropy is important in reducing aliasing.) For ready access during the analysis, the subscripts of the neighbors for each gridpoint are packed into a single work and stored in an array of the same size as the grid.

6.2.2 Weighting Factor Determination

The degree to which a neighboring observation is per-mitted to influence a gridpoint is determined by the separating distance and the degree to which all stations on that latitude zone fit the initial estimate (or the result of a previous scan). Basically, if all observations indicate that the estimate is a close fit to the data, there is little reason to change the estimate, and the weighting factor should be small. Also, empirical studies (e.g. Bengtsson and Gustavssen) show that the autocorrelation of error in forecasts (initial estimates) falls off rapidly with distance, so a weighting factor should likewise fall off rapidly. A number of experiments were conducted with real temperature data and real forecasts to determine empirical curves re-lating autocorrelation to distance and to forecast error. It was discovered that these could be fairly represented by the expression

$$W = 1 - S \cdot D^{1/2} \tag{122}$$

where W is the autocorrelation, S is the standard deviation of the forecast error in the latitude and D is the distance in hundreds of kilometers. This expression was adopted directly for a weighting function with the limitations

$$W \geq 0; \quad S \leq 5.$$

There are 5 latitude zones in each hemisphere which are used to determine standard deviations of the data from the current estimate. These are bounded by: 90-74; 74-58; 58-42; 42-26; 26-0 degrees.

6.2.3 Report Quality Control

In common with most objective analysis systems, the validity of data is determined by comparison with the initial estimate for previous scan and with nearby data. In this analysis system there are two levels at which data can be rejected on each scan. First they are subject to fixed tolerances and secondly they are tested against the standard error for their latitude zone, which is determined from the data passing the gross tolerance tests.

(1) To determine if data are to be rejected from fixed tolerances, it is first asked if a value deviates from the current estimate by more than 10°C. If so, it is then asked if this deviation exceeds the deviation of the nearest neighboring data by more than a fixed amount. If so, the value is rejected for the current scan. The fixed amount is a function of scan, decreasing as the scans proceed. Limits imposed in this system are 5, 3, 2, and 1.5°C for the four scans respectively.

(2) To determine if data are to be rejected at the second level, the correction which is indicated by each station at its closest neighboring gridpoint is evaluated against the corrections implied by other neighboring reports which influence that gridpoint. The individual correlations are given by

$$C_i = W_i (O_i - F_i) , \qquad (123)$$

where W is the weighting function, O is the observed value, and F is the value interpolated from the gridpoint estimates. If 2 or less corrections are influencing the gridpoint, the report in question is rejected if its indicated correction exceeds twice the standard error of the latitude zone. If 3 or more corrections are influencing the gridpoint, the report in question is evaluated against an average of all the corrections. The average is formed, subject to the condition that none of the corrections deviate from the average by more than the standard error of the latitude zone. However, if any correction does, it is eliminated from the average. If that correction happens to be for the report in question, the report is rejected. If the number comprising the average falls below 3, the testing reverts to the procedure for 2 or less influencing reports.

Report quality control can be bypassed by a sense switch option. The quality of radiance data has been found to be sufficiently good to obviate the need for quality control during the radiance analyses.

6.2.4 Gridpoint Correction

The correction applied to each gridpoint on the first two scans is a simple average of the individual corrections as obtained from 6.2.3 (2). For the final two scans a modification is made to increase the correction with emphasis on the nearest reports. The procedure is to sum the corrections ordered by distance until the total sum of the weights reaches 0.8. At that point the remaining corrections are added but with diminished weight according to:

$$\hat{W}_k = \left(0.8 - \sum_{i=1}^{k-1} W_i + W_k\right) \tag{124}$$

where $\hat{W}_k$ is the new weight of the kth report. This modification was added when the ITPR scan mechanism failed since reports from rather distant but adjacent orbits appeared to be having too much influence on gridpoints close to the sub-orbital path. In the scanning mode reports from distant adjacent orbits are not usually selected as neighbors to a gridpoint. This modification has also been found useful for analyzing radiosonde reports.

Either or both of the initial two scans may be skipped if the average of the standard error of all latitude zones is less than a pre-determined number, 3.1 and 2.2, respectively. This criteria is frequently met during the summer at stratospheric levels in both hemispheres.

6.3 Computer Programs

All of the analysis programs are done in three sections. The initial section obtains the gridpoint initial estimates from an archive tape and writes them on disc. The second section reads in data and initial estimates, performs the analysis, and writes the final gridded fields on disc. The final section adds the final fields to the archive tape and establishes disc files for use with other programs in the retrieval package. A schematic of the basic steps is as follows

SECTION 1
GETGUES

PRELIMINARY STEPS

A - Read data flag and file skip number

B - Flag <o Read to last file on input tape
       >o Skip designated number of files on input tape
       =o Do nothing

FOR N INITIAL ESTIMATES

A - Read 664 sixty-bit word record

B - Unpack 5:1 to 3320 word record (72 x 43 + 8 word of identification)

C - Write words 1657-3312 (Southern Hemisphere) into ECS

D - Encode level and date into words 1657 and 1658

E - Write words 1-1658 (Northern Hemisphere) as disc record

FOR N INITIAL ESTIMATES

A - Read Southern Hemisphere from ECS

B - Invert field to orient like Northern Hemisphere

C - Write Southern Hemisphere as disc record

SECTION 2
ANALYSIS

PRELIMINARY STEPS

A - Set constants

B - Read sense switches for rejections, output print options
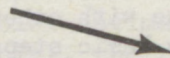
REPORTS

READ IN DATA

A - Read 505 word retrieval record of five 101 word retrievals

B - From first record extract date and time for return to analysis
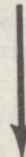
SAVE DATA

A - Loop through 5 retrievals; from
latitude/longitude set up grid
indices to store

B - Store data sequentially in 900
word buffers for N fields,
Northern Hemisphere; N fields,
Southern Hemisphere

C - Read next record and repeat A and
B until end of data

STORE DATA

A - Write 900 word buffers into ECS,
grid indices (I and J) followed
by levels, northern then
southern hemisphere

B - Print sample of data

C - Return number of reports for
each hemisphere

1000

BEGIN ANALYSIS FOR EACH HEMISPHERE

A - Read locations from ECS and increment
address pointer

B - Order a subscript array in increasing
values of J (pole to equator)

C - Find number of stations in each of
5 latitude zones

SORT

FIND NEIGHBORS FOR EACH GRIDPOINT

A - Find beginning and end points in
ordered subscript array for stations
within 20 degree latitude.

B - Store distance and subscript number
of all stations also within longi-
tude limit

C - Sort eligible station by distance

D - Beginning with closest station
find quadrant about gridpoint
and save if quadrant is not
represented or no quadrant has
been represented twice

E - After finding 5 neighbors or
exhausting eligible stations, pack
5 neighbors' subscripts into 1
word and store in array dimen-
sioned 72x23 in position appro-
priate to gridpoint

F - Return to A until all gridpoints
finished

FIND GRIDPOINT NEAREST EACH STATION

A - Store in array the linear gridpoint
subscript of the gridpoint nearest
each station

100

DO ALL FIELDS FOR HEMISPHERE

A - Read initial estimate from disc

B - Read data from ECS and increment
address pointer

C - Test option to print contoured polar
stereographic display of guess

ANALYZE FIELD

POLSIER

FORM POLSIER STEROGRAPHIC ARRAY

A - Convert from 72x23 geographic grid
to 53x57 polar stereographic

PRTW

PRINT CONTROLLED MAP

ANALYSER

DO 4 SCANS OF GRIDPOINT CORRECTIONS

A - Calculate array of values inter-
polated on gridpoint field to
location of each report

B - Test reports against fixed criteria
for rejection (if rejection option
on). Print rejected reports

C - Compute and print standard error
for 5 latitude zones from retained
reports

D - Test average standard error to stop
scan

E - If rejection option on, for each
test its influence on closest
gridpoint as compared with influence
of neighbors. Reject according to
standard error of latitude zone,
using maximum of 5, minimum of 0.9

F - For each gridpoint (except pole
row) compute correction from
retained reports and weighting
function

G - Add corrections to each gridpoint
except pole row

H - Assign average value of row next
to pole to pole point.

SUMMARIZE FIT

A - Calculate array of values inter-
polated in final gridpoint field
to location of reports

B - Test reports for final rejection
against fixed criteria

C - Compute and print final standard
error for 5 latitude zones

D - Print all reports which deviate
by more than 2 standard errors

APPLY LIGHT SMOOTHER

FIVE PT

DO THREE PASSES WITH LIGHT
5-POINT SMOOTHER

PREPARE OUTPUT

OUT

WRITE OUTPUT FIELD

A - If northern hemisphere save 1656
gridpoint field in ECS and return

B - If southern hemisphere invert so
pole row is last and store in
second half of 3312 array

C - Read northern hemisphere from ECS
into first half of 3312 array,
store identification at end of array

D - Pack 5:1 into 664 word array

E - Write record on disc

TEST OPTION FOR PRINT OF ANALYZED FIELD

POLSTER
PRTW

100 ← RETURN FOR NEXT FIELD OR
PRINT REPORT COVERAGE

POUT

PRINT POLAR STEREOGRAPHIC MAP
OF REPORT LOCATIONS ON SAME
BASE AS CONTOURED MAPS

1000 ← RETURN FOR SOUTHERN HEMISPHERE
OR STOP
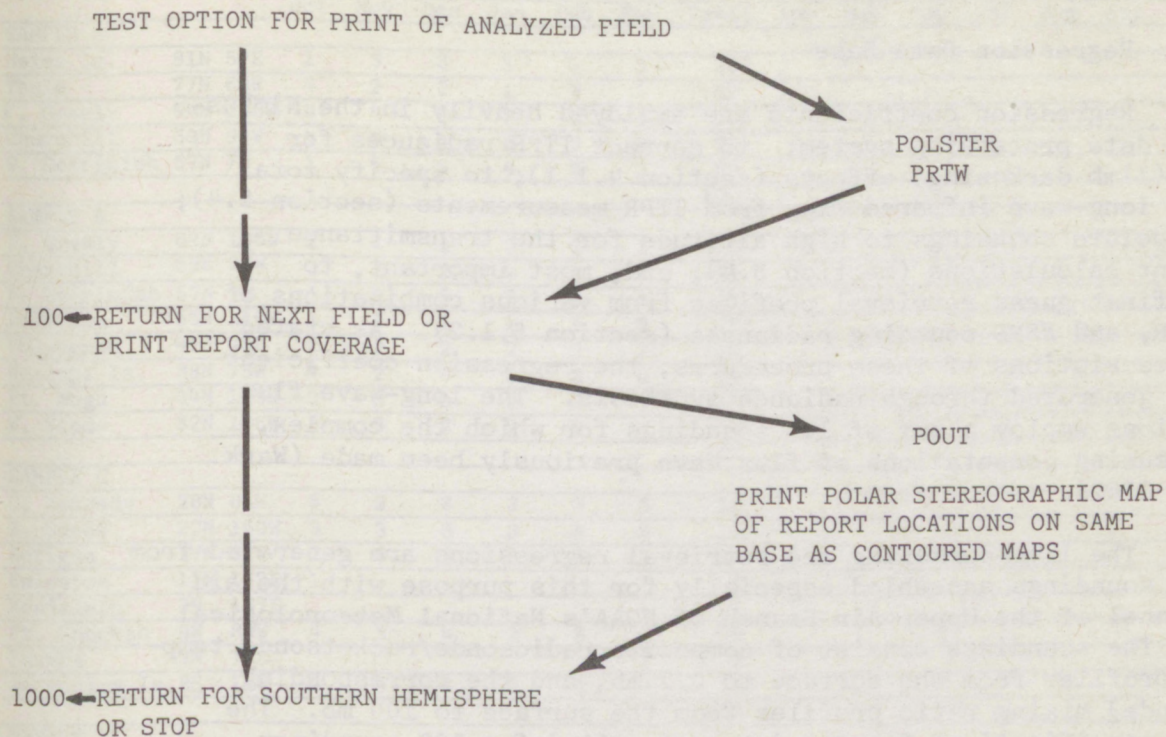
SECTION 3

SYSTEM HARDWARE AND UTILITY ROUTINES

COPY OUTPUT FROM DISC TO ARCHIVE TAPE
FOR ALL LEVELS

COPY OUTPUT ONTO PERMANENT DISC
FILE FOR USE WITH OTHER PROGRAMS

7.0 Appendix

7.1 Regression Data Base

Regression coefficients are employed heavily in the Nimbus-5
sounding data processing system: to correct ITPR radiances for
angular (limb darkening) effects (section 4.1.1); to specify total
outgoing long-wave infrared flux from ITPR measurements (section 5.4);
to extrapolate soundings to high altitude for the transmittance
adjustment calculations (section 3.4); and, most important, to
specify first-guess retrieval profiles from various combinations of
ITPR, SCR, and NEMS sounding radiances (section 5.1.2). As stated
in the descriptions of these procedures, the regression coefficient
sets are generated through radiance synthesis. The long-wave flux
calculations employ a set of 100 soundings for which the complex,
time-consuming computations of flux have previously been made (Wark
et. al., 1962).

The limb-darkening and retrieval regressions are generated from
a set of soundings assembled especially for this purpose with the aid
of personnel of the Upper Air Branch of NOAA's National Meteorological
Center. The soundings consist of composite radiosonde/rocketsonde temp-
erature profiles from the surface to 0.2 mb, and the corresponding
(radiosonde) mixing ratio profiles from the surface to 100 mb. The
original specifications for the data set called for 100 soundings,
distributed as uniformly as possible in time of year, in each of six
latitude bands: 90N-60N, 60N-30N, 30N-Eq, Eq-30S, 30S-60S, 60S-90S.
Because of the relative scarcity of rocketsonde observations in the
Southern Hemisphere, it was necessary to "mirror", by six months, several
Northern Hemisphere soundings. The actual distribution of soundings by
month and observation site in each latitude zone is given in the accom-
panying table 7-1.

Because of range safety constraints on the launching of small
meteorological rockets, the associated radiosondes tend to be biased
toward fair weather conditions - light winds, small amounts of cloudiness -
in the troposphere. Time-series analysis by the Upper Air Branch of a
small sample of data indicated that most rocket firings took place at
the beginning of a period of fine weather. To lessen the obvious fair-
weather bias of the original data set, each rocket sounding was mated to
another radiosonde, from either the launch site itself or a nearby
regular upper-air station, taken one to two days before the rocket ob-
servation. Since upper-stratospheric temperature changes are generally
slow, this "doubling" of soundings did not induce any significant
"smearing" of high-level thermal structure. In those few situations
where rapid changes were occurring, such as in December 1967 at West
Geirinish, Scotland, the soundings were not doubled. Some independent
additions were made, and the data set was finalized at 1200 soundings.
After some initial experimentation, the latitudinal stratification was
broadened: the 90-60, 60-30, and 30-0 degree bands in both hemispheres
were combined, giving three zones of 400 soundings each.

TABLE 7-1. Source and Distribution of Soundings in Regression Data Base

		Oct	Nov	Dec	Jan	Feb	Mar	Total	Apr	May	Jun	Jul	Aug	Sep	Total
SAMPLE A															
Heiss Is.	81N 57E	1	3	3	5	5	3	20							
Thule	77N 69W	4	2	0	1	3	2	12							
F. Greely	64N 146W	4	4	4	7	3	3	25							
Churchill	59N 94W	4	3	4	6	3	3	23							
W. Geirinish	57N 7W	1	2	6	4	5	2	20							
								100							
SAMPLE B															
F. Greely	64N 146W	1	1	1	3	2	1	9							
Churchill	59N 94W	2	1	2	4	1	1	11							
W. Geirinish	57N 7W	1	1	5	2	1	1	11							
Primrose	55N 110W	1	2	2	1	1	0	7							
Volgagrad	49N 45E	2	2	2	2	2	2	12							
Wallops Is.	38N 75W	4	2	3	3	3	4	19							
Pt. Mugu	34N 119W	3	3	3	2	2	2	15							
W. Sands	32N 106W	3	3	2	2	3	3	16							
								100							
SAMPLE C															
C. Kennedy	28N 81W	3	3	3	3	3	3	18							
B. Sands	22N 160W	3	3	3	3	3	3	18							
Antigua	17N 62W	2	3	3	3	3	2	16							
Eniwetok	11N 162E	1						1							
Kwajalein	9N 167E						1	1							
Ft. Sherman	9N 80W	4	3	4	3	3	3	20							
Thumba	9N 77E						2	2							
Ascension Is.	8S 14W	4	4	4	5	3	4	24							
								100							
SAMPLE D															
C. Kennedy	28N 81W								3	4	4	4	3	2	20
B. Sands	22N 160W								2	4	5	5	5	3	24
Antigua	17N 62W								3	3	4	2	3	1	16
Ft. Sherman	9N 80W								0	4	4	3	4	0	15
Ascension Is.	8S 14W								4	4	5	5	2	2	22
Natal	6S 35W	0	1	0	0	1	1								3
															100
SAMPLE E															
F. Greely	64N 146W								2	2	4	1	3	0	12
Churchill	59N 94W								6	1	4	4	3	0	18
Primrose	55N 110W								0	4	3	0	1	0	8
Wallops Is.	38N 75W								1	3	3	4	3	2	16
Pt. Mugu	34N 119W								2	3	4	3	3	2	17
W. Sands	32N 106W								1	6	1	4	4	3	19
Ship	30-60S	0	0	0	1	4	0								5
Chamical	30S 66W	1	0	0	0	0	0								1
Mar Chiquita	38S 57W	0	1	2	1	0	0								4
															100
SAMPLE F															
Thule	77N 69W								6	7	6	6	6	2	33
F. Greely	64N 146W								8	6	6	2	7	1	30
Churchill	59N 94W								8	3	5	6	4	0	26
Molodeznaja	68S 46E	0	0	0	4	3	2								9
McMurdo	78S 167E	0	0	0	2	0	0								2
															100

The retrieval regressions for generating guess profiles of temperature and mixing ratio are determined in the three zones, using the full sample. Limb-darkening and radiosonde extrapolation regressions are constructed from a global set of 120 soundings, 40 in each latitude band.

Statistics concerning the limb corrections are presented in table 7-2. Figure 7-1 presents the standard error of estimate (square root of the unexplained variance) as a function of pressure for the temperature-retrieval regressions, in the three latitude zones described above, for the three principal sensor/channel combinations described in section 5.1.5.

7.2 System Data Flow

The overall flow of data through the Nimbus-5 Sounding Data Software System is depicted in figure 7-2, in which the rectangles denote major software modules and the circles, rotating storage devices - magnetic tape and/or disk. The various processing steps have been described in detail in the main body of this report. The double arrow from surface analysis to sounding radiance, identified as "on-line, one-day delayed," indicates that "today's" analysis will be employed as the first guess for "tomorrow's" processing. The "as necessary" in the definition of the broken line occurs when there are significant changes in the transmittance-adjustment parameters β and γ.

As the system evolved at NOAA/NESS, data were processed in one-day batches of (usually) 12 orbits; hence the origin of the word "day" in the legend of the flow diagram. The system has been implemented at GISS, with a basic processing unit of three orbits; while there have been major modifications to the software, the fundamental data flow remains essentially the same. Thus the word "run" may be substituted for "day".

The meteorological output of the Nimbus-5 sounding system is summarized in table 7-3.

TABLE 7-2.   ITPR Angular Correction Statistics

ZENITH ANGLE = 1.06 DEGREES

CHANNEL	STANDARD ERROR	EXPLAINED VARIANCE
1	.1028E-01	.6992
2	.1170E+01	.7008
3	.4364E-04	.9955
4	.2706E-04	.9985
5	.5396E-04	.9499
6	.7349E-04	.9864
7	.7668E-04	.9651

REGRESSION COEFFICIENTS

CHANNEL	C0	C2	C3	C4	C5	C6	C7
1	-.2590E-01	.2218E-02	-.1920E-02	.4477E-02	-.2458E-02	.7093E-03	-.2678E-02
2	-.2329E+01	.1572E+00	.7219E-01	.3599E+00	-.1662E+00	.2099E-01	-.3940E+00
3	-.2284E-03	.3399E-04	.2007E-04	-.3694E-04	.7062E-05	-.2309E-05	-.1748E-04
4	-.8581E-04	-.9971E-05	.7673E-04	-.3194E-04	.2308E-04	-.1325E-06	-.8561E-05
5	.4408E-03	.1616E-04	-.5883E-04	.8410E-04	-.8473E-05	-.4101E-04	.4333E-05
6	.3572E-03	-.8884E-05	.3038E-04	-.3351E-04	.2222E-03	-.2053E-03	-.3493E-05
7	-.1604E-03	-.3120E-05	.9630E-04	-.8351E-04	.2470E-04	-.9054E-06	-.3220E-04

ZENITH ANGLE = 3.17 DEGREES

CHANNEL	STANDARD ERROR	EXPLAINED VARIANCE
1	.1027E-01	.7008
2	.1168E+01	.7026
3	.3940E-03	.9955
4	.2394E-03	.9986
5	.4733E-03	.9525
6	.6547E-03	.9867
7	.6848E-03	.9657

REGRESSION COEFFICIENTS

CHANNEL	C0	C2	C3	C4	C5	C6	C7
1	-.2848E-01	.2220E-02	-.1907E-02	.4522E-02	-.2376E-02	.6624E-03	-.2706E-02
2	-.2627E+01	.1612E+00	.6391E-01	.3676E+00	-.1619E+00	.1856E-01	-.3932E+00
3	-.2052E-02	.3179E-03	.1462E-03	-.3138E-03	.5786E-04	-.1951E-04	-.1491E-03
4	-.8025E-03	-.8976E-04	.6905E-03	-.2852E-03	.2071E-03	-.2355E-05	-.7765E-04
5	.3853E-02	.1626E-03	-.5865E-03	.7963E-03	-.8652E-04	-.3692E-03	.5317E-04
6	.3183E-02	-.1004E-03	.3356E-03	-.3354E-03	.2010E-02	-.1850E-02	-.4794E-04
7	-.1428E-02	-.3174E-04	.8834E-03	-.7621E-03	.2310E-03	-.1258E-04	-.2962E-03

ZENITH ANGLE = 5.28 DEGREES

CHANNEL	STANDARD ERROR	EXPLAINED VARIANCE
1	.1033E-01	.6985
2	.1174E+01	.7003
3	.1081E-02	.9956
4	.6692E-03	.9986
5	.1336E-02	.9510
6	.1885E-02	.9858
7	.1927E-02	.9649

REGRESSION COEFFICIENTS

CHANNEL	C0	C2	C3	C4	C5	C6	C7
1	-.2611E-01	.2183F-02	-.1781E-02	.4388E-02	-.2435E-02	.7198E-03	-.2724E-02
2	-.2373E+01	.1563E+00	.7931E-01	.3517E+00	-.1670E+00	.2435E-01	-.3952E+00
3	-.5714E-02	.8553E-03	.4921E-03	-.9306E-03	.1788E-03	-.5526E-04	-.4311E-03
4	-.2304E-02	-.2340E-03	.1877E-02	-.7722E-03	-.5832E-03	.2591E-05	-.2047E-03
5	.1116E-01	.4011E-03	-.1471E-02	.2111E-02	-.2235E-03	.1022E-02	.1096E-03
6	.9105E-02	-.2467E-03	.8330E-03	-.8793E-03	.5573E-02	-.5141E-02	-.1081E-03
7	-.4271E-02	-.6062E-04	.2368E-02	-.2069E-02	.6329E-03	-.3296E-04	-.7985E-03

ZENITH ANGLE = 7.39 DEGREES

CHANNEL	STANDARD ERROR	EXPLAINED VARIANCE
1	.1045E-01	.6931
2	.1187E+01	.6957
3	.2177E-02	.9954
4	.1301E-02	.9986
5	.2635E-02	.9505
6	.3622E-02	.9864
7	.3733E-02	.9659

REGRESSION COEFFICIENTS

CHANNEL	C0	C2	C3	C4	C5	C6	C7
1	-.2812E-01	.2247E-02	-.1958E-02	.4551E-02	-.2380E-02	.6602E-03	-.2708E-02
2	-.2664E+01	.1601E+00	.6836E-01	.3678E+00	-.1611E+00	.1842E-01	-.3959E+00
3	-.1136E-01	.1722E-02	.8415E-03	-.1726E-02	.3323E-03	-.1186E-03	-.8290E-03
4	-.4145E-02	-.4877E-03	.3778E-02	-.1580E-02	-.1134E-02	-.6454E-05	-.4228E-03
5	.2124E-01	.8024E-03	-.2935E-02	.4198E-02	-.4553E-03	.1997E-02	.2150E-03
6	.1812E-01	-.5454E-03	.1837E-02	-.1857E-02	.1099E-01	-.1010E-01	-.2632E-03
7	-.7745E-02	-.1729E-03	.4827E-02	-.4178E-02	.1288E-02	-.8664E-04	-.1613E-02

ZENITH ANGLE = 9.51 DEGREES

CHANNEL	STANDARD ERROR	EXPLAINED VARIANCE
1	.1050E-01	.6930
2	.1187E+01	.6982
3	.3560E-02	.9955
4	.2162E-02	.9986
5	.4329E-02	.9512
6	.6037E-02	.9863
7	.6157E-02	.9662

REGRESSION COEFFICIENTS

CHANNEL	C0	C2	C3	C4	C5	C6	C7
1	-.2491E-01	.2063E-02	-.1385E-02	.4128E-02	-.2336E-02	.6783E-03	-.2820E-02
2	-.2349E+01	.1455E+00	.1164E+00	.3318E+00	-.1530E+00	.1640E-01	-.4063E+00
3	-.1891E-01	.2833E-02	.1465E-02	-.2916E-02	.5639E-03	-.1889E-03	-.1390E-02
4	-.7750E-02	-.8156E-03	.6274E-02	-.2649E-02	-.1872E-02	.6723E-05	-.6848E-03
5	.3677E-01	.1385E-02	-.5003E-02	.7009E-02	-.7762E-03	-.3323E-02	.3929E-03
6	.2716E-01	-.6304E-03	.2192E-02	-.2536E-02	.1788E-01	-.1654E-01	-.2252E-03
7	-.1438E-01	-.2907E-03	.7996E-02	-.6952E-02	.2121E-02	-.9487E-04	-.2648E-02

ZENITH ANGLE = 11.63 DEGREES

CHANNEL	STANDARD ERROR	EXPLAINED VARIANCE
1	.1050E-01	.6960
2	.1194E+01	.6977
3	.5381E-02	.9954
4	.3260E-02	.9986
5	.6438E-02	.9518
6	.8966E-02	.9866
7	.9276E-02	.9659

REGRESSION COEFFICIENTS

CHANNEL	C0	C2	C3	C4	C5	C6	C7
1	-.3044E-01	.2324E-02	-.2205E-02	.4923E-02	-.2351E-02	.5284E-03	-.2723E-02
2	-.2859E+01	.1741E+00	.2703E-01	.4156E+00	-.1600E+00	.5007E-02	-.3954E+00
3	-.2769E-01	.4092E-02	.2640E-02	-.4644E-02	.8859E-03	-.2627E-03	-.2180E-02
4	-.1173E-01	-.1250E-02	.9458E-02	-.3939E-02	-.2857E-02	.3078E-04	-.1053E-02
5	.5403E-01	.2073E-02	-.7501E-02	.1045E-01	-.1132E-02	-.4968E-02	.6252E-03
6	.4405E-01	-.1499E-02	.4942E-02	-.4800E-02	.2704E-01	-.2481E-01	-.7376E-03
7	-.2033E-01	-.4449E-03	.1199E-01	-.1033E-01	.3093E-02	-.1221E-03	-.4010E-02

ZENITH ANGLE = 13.76 DEGREES

CHANNEL	STANDARD ERROR	EXPLAINED VARIANCE
1	.1064E-01	.6918
2	.1209E+01	.6935
3	.7534E-02	.9955
4	.4556E-02	.9986
5	.9201E-02	.9498
6	.1267E-01	.9865
7	.1315E-01	.9652

REGRESSION COEFFICIENTS

CHANNEL	C0	C2	C3	C4	C5	C6	C7
1	-.2513E-01	.2206E-02	-.1781E-02	.4388E-02	-.2583E-02	.8207E-03	-.2745E-02
2	-.2346E+01	.1594E+00	.7953E-01	.3545E+00	-.1811E+00	.3400E-01	-.3993E+00
3	-.3920E-01	.5909E-02	.3205E-02	-.6251E-02	.1157E-02	-.3470E-03	-.2928E-02
4	-.1674E-01	-.1701E-02	.1320E-01	-.5522E-02	.3968E-02	.2511E-04	-.1476E-02
5	.7730E-01	.2806E-02	-.1026E-01	.1449E-01	-.1660E-02	-.6878E-02	.8287E-03
6	.6041E-01	-.1762E-02	.5873E-02	-.6163E-02	.3754E-01	-.3453E-01	-.7422E-03
7	-.3040E-01	-.4029E-03	.1623E-01	-.1418E-01	.4368E-02	-.2296E-03	-.5497E-02

ZENITH ANGLE = 15.89 DEGREES

CHANNEL	STANDARD ERROR	EXPLAINED VARIANCE
1	.1070E-01	.6937
2	.1216E+01	.6945
3	.1016E-01	.9954
4	.6238E-02	.9986
5	.1215E-01	.9509
6	.1713E-01	.9862
7	.1753E-01	.9655

REGRESSION COEFFICIENTS

CHANNEL	C0	C2	C3	C4	C5	C6	C7
1	-.2641E-01	.2263E-02	-.1950E-02	.4533E-02	-.2673E-02	.8804E-03	-.2727E-02
2	-.2395E+01	.1619E+00	.7424E-01	.3604E+00	-.1920E+00	.4246E-01	-.4003E+00
3	-.5193E-01	.8043E-02	.3903E-02	-.8072E-02	.1483E-02	-.4854E-03	-.3873E-02
4	-.2095E-01	-.2361E-02	.1790E-01	-.7493E-02	.5297E-02	.1530E-04	-.2046E-02
5	.9889E-01	.4022E-02	-.1449E-01	.1990E-01	-.2252E-02	-.9240E-02	.1277E-02
6	.8549E-01	-.2396E-02	.8012E-02	-.8335E-02	.4951E-01	-.4564E-01	-.1040E-02
7	-.3546E-01	-.8974E-03	.2273E-01	-.1963E-01	.5836E-02	-.2205E-03	-.7569E-02

ZENITH ANGLE = 18.03 DEGREES

CHANNEL	STANDARD ERROR	EXPLAINED VARIANCE
1	.1094E-01	.6853
2	.1237E+01	.6890
3	.1304E-01	.9955
4	.7953E-02	.9986
5	.1599E-01	.9488
6	.2082E-01	.9879
7	.2251E-01	.9659

REGRESSION COEFFICIENTS

CHANNEL	C0	C2	C3	C4	C5	C6	C7
1	-.2484E-01	.2102E-02	-.1365E-02	.4131E-02	-.2545E-02	.8480E-03	-.2883E-02
2	-.2302E+01	.1444E+00	.1380E+00	.3166E+00	-.1754E+00	.3698E-01	-.4165E+00
3	-.6631E-01	.1027E-01	.5425E-02	-.1067E-01	.2054E-02	-.6870E-03	-.5097E-02
4	-.2751E-01	-.2835E-02	.2261E-01	-.9411E-02	-.6816E-02	-.5329E-04	-.2546E-02
5	.1299E+00	.4726E-02	-.1742E-01	.2480E-01	-.2974E-02	-.1168E-01	.1450E-02
6	.1027E+00	-.2932E-02	.1016E-01	-.1053E-01	.6401E-01	-.5889E-01	-.1460E-02
7	-.4625E-01	-.7032E-03	.2828E-01	-.2482E-01	.7715E-02	-.4996E-03	-.9596E-02

ZENITH ANGLE = 20.17 DEGREES

CHANNEL	STANDARD ERROR	EXPLAINED VARIANCE
1	.1093E-01	.6922
2	.1241E+01	.6927
3	.1638E-01	.9955
4	.1001E-01	.9985
5	.2001E-01	.9489
6	.2645E-01	.9877
7	.2881E-01	.9647

REGRESSION COEFFICIENTS

CHANNEL	C0	C2	C3	C4	C5	C6	C7
1	-.2899E-01	.2317E-02	-.2095E-02	.4862E-02	-.2650E-02	.7707E-03	-.2786E-02
2	-.2691E+01	.1728E+00	.4551E-01	.4040E+00	-.1880E+00	.2816E-01	-.4044E+00
3	-.8285E-01	.1293E-01	.6717E-02	-.1346E-01	.2455E-02	-.7338E-03	-.6339E-02
4	-.3257E-01	-.3662E-02	.2883E-01	-.1217E-01	-.8660E-02	.8737E-04	-.3303E-02
5	.1634E+00	.6025E-02	-.2226E-01	.3149E-01	-.3854E-02	-.1469E-01	.1933E-02
6	.1249E+00	-.3548E-02	.1224E-01	-.1267E-01	.7949E-01	-.7322E-01	-.1786E-02
7	-.6023E-01	-.5245E-03	.3450E-01	-.3050E-01	.9384E-02	-.4713E-03	-.1189E-01

ZENITH ANGLE = 22.32 DEGREES

CHANNEL	STANDARD ERROR	EXPLAINED VARIANCE
1	.1125E-01	.6807
2	.1271E+01	.6845
3	.2032E-01	.9954
4	.1206E-01	.9986
5	.2458E-01	.9488
6	.3269E-01	.9877
7	.3458E-01	.9664

REGRESSION COEFFICIENTS

CHANNEL	C0	C2	C3	C4	C5	C6	C7
1	-.2508E-01	.2229E-02	-.1699E-02	.4449E-02	-.2707E-02	.8784E-03	-.2859E-02
2	-.2247E+01	.1592E+00	.9941E-01	.3527E+00	-.1962E+00	.4331E-01	-.4148E+00
3	-.1045E+00	.1577E-01	.8690E-02	-.1669E-01	.3078E-02	-.8852E-03	.7971E-02
4	-.4085E-01	-.4562E-02	.3583E-01	-.1541E-01	-.1056E-01	.1798E-03	-.4108E-02
5	.2022E+00	.7477E-02	-.2761E-01	.3889E-01	-.5035E-02	-.1789E-01	.2476E-02
6	.1435E+00	-.4920E-02	.1626E-01	-.1579E-01	.9692E-01	-.8924E-01	.2442E-02
7	-.7388E-01	-.1206E-02	.4431E-01	-.3905E-01	.1207E-01	-.5726E-03	.1499E-01

ZENITH ANGLE = 24.49 DEGREES

CHANNEL	STANDARD ERROR	EXPLAINED VARIANCE
1	.1134E-01	.6825
2	.1281E+01	.6860
3	.2488E-01	.9953
4	.1477E-01	.9986
5	.2954E-01	.9491
6	.3863E-01	.9883
7	.4213E-01	.9660

REGRESSION COEFFICIENTS

CHANNEL	C0	C2	C3	C4	C5	C6	C7
1	-.2747E-01	.2102E-02	-.1269E-02	.4173E-02	-.2779E-02	.1011E-02	-.2953E-02
2	-.2558E+01	.1509E+00	.1306E+00	.3371E+00	-.2031E+00	.5382E-01	-.4237E+00
3	-.1253E+00	.1959E-01	.9076E-02	-.1948E-01	.3606E-02	-.1096E-02	.9296E-02
4	-.4898E-01	-.5396E-02	.4310E-01	-.1848E-01	-.1274E-01	.1471E-03	-.4953E-02
5	.2409E+00	.8816E-02	-.3305E-01	.4691E-01	-.6350E-02	-.2136E-01	.3066E-02
6	.1793E+00	-.5502E-02	.1886E-01	-.1859E-01	.1158E+00	-.1067E+00	.3026E-02
7	-.8657E-01	-.9452E-03	.5235E-01	-.4652E-01	.1469E-01	-.8991E-03	.1798E-01

ZENITH ANGLE = 26.66 DEGREES

CHANNEL	STANDARD ERROR	EXPLAINED VARIANCE
1	.1150E-01	.6828
2	.1305E+01	.6824
3	.2964E-01	.9953
4	.1724E-01	.9986
5	.3534E-01	.9484
6	.4622E-01	.9883
7	.5088E-01	.9651

REGRESSION COEFFICIENTS

CHANNEL	C0	C2	C3	C4	C5	C6	C7
1	-.2916E-01	.2422E-02	-.2324E-02	.5221E-02	-.2805E-02	.7659E-03	-.2843E-02
2	-.2759E+01	.1826E+00	.2949E-01	.4349E+00	-.2041E+00	.3055E-01	-.4128E+00
3	-.1530E+00	.2316E-01	.1126E-01	-.2314E-01	.4300E-02	-.1366E-02	-.1126E-01
4	-.6459E-01	-.6506E-02	.5196E-01	-.2235E-01	-.1493E-01	.7650E-04	-.6126E-02
5	.2953E+00	.1081E-01	-.4046E-01	.5633E-01	-.8546E-02	-.2476E-01	.4029E-02
6	.2058E+00	-.6158E-02	.2129E-01	-.2076E-01	.1359E+00	-.1257E+00	-.3558E-02
7	-.1156E+00	-.4581E-03	.6062E-01	-.5390E-01	.1776E-01	-.1577E-02	-.2125E-01

ZENITH ANGLE = 28.85 DEGREES

CHANNEL	STANDARD ERROR	EXPLAINED VARIANCE
1	.1176E-01	.6779
2	.1324E+01	.6823
3	.3500E-01	.9953
4	.2054E-01	.9986
5	.4163E-01	.9480
6	.5242E-01	.9893
7	.5907E-01	.9662

REGRESSION COEFFICIENTS

CHANNEL	C0	C2	C3	C4	C5	C6	C7
1	-.2918E-01	.2096E-02	-.1188E-02	.4323E-02	-.2856E-02	.1006E-02	-.3059E-02
2	-.2665E+01	.1443E+00	.1609E+00	.3333E+00	-.2079E+00	.5487E-01	-.4381E+00
3	-.1825E+00	.2757E-01	.1244E-01	-.2682E-01	.5095E-02	-.1636E-02	-.1309E-01
4	-.7583E-01	-.7291E-02	.6008E-01	-.2583E-01	-.1798E-01	.3402E-03	-.6843E-02
5	.3443E+00	.1246E-01	-.4672E-01	.6593E-01	-.1000E-01	-.2907E-01	.4485E-02
6	.2385E+00	-.6621E-02	.2322E-01	-.2329E-01	.1576E+00	-.1459E+00	-.3812E-02
7	-.1315E+00	-.8059E-03	.7223E-01	-.6475E-01	.2099E-01	-.1465E-02	-.2499E-01

ZENITH ANGLE = 31.06 DEGREES

CHANNEL	STANDARD ERROR	EXPLAINED VARIANCE
1	.1206E-01	.6729
2	.1360E+01	.6755
3	.4065E-01	.9954
4	.2528E-01	.9984
5	.4898E-01	.9467
6	.6127E-01	.9893
7	.6952E-01	.9657

REGRESSION COEFFICIENTS

CHANNEL	C0	C2	C3	C4	C5	C6	C7
1	-.3137E-01	.2286E-02	-.1674E-02	.4726E-02	-.2969E-02	.1016E-02	-.3014E-02
2	-.1315E+00	-.8059E-03	.7223E-01	-.6475E-01	.2099E-01	-.1465E-02	-.2499E-01
3	-.3137E-01	.2286E-02	-.1674E-02	.4726E-02	-.2969E-02	.1016E-02	-.3014E-02
4	-.2851E+01	.1680E+00	.1001E+00	.3815E+00	-.2248E+00	.5910E-01	-.4324E+00
5	-.2068E+00	.3227E-01	.1433E-01	-.3120E-01	.5796E-02	-.1848E-02	-.1532E-01
6	-.9115E-01	-.7837E-02	.6846E-01	-.2893E-01	-.2105E-01	.1791E-03	-.7784E-02
7	.3933E+00	.1426E-01	-.5427E-01	.7669E-01	-.1247E-01	-.3309E-01	.5576E-02

ZENITH ANGLE = 33.28 DEGREES

CHANNEL	STANDARD ERROR	EXPLAINED VARIANCE
1	.1244E-01	.6643
2	.1399E+01	.6680
3	.4797E-01	.9952
4	.2889E-01	.9985
5	.5680E-01	.9460
6	.7066E-01	.9895
7	.7939E-01	.9666

REGRESSION COEFFICIENTS

CHANNEL	C0	C2	C3	C4	C5	C6	C7
1	.2987E+00	-.8133E-02	.2827E-01	-.2858E-01	.1810E+00	-.1675E+00	-.4387E-02
2	-.1410E+00	-.6746E-04	.8212E-01	-.7453E-01	.2437E-01	-.1873E-02	-.2883E-01
3	-.3149E-01	.2201E-02	-.1318E-02	.4487E-02	-.2950E-02	.1041E-02	-.3114E-02
4	-.2885E+01	.1551E+00	.1552E+00	.3420E+00	-.2203E+00	.6424E-01	-.4475E+00
5	-.2460E+00	.3764E-01	.1558E-01	-.3525E-01	.6651E-02	-.2225E-02	-.1756E-01
6	-.1024E+00	-.9626E-02	.8134E-01	-.3555E-01	-.2407E-01	.5690E-03	-.9323E-02
7	.4624E+00	.1568E-01	-.6033E-01	.8705E-01	-.1468E-01	-.3776E-01	.6019E-02

ZENITH ANGLE = 35.52 DEGREES

CHANNEL	STANDARD ERROR	EXPLAINED VARIANCE
1	.1270E-01	.6642
2	.1424E+01	.6681
3	.5490E-01	.9953
4	.3288E-01	.9985
5	.6479E-01	.9462
6	.7887E-01	.9901
7	.9198E-01	.9661

REGRESSION COEFFICIENTS

CHANNEL	C0	C2	C3	C4	C5	C6	C7
1	.3250E+00	-.7357E-02	.2712E-01	-.2851E-01	.2055E+00	-.1912E+00	-.4432E-02
2	-.1698E+00	-.1318E-03	.9583E-01	-.8731E-01	.2947E-01	-.2633E-02	-.3364E-01
3	-.3285E-01	.2338E-02	-.1686E-02	.5000E-02	-.2945E-02	.8906E-03	-.3155E-02
4	-.3016E+01	.1720E+00	.1094E+00	.4056E+00	-.2139E+00	.3996E-01	-.4520E+00
5	-.2745E+00	.4312E-01	.1840E-01	-.4119E-01	.7366E-02	-.2116E-02	-.2029E-01
6	-.1097E+00	-.1137E-01	.9529E-01	-.4234E-01	.2762E-01	.9359E-03	-.1133E-01
7	.5187E+00	.1911E-01	-.7324E-01	.1029E+00	-.1789E-01	-.4311E-01	.8086E-02

ZENITH ANGLE = 37.79 DEGREES

CHANNEL	STANDARD ERROR	EXPLAINED VARIANCE
1	.1299E-01	.6637
2	.1461E+01	.6647
3	.6428E-01	.9951
4	.3796E-01	.9985
5	.7409E-01	.9456
6	.8742E-01	.9908
7	.1049E+00	.9663

REGRESSION COEFFICIENTS

CHANNEL	C0	C2	C3	C4	C5	C6	C7
1	.3647E+00	-.1019E-01	.3603E-01	-.3462E-01	.2321E+00	-.2155E+00	-.6472E-02
2	-.1836E+00	.9878E-04	.1098E+00	-.1007E+00	.3342E-01	-.2478E-02	-.3872E-01
3	-.3235E-01	.2397E-02	-.1824E-02	.5124E-02	-.3213E-02	.1068E-02	-.3156E-02
4	-.3047E+01	.1803E+00	.8809E-01	.4216E+00	-.2447E+00	.6192E-01	-.4495E+00
5	-.3194E+00	.4976E-01	.1898E-01	-.4509E-01	.8189E-02	-.2754E-02	-.2279E-01
6	-.1240E+00	-.1244E-01	.1077E+00	-.4734E-01	.3196E-01	.1041E-02	-.1293E-01
7	.5887E+00	.2171E-01	-.8359E-01	.1170E+00	-.2148E-01	-.4799E-01	.9614E-02

ZENITH ANGLE = 40.08 DEGREES

CHANNEL	STANDARD ERROR	EXPLAINED VARIANCE
1	.1334E-01	.6619
2	.1498E+01	.6623
3	.7355E-01	.9950
4	.4266E-01	.9985
5	.8431E-01	.9449
6	.9753E-01	.9912
7	.1182E+00	.9669

REGRESSION COEFFICIENTS

CHANNEL	C0	C2	C3	C4	C5	C6	C7
1	.4150E+00	-.1089E-01	.4056E-01	-.3820E-01	.2613E+00	-.2428E+00	-.8392E-02
2	-.2043E+00	.1326E-02	.1224E+00	-.1129E+00	.3868E-01	-.3760E-02	-.4401E-01
3	-.3599E-01	.2491E-02	-.2057E-02	.5476E-02	-.3411E-02	.1146E-02	-.3186E-02
4	-.3327E+01	.1926E+00	.5948E-01	.4646E+00	-.2696E+00	.7119E-01	-.4549E+00
5	-.3598E+00	.5626E-01	.2252E-01	-.5204E-01	.9386E-02	-.2863E-02	-.2618E-01
6	-.1562E+00	-.1461E-01	.1244E+00	-.5557E-01	-.3534E-01	.1151E-02	-.1495E-01
7	.6864E+00	.2454E-01	-.9462E-01	.1327E+00	-.2614E-01	-.5336E-01	.1100E-01

ZENITH ANGLE = 42.40 DEGREES

CHANNEL	STANDARD ERROR	EXPLAINED VARIANCE
1	.1393E-01	.6502
2	.1560E+01	.6515
3	.8352E-01	.9950
4	.4838E-01	.9985
5	.9720E-01	.9423
6	.1107E+00	.9912
7	.1332E+00	.9673

REGRESSION COEFFICIENTS

CHANNEL	C0	C2	C3	C4	C5	C6	C7
1	.4397E+00	-.1198E-01	.4224E-01	-.3928E-01	.2871E+00	-.2684E+00	-.7897E-02
2	-.2454E+00	.1610E-02	.1388E+00	-.1295E+00	.4511E-01	-.4249E-02	-.4951E-01
3	-.3757E-01	.2549E-02	-.2169E-02	.5736E-02	-.3599E-02	.1214E-02	-.3247E-02
4	-.3405E+01	.1941E+00	.6849E-01	.4676E+00	-.2857E+00	.8138E-01	-.4638E+00
5	-.4109E+00	.6352E-01	.2630E-01	-.5926E-01	.1103E-01	-.3366E-02	-.3011E-01
6	-.1648E+00	-.1594E-01	.1408E+00	-.6402E-01	-.4004E-01	.1636E-02	-.1719E-01
7	.7761E+00	.2609E-01	-.1035E+00	.1476E+00	-.3044E-01	-.5899E-01	.1265E-01
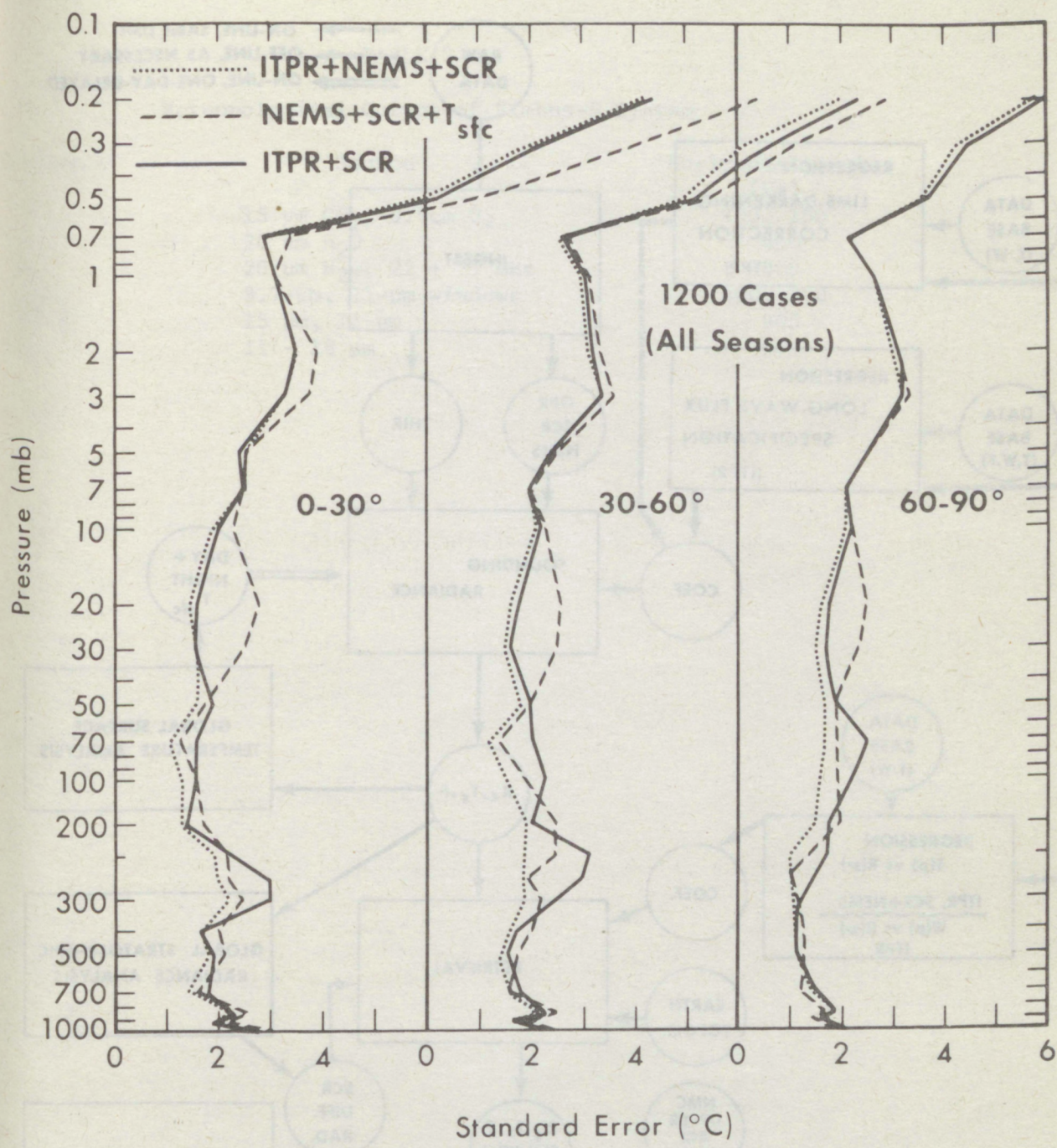
Fig. 7 - 1

NIMBUS 5 SOUNDING DATA PROCESSING SYSTEM
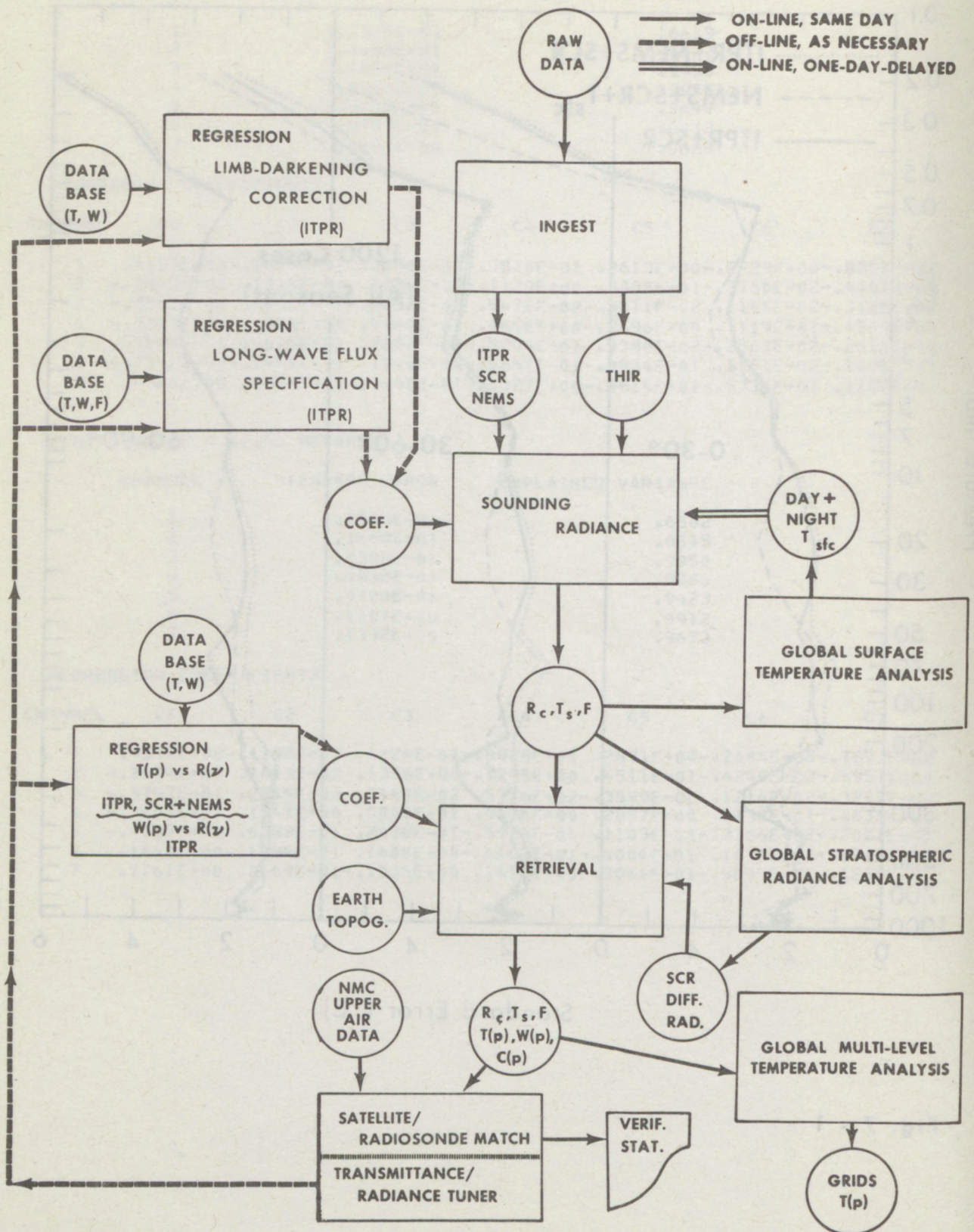
Fig. 7- 2

TABLE 7-3

Meteorological Output of Nimbus-5 System

Parameter	Source	Horizontal Scale (km)
$T(p)$	15 μm CO_2, 0.5cm O_2	400, 150
$q(p)$	20 μm H_2O	400
W_T	20 μm H_2O, 22 + 31 GHz	400
T_{sfc}	3.7-μm, 11-μm windows	400, 150
P_C,N	15 μm, 11 μm	400
$F_T^\uparrow$	11 - 18 μm	400

REFERENCES

Barrett, A. H., and Chung, V. K., "A Method for the Determination of
High-Altitude Water-Vapor Abundance from Ground-Based Microwave
Observations," Journal of Geophysical Research, Vol. 67, No. 11,
1962, pp. 4259-4266.

Bengtsson, L., and Gustavsson, N., "An Experiment in the Assimilation
of Data in Dynamical Analysis," Tellus, 23, 1971, pp. 328-336.

Davis, P. A., "Universal Transmittance Representations for Application
to ITPR Measurements," Final Report prepared for NOAA/NESS, Contract
2 - 35136, Stanford Research Institute, Menlo Park, California,
May 1972, 45 pp.

Fritz, S., Wark, D. Q., Fleming, H. E., Smith, W. L., Jacobowitz, H.,
Hilleary, D. T., Alishouse, J. C., "Temperature Sounding From Satellites,"
NOAA Technical Report NESS 59, July 1972, 49 pp. (Available from the
National Technical Information Service.)

Grody, N., Unpublished Memo, 1974.

McClatchey, R. A., et. al., Environmental Research Papers No. 331
(ARCRL 70-0527) AF Cambridge Res. Lab., 1970.

Meeks, M. L., and Lilley, A. E., "The Microwave Spectrum of Oxygen
in the Earth's Atmosphere," Journal of Geophysical Research, Vol. 68,
No. 6, 1963, pp. 1683-1703.

Nimbus Project "The Nimbus-5 User's Guide," Goddard Space Flight
Center, NASA, Nov. 1972, 161 pp.

Smith, W. L., "Iterative Solution of the Radiative Transfer Equation for
Temperature and Absorbing Gas Profiles of an Atmosphere," Applied
Optics, Vol. 9, No. 9, Sept. 1970, pp. 1993-1999.

Smith, W. L., Woolf, H. M., and Jacob, W. J., "A Regression Method for
Obtaining Real Time Temperature and Geopotential Height Profiles from
Satellite Spectrometer Measurements and Its Application to Nimbus III
'SIRS' Observations," Monthly Weather Review, Vol. 98, No. 8, Aug 1970,
pp. 582-603.

Smith, W. L., Woolf, H. M., and Fleming, H. E., "Retrieval of Atmospheric
Temperature Profiles from Satellite Measurements for Dynamical Fore-
casting," Journal of Applied Meteorology, Vol. 11, No. 1, Feb. 1972,
pp. 113-122.

Smith, W. L., Hilleary, D. T., Baldwin, E. C., Jacob, W. J., Jacobowitz, H., Nelson, G., Soules, S. D., and Wark, D. Q., "The Airborne ITPR Brassboard Experiment," NOAA Technical Report, NESS 58, Mar. 1972, 74 pp. (Available from the National Technical Information Service).

Smith, W. L., Wydick, J., Howell, H. B., and Pellegrino, P. P., "Results From the CV-990 ITPR Experiment During BESEX," to be published as a NOAA Tech. Report, 1974.

VanVleck, J. H., and Weisskopf, V. F., "On the Shape of Collision Broadened Lines," Reviews of Modern Physics, Vol. 17, Nos. 2 and 3, 1945, pp. 227-236.

Wark, D. Q., Yamamoto, G. and Lienesch, J., "Infrared Flux and Surface Temperature Determinations From TIROS Radiometer Measurements," M.S.L. Report No. 10, U. S. Dept. of Commerce, Wash. D.C., Aug. 1962 84 pp.

Wark, D. Q., and Hilleary D., ESSA, "Atmospheric Temperature: Successful Test of Remote Probing," Science, 165, Sept. 1969, pp. 1256-1258.

Winston, J. S., Smith, W. L., and Woolf, H. M., "The Global Distribution of Outgoing Long-Wave Radiation Derived From SIRS Radiance Measurements," Proceedings of the Conference on Atmospheric Radiation, Fort Collins, Colorado, Aug. 7-9, 1972, pp. 221-227.